STUDY OF DISORDERED SYSTEMS

A Thesis

Submitted to the University of Roorkee

for the Award of the Degree of

DOCTOR OF PHILOSOPHY

in

PHYSICS

By

VIPIN SRIVASTAVA

Department of Physics

University of Roorkee

Roorkee (India)

May 1976

CERTIFICATE

This is to certify that the thesis entitled 'STUDY OF DISORDERED SYSTEMS', which is being submitted by Mr. Vipin Srivastava in fulfilment for the award of the degree of Doctor of Philosophy in Physics from the University of Roorkee, is a record of his own work carried out by him under my supervision and guidance. The matter embodied in this thesis has not been submitted for the award of any other degree.

This is further to certify that he has worked for a period equivalent to 24 months full time research for preparing his thesis for Ph.D. degree at this University.

Dated: 15th May 1976

S.K. Joshi

(S.K. Joshi)

Professor and Head,
Physics Department,
Roorkee University,
Roorkee 247667, INDIA.

ACKNOWLEDGMENTS

I extend my gratitude to Professor S.K.Joshi, but for whose guidance and cooperation, this thesis would not have been possible. It is a pleasure to record my deep appreciation of warm helpfulness and good colleagueship enjoyed in the department of Physics, University of Roorkee during the course of my research work. I am thankful to the Council of Scientific and Industrial Research (New Delhi) for providing financial support in the form of a research fellowship.

RÉSUMÉ

The present thesis contains some of the author's theoretical investigations aimed at understanding the behaviour of electrons and phonons in disordered systems. The usual tools of band theory are not applicable to such systems because of the lack of translational invariance. With the breakdown of Bloch-Floquet theorem in disordered systems, the nature and distribution of their eigen-states in energy become the foci of theoretical interest. With the availability of high-speed computers, it has become possible to apply sophisticated Green-function techniques to the present problem. Amongst the analytical tools developed for studying disordered systems the Coherent potential approximation (CPA) occupies a central position. This theory has proved extremely helpful in providing a semi-quantitative description of a wide class of elementary excitations (electrons, phonons, excitons etc.).in disordered systems.

We applied this theory for phonons in Si-Ge alloy and tried to interpret the Raman-data available for this system. This study led us to conclude that it is necessary to modify some of the simplifying assumptions in CPA theory for a fruitful confrontation of theory and experiment.

Our efforts aimed at improving upon CPA have followed two different directions. First, following the

line of CPA we developed a coherent pseudopotential approximation. This is capable of taking into account the difference in band-widths and shapes of density of states curves of the constituents of the alloy. This is a self-consistent, single-site, single-band theory and is valid for any number of subbands. Its application to Cu-Ni alloys has been quite promising. Secondly, we have attempted to synthesize the numerous approaches to improve upon the single-site nature of CPA. This type of generalization of CPA is non-unique. All the generalizations to include the cluster effects can be categorised into two classes based on two types of decoupling schemes. It becomes interesting to compare the numerical results obtained from the two methods. Numerical results are available for two-site clusters from one of these methods. We have performed the calculations using the other method. The results are quite different.

The studies mentioned so far were concerned with the distribution of eigenstates in energy. The other important aspect studied in the thesis is the nature of the wave functions in disordered systems. Anderson introduced the idea of non-diffusion of an electron in a disordered system. Further charm was added to the idea by Mott, Cohen, Fritsche and Ovshinsky, who conjectured that in a disordered system the localized and extended eigenstates are separated by a well-defined energy called

mobility edge. Anderson's original work was extended to determine the mobility edges, by two sets of authors, Economou and Cohen, and Abou-Chacra, Anderson and Thouless. They used renormalized perturbation expansion of self-energy and dealt with the convergence and divergence of the series. The former authors assumed all the terms in the series to be strongly correlated whereas the latter ones took them to be uncorrelated. The convergence of the series implies localization and divergence implies extension.

We have modified the Economou-Cohen criteria by avoiding a mathematical approximation made by them, and have calculated the percolation concentration. This concentration comes out to be 7% and 8% against the corresponding old values of 17% and 24% yielded by two of Economou-Cohen criteria. Percolation studies of localization yield the value 31% . We have made some preliminary studies regarding the influence of short range order on localization, and the meaning of localization of phonons.

The shape of localized wave functions is a subject of great interest in localization studies. Assuming the mobility edge to be known we have studied for a Cayley tree lattice the extent of localized wave function as a function of energy. We have found that the extent of wave-function diverges at the mobility edge — an observation

consistent with Mott's contentions. It is interesting to note that the extent also increases gradually as energy moves deep into the band tail. This behaviour can be explained by the probabilistic arguments proposed by Lifshitz.

In the end of the thesis we have critically examined the recent approach to localization problem proposed by Mattis and Yonezawa.

CONTENTS

CHAPTER 1

Preamble

Disorder means deviation from order. In the natural world, there exists an enormous amount of important materials whose microscopic structures are far from periodic. As a matter of fact as has been described by Krumhansl[1], it is really a random world. It is now conceded that many materials possess interesting properties largely on account of their disorder, and solid state philosophers freely predict that the non-crystalline state, when fully unravelled will be found to exhibit its own range of phenomena, no less rich and varied than that shown by the other aggregations of matter.

1. Range of Disordered Systems.

Disorder is mainly divided into two classes.

(a) Substitutional or Cellular Disorder.

The lattice structure is retained but each atomic site is randomly occupied by atoms of different isotopic or chemical species. We also include in this class vacancy defects due to absence of atoms from a lattice site, or interstitial defects due to the presence of additional atoms in the lattice interstices. As a general definition it is best to think of cellular disorder as a disorder where properties vary from cell to cell in a lattice. Cells may contain molecular units which may vary in their orientation, then we have an orientationally disordered crystal.

(b) Topological Disorder.

Topological disorder is associated with glassy or liquid like characteristics. Two extreme situations occur. In the first case each atomic species has its own well defined coordination requirement and its nearest neighbour environment is similar to that in corresponding crystal. In the second case this short range coordination order is absent.

There is an intermediate situation between the orientational disorder and topological disorder which is present in liquid crystals. They are devoid of any lattice structure but the molecules tend to be lined up parallel over long distances.

Before we move on to the problem as to how to study disordered systems, we explain some relevant basic concepts and definitions.

2. Probability Distributions and Ensemble Averages:

In a random system we never have complete information about the structural details of a given specimen. What we can know at most is the probability for a particular structure (or configuration) to appear. Thus we are led to the concept of an ensemble as a mental collection of replicas of the system, each member of the ensemble corresponding to a particular possible structure of the system. Experiments are performed on particular specimens, so we assume that experimentally observable quantities pertinent

to macroscopic systems are sharply distributed around the ensemble average value. In other words we assume that the value of an observable quantity for a member of the ensemble chosen at random differs from the ensemble average value of the same quantity by an amount which is vanishingly small. It therefore follows that purpose of a theory is to calculate ensemble averages or, even more generally, probability distributions for the quantities of physical interest. At which stage the ensemble average will be performed depends on the operational definition of the quantity of interest. This will be made clear later when the averaging is employed.

3. One-body Approximation.

The propagation of the particle or wave we shall consider here will be governed completely by a one-body Hamiltonian, whose matrix elements will be random variables with a known probability distribution. This randomness in the Hamiltonian stems from the randomness in the structure of the material. We will omit many body effects. It should be pointed out that many body effects may be important and possibly different than in a periodic structure.

4. Short- and Long-range Order, Correlation Functions, Degree of Randomness.

In almost all disordered systems there are some elements of order remaining. Usually the material is ordered

to a high degree locally. This means that in the neighbourhood of any arbitrary atom the structure is always very similar to that of a corresponding periodic system. We say that the system possesses short-range order. As the size of the considered neighbourhood increases, its structure for the disordered system usually becomes more and more different than that of a corresponding periodic system and eventually for the very distant atoms there is no correlation at all between the two. This situation is characterized as absence of long-range order. Mathematically speaking, the existence of disorder implies that at least some matrix elements of the Hamiltonian are random variables. Existence of short-range order implies that the matrix elements referring to neighbour atoms are strongly correlated random variables; absence of long-range order means that matrix elements referring to distant atoms become statistically independent as the distance between the atoms becomes infinite.

To decide that one system is more random than another, we make the following considerations. (a) The wider the probability distribution of each matrix element is, the more random the system is, provided all other parameters characterizing the probability distribution remain unchanged;(b) the smaller the range of statistical correlation is, the more random the system is;(c) the weaker the statistical correlation is, the more random the system is.

5. Quantities of Interest.

Having discussed the above basic input informations for a theory, we now examine briefly what the output is, i.e. the quantities we calculate. The most basic information we need is how the eigenstates are distributed in energy, i.e. the density of states. Second, we like to have information about the nature of eigenstates, their spatial extent, i.e. whether they are localized or extended.

5.1. Localized Eigenstates.

A wave function $\psi(\vec{r})$ is defined as localized if it decays fast enough as $|\vec{r}| \to \infty$ so that the integral $\int \psi^* \psi d^3r$ exists. When $\psi(\vec{r})$ is localized, it is assumed to decay in an exponential way, $\psi(\vec{r}) \underset{r\to\infty}{\longrightarrow} e^{-|\vec{r}|/R_d}$, where R_d is called the decay localization length. The quantity R_d determines the behaviour of the wave function only at very large distances; for finite distances $|\psi(\vec{r})|^2$ may exhibit a very complicated behaviour. One possibility is that $|\psi(\vec{r})|^2$ remains more or less constant within a finite simply connected region of space of simple geometrical shape characterized by a linear dimension R_f, termed as fluctuation localization length. More exhaustive definitions of localized eigenstates will be given in the Chapter 5 while doing the physics of such eigenstates.

5.2 Extended Eigenstates.

Extended eigenstates are characterized by the shape of the multiply connected channel type region

extending to infinity, where $|\Psi(\vec{r})|^2$ is appreciable.

An essential difference in theoretical treatments of periodic systems and disordered systems lies in the fact that in the former the problem is reduced, owing to the Bloch theorem, to that of solving a Schrödinger equation in an unit cell. For systems which lack in perfect periodicity, the Bloch theorem fails to work ($\vec{k}$-selection rules are also lost) and thus the Schrödinger equation with an aperiodic potential of infinite extent must be treated. Therefore, for disordered systems it is impossible to solve this equation exactly. Statistical physics provides us methods for deriving macroscopic properties of these disordered materials from quantum mechanical rules governing the microscopic world.

In this thesis we present some of our attempts to tackle with two main themes in the study of phonons and electrons in disordered systems. The first theme is related to the distribution of the eigenvalues of the wave functions for these systems. This is concerned with the problem of the energy spectrum and other one-particle properties of the elementary excitations which are to be discussed by means of the ensemble-averaged one-particle Green's function $\langle G \rangle$, where the ensemble consists of elements corresponding to all possible microscopic configurations of atoms which can not be distinguished macroscopically. The second theme is associated with the

behaviour or the character of the eigenstates, i.e. whether it is spatially localized in a restricted region, or extended throughout the sample.

The organization of the thesis is as follows. Chapter 2 contains a general formulation of the self-consistent single site approximation, the so-called coherent potential approximation[2,3] for obtaining ensemble averages of the quantities of interest. It has been subsequently generalized for the case of phonons for lattices containing more than one atom per unit cell. This has been applied to Si-Ge alloys of arbitrary composition and comparison has been made with the available Raman spectra. In Chapter 3 a coherent pseudo-potential approximation has been reported. This is again a self-consistent single site theory but enables one to deal with realistic systems having arbitrary shape and any number of sub-bands of density of states. Comparison of the computed results for Cu-Ni alloys has been made with the photo-emission results. Generalization of CPA to include the effects due to clusters of like atoms has been given in Chapter 4. Various decoupling schemes have been compared and critically studied with special emphasis upon the pairs embedded in an effective medium. Calculations within self-consistent pair approximation have been reported for simple cubic lattice and results have been compared with other similar but not so exact calculations. The fifth and the final chapter deals with the difficult problem of localization in disordered lattices. Three

methodologies in the field have been stated and discussed. Results for the extent of wave functions in the localized regime obtained for the first time for three dimensional lattices, have been given for infinite Cayley tree lattice with Lorenzian shape of site-energy distribution. The famous Economou-Cohen criteria for localization have been modified. Attempts have been made to understand the localization of phonons. Qualitative arguments have been stated and supported to a good extent by the quantitative results obtained by adapting the Economou-Cohen criteria to the case of phonons. The final section of the chapter reports the socalled new criterion for localization given by Mattis and Yonezawa.[111] This method has been shown to rest on erroneous arguments.

CHAPTER 2

Coherent Potential Approximation

We present a brief systematic derivation of the so-called coherent potential approximation (CPA)[2,3], which is a powerful approximation scheme for obtaining the ensemble average. We clarify its meaning and limitations and discuss a moderately realistic single band model corresponding to a three-dimensional system.

The CPA is a self-consistent single site approximation within the multiple-scattering framework[4-6]. In this approach the propagation of an electron or lattice wave in an alloy is regarded as a succession of elementary scatterings on the random atomic scatterers, which are then averaged over all configurations of atoms. A scatterer is viewed as being embedded in a fictitious medium described by a yet undetermined effective Hamiltonian, H_{eff} which possesses the same symmetry properties as the average Hamiltonian (i.e. it is periodic). An incident wave associated with this effective Hamiltonian is introduced which is scattered in the real material by the scattering potential $(H-H_{eff})$ (H is the actual Hamiltonian of the disordered system). H_{eff} is then determined by the requirement that the scattering on the average is minimal. The so-determined H_{eff} is called the coherent potential Hamiltonian and is used to describe the average properties of the material. A detailed study of CPA has been done by Velicky, Kirkpatrick and Ehrenreich[7] and all the parallel methodologies have been reviewed by Yonezawa and Morigaki.[8]

1. GENERAL FORMULATION:

We derive results that are valid within single site approximation for any single-particle Hamiltonian which can be decomposed into a sum of contributions associated with each site. The N equivalent sites of a lattice are randomly occupied by two kinds of atoms, A and B. The probabilities for a site of being occupied by A and B are proportional to their concentrations per unit cell, which are respectively x and y = 1-x, both varying from 0 to 1. The one-electron Hamiltonian corresponding to a given configuration is denoted by H. The single particle properties are derived from the Green's function $G(Z) = (Z-H)^{-1}$. The quantity of interest is $\langle G(Z) \rangle$ which determines all the macroscopic quantities and has the full symmetry of the empty lattice. The effective Hamiltonian characterizing the average crystal is defined by the relation $\langle G(Z) \rangle = (Z-H_{eff})^{-1}$. An approximation $\tilde{H}(Z)$ is made for the exact $H_{eff}(Z)$ and a perturbation equation is written,

$$\langle G \rangle = \tilde{G} + \tilde{G}(H_{eff}-\tilde{H}) \langle G \rangle . \qquad \ldots (1.1)$$

Here,

$$\tilde{G} = (Z-\tilde{H})^{-1} , \qquad \ldots (1.2)$$

is the unperturbed (reference medium) Green's function. In the multiple scattering theory a T matrix is defined by a relation similar to (1.1),

$$G = \tilde{G} + \tilde{G}T\tilde{G}. \qquad \ldots (1.3)$$

On averaging one gets,

$$\langle G \rangle = \tilde{G} + \tilde{G}\langle T \rangle \tilde{G}. \qquad \ldots (1.4)$$

From (1.1) and (1.4) we get,

$$H_{eff} = \tilde{H} + \langle T \rangle (1+\tilde{G}\langle T \rangle)^{-1}. \qquad \ldots (1.5)$$

This equation can be solved in two ways.

(a) Non-self consistent method:

$\langle T(\tilde{H}) \rangle$ corresponding to a given $\tilde{H}$ is inserted.

(b) Self-consistent method:

$$\langle T(\tilde{H}) \rangle = 0, \qquad \ldots (1.6)$$

is solved. Approach (a) is simpler than (b).

1.1 Single Site Approximation(SSA):

The random-perturbing potential $(H-\tilde{H})$ is decomposed into a sum of contributions from individual scatterer,

$$H - \tilde{H} = \sum_n V_n. \qquad \ldots (1.7)$$

The multiple scattering method is applicable if such a decomposition is possible. Combination of (1.3) and

$$G = \tilde{G} + \tilde{G}(H - \tilde{H})G, \qquad \ldots (1.8)$$

yields,

$$T = (H-\tilde{H})(1+\tilde{G}T), \qquad \ldots (1.9)$$

$$= \sum_n V_n(1+\tilde{G}T) = \sum_n T_n. \qquad \ldots (1.10)$$

T_n is the contribution of an individual scatterer to T. We now introduce t_n, the atomic T matrix associated with the isolated site n,

$$t_n = V_n(1-V_n\tilde{G})^{-1}. \qquad \ldots (1.11)$$

With the help of (1.10) and (1.11), T_n is written in terms of t_n as,

$$T_n = t_n(1 + \tilde{G}\sum_{m\neq n} T_m). \qquad \ldots (1.12)$$

T_n is the strength of a scatterer in alloy. t_n is the strength of an isolated scatterer. $(1+\tilde{G}\sum_{m\neq n} T_m)$ describes the multiple scattering from all the scatterers (except n) in the alloy of an unperturbed wave incident on n. After iterations (1.12) evolves into an hierarchy of atomic T matrices,

$$T = \sum_n t_n + \sum_n t_n \tilde{G} \sum_{m\neq n} t_m + \ldots. \qquad \ldots (1.13)$$

Averaging the exact relations (1.10)-(1.12), we get,

$$\langle T\rangle = \sum_n \langle T_n\rangle, \qquad \ldots (1.14)$$

$$\langle T_n\rangle = \langle t_n(1+\tilde{G}\sum_{m\neq n} T_m)\rangle, \qquad \ldots (1.15)$$

$$= \langle t_n\rangle(1+\tilde{G}\sum_{m\neq n}\langle T_m\rangle) + \langle t_n\tilde{G}\sum_{m\neq n}(T_m - \langle T_m\rangle)\rangle \quad \ldots (1.16)$$

The first term describes the effect of the averaged effective wave seen by the n^{th} atom and the second term corresponds to the fluctuations of the effective wave. We neglect this fluctuation term which amounts to assuming that all statistical correlations between n and all other sites m are neglected. So that,

$$\langle T_n\rangle = \langle t_n\rangle\, 1+\tilde{G}\sum_{m\neq n}\langle T_m\rangle). \qquad \ldots (1.17)$$

This decoupling of average in (1.15) is termed as <u>single-site</u> decoupling scheme because it isolates the average

scattering from n^{th} scatterer from the multiple scatterings from rest of the sites in the system. Since $\sum_{m\neq n} T_m = T-T_n$, we get from (1.17),

$$\langle T_n \rangle = \langle t_n \rangle (1+\tilde{G}\langle T \rangle)(1+\tilde{G}\langle t_n \rangle)^{-1}, \qquad \ldots (1.18)$$

so that (1.5) can be rewritten as,

$$H_{eff} = \tilde{H} + \sum_n \langle t_n \rangle (1+\tilde{G}\langle t_n \rangle)^{-1}. \qquad \ldots (1.19)$$

Thus the non-self consistent and self consistent methods described above may be done in terms of t_n within SSA. Within SSA the self consistency condition (1.6) is equivalent to solving,

$$\langle t_n(\tilde{H}) \rangle = 0, \qquad \ldots (1.20)$$

for all n. Determination of an effective medium through the fulfilment of the condition (1.20) within the set of approximations made in arriving at (1.20) is called the coherent Potential Approximation(CPA).

2. CPA FOR PHONONS:

We essentially repeat the CPA formulation of Taylor[3] for phonons in disordered alloys, generalizing it for more than one atom in a unit cell.[9] We discuss a single-band model which is closely related to the tight-binding approximation. The Hamiltonian for the harmonic lattice containing impurities is

$$H = H_o + H', \qquad \ldots (2.1)$$

where,

$$H_o = \sum_{\ell k} \frac{p^2(\ell k)}{2M_o} + \frac{1}{2} \sum_{\substack{\ell,\ell' \\ k,k'}} \sum_{\alpha,\beta} \phi_{\alpha\beta}(\ell k, \ell' k') u_\alpha(\ell k) u_\beta(\ell' k'), \quad \ldots (2.1)$$

is the perfect lattice Hamiltonian, $p(\ell k)$ is the momentum operator for the atom of mass M_o in the ℓ^{th} unit cell with basis index k, and $u_\alpha(\ell k)$ is the α^{th} Cartesian component of the displacement operator for this atom. $\phi_{\alpha\beta}(\ell k, \ell' k')$ are force constants. If we confine ourselves to the mass disorder only, the perturbation part of H is written as,

$$H' = \sum_{\ell k} \frac{p^2(\ell k)}{2} \left(\frac{1}{M(\ell k)} - \frac{1}{M_o} \right). \quad \ldots (2.3)$$

Such an assumption makes the disorder cell localized. Contributions to H' come from impurity sites only. The displacement-displacement double-time thermal Green's functions[10] are defined as

$$G^{ret}_{\alpha\beta}(\ell k, \ell' k'; t-t') \equiv 2\pi \ll u_\alpha(\ell k, t); u_\beta(\ell' k', t') \gg_{ret}$$
$$= -2\pi i \langle [u_\alpha(\ell k, t), u_\beta(\ell' k', t')] \rangle_T \theta(t-t'), \quad \ldots (2.4a)$$

$$G^{adv}_{\alpha\beta}(\ell k, \ell' k'; t-t') \equiv 2\pi \ll u_\alpha(\ell k, t); u_\beta(\ell' k', t) \gg_{adv}$$
$$= 2\pi i \langle [u_\alpha(\ell k, t), u_\beta(\ell' k', t')] \rangle_T \theta(t'-t), \quad \ldots (2.4b)$$

$$\theta(t) = 1, \quad t > 0$$
$$= 0, \quad t < 0.$$

α,β denote the Cartesian components and $\langle\rangle_T$ denotes the thermal average. The average over different configurations is denoted simply by $\langle\rangle$. The Fourier time transform of G is given by

$$G_{\alpha\beta}(\ell k,\ell' k';\omega\pm i\delta) = \frac{1}{2\pi}\int_{-\infty}^{\infty} G^{ret,adv}_{\alpha\beta}(\ell k,\ell' k';t)\, e^{i(\omega\pm i\delta)t}\, dt \qquad \ldots (2.5)$$

We shall suppress the infinitesimal quantity δ and understand that for the retarded and advanced cases ω approaches the real axis from the upper and lower half planes, respectively. For a harmonic lattice, both Green's functions of (2.4) for a system described by eqns. (2.1)-(2.3) satisfy identical second order differential equations of motion which, when transformed according to (2.5), give the following equation for G:

$$-M_o\omega^2 G_{\alpha\beta}(\ell k,\ell' k';\omega) + \sum_{\substack{\ell'',\gamma \\ k'',k'}} \Phi_{\alpha\gamma}(\ell k,\ell'' k'')\, G_{\gamma\beta}(\ell'' k'',\ell' k';\omega)$$

$$= -\delta_{\alpha\beta}\delta(\ell k,\ell' k') + \sum_{\substack{\ell'',\gamma \\ k',k''}} C_{\alpha\gamma}(\ell k,\ell'' k'';\omega)\, G_{\gamma\beta}(\ell'' k'',\ell' k';\omega), \qquad \ldots (2.6)$$

$$C_{\alpha\beta}(\ell k,\ell' k';\omega) = \left[M_o - M(\ell k)\right]\omega^2\delta_{\alpha\beta}(\ell k,\ell' k'). \qquad \ldots (2.7)$$

For a defect atom at $\ell_i k_i$, it is convenient to describe the change in mass,

$$M_o - M(\ell_i k_i) = M_o\varepsilon^{(\ell_i k_i)}, \qquad \ldots (2.8)$$

by the matrix,

$$C^{(\ell_i k_i)}_{\alpha\beta}(\ell k,\ell' k';\omega) = M_o\varepsilon^{(\ell_i k_i)}\omega^2\delta_{\alpha\beta}\delta(\ell k,\ell' k')\delta(\ell k,\ell_i k_i) \qquad \ldots (2.9)$$

$\varepsilon^{(\ell_i k_i)}$ therefore gives the fractional mass change at $(\ell_i k_i)$ occupied by an atom of type p. If the Green's function for the perfect lattice [i.e., $\underline{C} = 0$ in eq.(2.6)], denoted by $\underline{P}$, is known, then one obtains for $\underline{G}$

$$G_{\alpha\beta}(\ell k,\ell' k';\omega) = P_{\alpha\beta}(\ell k,\ell' k';\omega)+M_o\varepsilon\omega^2 \sum_{\substack{s,\gamma \\ k_s}} P_{\alpha\gamma}(\ell k,sk_s;\omega)\times G_{\gamma\beta}(sk_s,\ell' k';\omega) \quad \ldots (2.10)$$

(sk_s) denotes the impurity site. Now

$$P_{\alpha\beta}(\ell k,\ell' k';\omega) = \frac{1}{NM_o}\sum_{\vec{q},j} \frac{\sigma_\alpha^{j*}(\vec{q})\sigma_\beta^{j}(\vec{q})e^{-i\vec{q}.(\vec{R}_{\ell k}-\vec{R}_{\ell' k'})}}{\omega^2-\omega_j^2(\vec{q})}, \quad \ldots (2.11)$$

N is the number of unit cells and j specifies the 3s branches, where s is the number of atmos per unit cell. $\omega_j(\vec{q})$ are the eigenvalues and $\sigma_\alpha^j(\vec{q})$ are the eigenvectors of the dynamical matrix for a perfect crystal. Eq.(2.10) for the Green's function of the imperfect crystal $\underline{G}$ can be rewritten in the form

$$\underline{G}(\ell k,\ell' k';\omega) = \underline{P}(\ell k,\ell' k';\omega)+ \sum_{\substack{\ell_1,\ell_2 \\ k_1,k_2}} \underline{P}(\ell k,\ell_1 k_1;\omega)\underline{C}(\ell_1 k_1,\ell_2 k_2;\omega)\cdot \underline{G}(\ell_2 k_2,\ell' k';\omega), \quad \ldots (2.12)$$

where the defect matrix is given by

$$\underline{C}(\ell k,\ell' k',\omega) = \sum_{\ell_i k_i} \underline{C}^{(\ell_i k_i)}(\ell k,\ell' k';\omega). \quad \ldots (2.13)$$

Equation (2.12) is the usual Dyson equation with $\underline{C}$ as perturbation. If we introduce the t-matrix,

$$\underline{T}(\ell_1 k_1, \ell_2 k_2; \omega) = \frac{\underline{C}(\ell_1 k_1, \ell_2 k_2; \omega)}{1 - \underline{C}(\ell_1 k_1, \ell_2 k_2; \omega)\underline{P}(\ell_1 k_1, \ell_2 k_2; \omega)} , \quad \ldots (2.14)$$

We can write

$$\underline{G}(\ell k, \ell' k'; \omega) = \underline{P}(\ell k, \ell' k'; \omega) + \sum_{\substack{\ell_1, \ell_2 \\ k_1, k_2}} \underline{P}(\ell k, \ell_1 k_1; \omega)\underline{T}(\ell_1 k_1, \ell_2 k_2; \omega) \times \underline{P}(\ell_2 k_2, \ell' k'; \omega) . \quad \ldots (2.15)$$

Averaging (2.15) over all configurations, we have

$$\langle \underline{G}(\ell k, \ell' k'; \omega) \rangle = \underline{P}(\ell k, \ell' k'; \omega) + \sum_{\substack{\ell_1, \ell_2 \\ k_1, k_2}} \underline{P}(\ell k, \ell_1 k_1; \omega) \langle \underline{T}(\ell_1 k_1, \ell_2 k_2; \omega) \rangle \times \underline{P}(\ell_2 k_2, \ell' k'; \omega) . \quad \ldots (2.16)$$

On iterating eqn.(2.12) and averaging, we have the result in terms of the self-energy $\underline{\Sigma}$:

$$\langle \underline{G}(\ell k, \ell' k'; \omega) \rangle = \underline{P}(\ell k, \ell' k'; \omega) + \sum_{\substack{\ell_1, \ell_2 \\ k_1, k_2}} \underline{P}(\ell k, \ell_1 k_1; \omega)\, \underline{\Sigma}(\ell_1 k_1, \ell_2 k_2; \omega) \times \langle \underline{G}(\ell_2 k_2, \ell' k'; \omega) \rangle . \quad \ldots (2.17)$$

Now we make an approximation $\underline{E}$ for the actual self-energy $\underline{\Sigma}$. A new Green's function is defined in terms of $\underline{E}$ as

$$\underline{G}^{\circ}(\ell k, \ell' k'; \omega) = \underline{P}(\ell k, \ell' k'; \omega) + \sum_{\substack{\ell_1, \ell_2 \\ k_1, k_2}} \underline{P}(\ell k, \ell_1 k_1; \omega)\underline{E}(\ell_1 k_1, \ell_2 k_2; \omega) \times \underline{G}^{\circ}(\ell_2 k_2, \ell' k'; \omega) . \quad \ldots (2.18)$$

Then writing Eqn.(2.12) in terms of $\underline{G}^{\circ}$ rather than $\underline{P}$, we obtain

$$\underline{G}(\ell k,\ell' k';\omega) = \underline{G}^{o}(\ell k,\ell' k';\omega) + \sum_{\substack{\ell_1,\ell_2 \\ k_1,k_2}} \underline{G}^{o}(\ell k,\ell_1 k_1;\omega)\underline{V}^{(\ell_2 k_2)}(\ell_1 k_1,\ell_2 k_2;\omega) \times \underline{G}(\ell_2 k_2,\ell' k';\omega), \quad \ldots (2.19)$$

with

$$\underline{V}^{(\ell_2 k_2)}(\ell_1 k_1,\ell_2 k_2;\omega) = -\underline{E}(\ell_1 k_1,\ell_2 k_2;\omega) \text{ for a host atom at } \ell_2 k_2 \quad \ldots (2.20a)$$

$$= -\underline{E}(\ell_1 k_1,\ell_2 k_2;\omega) + M_o \varepsilon \omega^2 \delta(\ell_1 k_1,\ell_2 k_2)\underline{I}$$

for a defect atom at $\ell_2 k_2$. ... (2.20b)

In the single-site CPA we choose our system such that besides the site, say, (ℓk) (which has the liberty of being occupied by the host atom or the defect atom), the rest of the sites are configurationally averaged. If we identify $\underline{E}$ with the exact $\underline{\Sigma}$, then $\underline{G}^{o}$ becomes equal to the exact $\underline{G}$ and the self-consistency condition for determining $\underline{E}$ is

$$\sum_{p} c^{p}\underline{T}^{p}(\vec{q},\omega) = 0. \quad \ldots (2.21)$$

c^{p} is the concentration of the p-type atoms in the lattice and hence is proportional to the probability of the occurrence of a p-type atom at a site. $\underline{T}$ is calculated in terms of the modified Green's function $\underline{G}^{o}$. Equation (2.21) is

$$(1-c)\underline{T}^{h} + c\underline{T}^{d} = 0,$$

with

$$\underline{T}^{p} = \frac{\underline{V}^{p}}{1 - \underline{G}^{o}\underline{V}^{p}},$$

where h and d stand for host and defect, respectively.

The explicit form of $\underline{V}^p$ is given in eqn.(2.20) and on simplification we get

$$\underline{E}(\vec{q}\,\omega)\Big(\underline{I}+\frac{1}{N}\sum_{q}\underline{G}^{o}(\vec{q}\,\omega)\underline{E}(\vec{q},\omega)^{-1}\times\big(\underline{I}-(1-c)M_{o}\varepsilon\omega^{2}\underline{G}^{o}(\omega)\big)$$

$$+\frac{1}{N}\sum_{q}\underline{G}^{o}(\vec{q},\omega)\underline{E}(\vec{q},\omega)\Big)=M_{o}c\varepsilon\omega^{2}\underline{I}, \qquad \ldots (2.22)$$

where $\underline{G}^{o}(\omega)=\underline{G}^{o}(\ell k,\ell k;\omega)=\frac{1}{N}\sum_{q}\underline{G}^{o}(\vec{q},\omega)$. $\qquad \ldots (2.23)$

Thus $\underline{E}(\vec{q},\omega)$ is independent of $\vec{q}$, so that

$$\frac{1}{N}\sum_{\vec{q}}\underline{G}^{o}(\vec{q},\omega)\underline{E}(\vec{q},\omega)=\underline{G}^{o}(\omega)\underline{E}(\omega),$$

and on further simplification eqn.(2.22) becomes

$$\underline{E}(\omega)-M_{o}c\varepsilon\omega^{2}\underline{I}-\underline{E}(\omega)\big[M_{o}\varepsilon\omega^{2}\underline{I}-\underline{E}(\omega)\big]\,\underline{G}^{o}(\omega)=0. \qquad \ldots (2.24)$$

We write

$$\underline{E}(\omega)=M_{o}\tilde{\varepsilon}(\omega)\omega^{2}\underline{I}, \qquad \ldots (2.25)$$

convert (2.18) into $\vec{q}$ representation, and change the unperturbed Green's function (2.11) from normal coordinate representation to qj representation. This enables us to write

$$G^{o}(\omega)=\frac{1}{M_{o}}\int\frac{\rho(\omega')}{\omega^{2}\big[1-\tilde{\varepsilon}(\omega)\big]-\omega'^{2}}\,d\omega', \qquad \ldots (2.26)$$

with $\rho(\omega')=\frac{1}{N}\sum_{qj}\delta\{\omega_{j}(\vec{q})-\omega'\}$, $\qquad \ldots (2.27)$

which is the phonon density of states of the unperturbed host crystal. Writing (2.26) as

$$G^{o}(\omega)=(1/M_{o})g^{o}(\omega),$$

and using (2.25), we write (2.24), finally, in the form

$$\tilde{\varepsilon}(\omega) = c\varepsilon+\tilde{\varepsilon}(\omega)\left[\varepsilon-\tilde{\varepsilon}(\omega)\right]\omega^2 g^{o}(\omega), \qquad \ldots (2.28)$$

where

$$g^{o}(\omega) = \int \frac{\rho(\omega')}{\omega^2\left[1-\tilde{\varepsilon}(\omega)\right]-\omega'^2}\, d\omega'. \qquad \ldots (2.29)$$

The averaged Green's function $G(\vec{q},\omega)$ is specified by the spectral density

$$\mathcal{A}(\vec{q}j,\omega) = -\pi^{-1}\,\mathrm{Im}\langle G(\vec{q}j,\omega)\rangle. \qquad \ldots (2.30)$$

We can cast the spectral density function into a form which is convenient for calculation. From eqns.(2.26) and (2.27) we have

$$G^{o}(\omega) = \frac{1}{NM_o}\sum_{\vec{q}j}\int \frac{\delta\{\omega_j(\vec{q})-\omega'\}}{\omega^2\left[1-\tilde{\varepsilon}(\omega)\right]-\omega'^2}\, d\omega'. \qquad \ldots (2.31)$$

$G^{o}(\omega)$ may be written in terms of the modes specified by $\vec{q},j$ as

$$G^{o}(\omega) = \frac{1}{N}\sum_{\vec{q},j} G^{o}(\vec{q}j,\omega), \qquad \ldots (2.32)$$

where $G^{o}(\vec{q}j,\omega) = \frac{1}{M_o}\left[\{\omega^2(1-\mathrm{Re}\tilde{\varepsilon}(\omega))-\omega_j^2(\vec{q})\}-i\omega^2\mathrm{Im}\tilde{\varepsilon}(\omega)\right]^{-1}$. $\qquad \ldots (2.33)$

In the CPA

$$\langle G(\vec{q}j,\omega)\rangle = G^{o}(\vec{q}j,\omega).$$

Separating the real and imaginary parts in (2.33), we get the imaginary part

$$\mathrm{Im}\langle G(\vec{q}j,\omega)\rangle = \frac{1}{M_o}\cdot\frac{\omega^2\mathrm{Im}\tilde{\varepsilon}(\omega)}{\{\omega^2\left[1-\mathrm{Re}\tilde{\varepsilon}(\omega)\right]-\omega_j^2(\vec{q})\}^2+\{\omega^2\mathrm{Im}\tilde{\varepsilon}(\omega)\}^2} \qquad \ldots (2.34)$$

This is the spectral density, which can be evaluated by calculating the self-energy from the self-consistent equations (2.28) and (2.29). $G^{o}(\vec{q}j,\omega)$, which is completely determined by $\mathcal{A}(\vec{q}j,\omega)$, contains full information about the one-particle properties and in particular permits discussion of the quasiparticle approximation. Because $\tilde{\varepsilon}(\omega)$ is $\vec{q}j$-independent in the CPA, $G^{o}(\vec{q}j,\omega)$ depends upon $\vec{q}j$ only through $\omega_j(\vec{q})$. If $\mathcal{A}(\vec{q}j,\omega)$ be calculated for the whole allowed range of $\vec{q}j$, one can get information about localization or delocalization of an eigenmode. In the spectral density two kinds of excitation appear, one related to the plane wave like eigenstates of pure host crystal and the other to the impurity states. A peak in $\mathcal{A}(\vec{q}j,\omega)$, if well localized in $\vec{q}j$ space as well as in ω space, has a quasiparticle character and hence corresponds to the delocalization in r-space (because of the uncertainty principle). On the contrary a flat peak extending over the entire band is expected of states localized in coordinate space.

A fairly comprehensive set of density of phonon states and spectral density obtained from CPA-equations (2.28), (2.29) and (2.34), has been given in Figs.1 and 2 for a series of compositions in Cu-Au alloys. The unperturbed density of states for Cu and the $\omega_j(\vec{q})$'s were taken from Svensson et.al. [Phys.Rev.155,619(1967)]. Only mass defect was considered. Figure 1 is a good illustration to see how CPA interpolates between the

unperturbed densities of states of pure Cu and Au. The Cu-Au system is further interesting because Au is slightly more than three times heavier than Cu, so that in-band resonance mode of Au in Cu-rich alloys and isolated impurity mode of Cu in Au-rich alloys can be distinctly seen. Figure 2 shows spectral densities for Cu containing 25%, 75% and 95% Au and for $\omega_j(\vec{q}) = 0.2$, 0.4, 0.6, 0.8 and 0.95 of ω_m^{Cu}, where ω_m^{Cu} is the maximum frequency in the frequency distribution of Cu. A comparison of spectral density plots and the density of states for the corresponding alloy gives some insight into the discussions made in the preceding paragraph about the spectral density.

3. PHONONS IN DISORDERED Si-Ge ALLOYS:

In recent years a lot of work has been done on lattice vibrations of disordered alloys. The vibrational spectra of a large number of binary and pseudobinary alloys have been studied by means of infrared absorption and Raman scattering.[11] Two distinct types of behaviour are found. For same systems only long-wavelength optical phonon frequencies occur which shift, in most cases, linearly with concentration from the mode frequencies of the lighter component downward to the mode frequencies of the heavier component. In other systems vibration frequencies related to each one of the constituents can be separately found in the middle of the concentration range. The first, or the one-mode-type behaviour, is obtained for most of the solid solutions of alkali halides, while the

second or two-mode-type behaviour is found in most of the solid solutions of zinc-blende-type crystals. Balkanski[12] suggests that the long-range average-crystal-potential variation may have been large enough for the one-mode systems to shift the eigenfrequencies of each constituent towards a unique value, and is not sufficient for the two-mode case. The alkali-halide mixed crystals are strongly ionic in character, and therefore each atom is subjected to electrostatic forces extending much further than the statistical cluster in which it is embedded. These forces therefore average for each pair of ions and yield a unique frequency for the mixture. On the contrary, in zinc-blende-type mixed crystals the first-neighbour interaction dominates and is responsible for the splitting of the vibrational spectrum.

A third type of multimode behaviour has been reported for the Raman spectra of Ge-Si alloys by Feldman et.al.[13] over a small composition range (0-33 at % Si in Ge) and by Renucci et.al.[14] and Brya[15] over the whole composition range. Three peaks have been found and are attributed to the vibrations of Ge-Ge, Ge-Si, and Si-Si nearest neighbour pairs. Silicon and germanium form a mixed crystal in all proportions.[16] Because the mass of silicon is much less than that of germanium, one would expect local modes to be associated with the motion of silicon atoms in germanium. Germanium and silicon have a common valency, so that such modes are not expected to be infrared active in first order; however they should

be Raman active. We have tried to understand the experimental observations for the Ge-Si system by Feldman et.al.[13] and Renucci et.al.[14], theoretically[9] within the framework of the coherent potential approximation. With the help of equations (2.28), (2.29) and (2.34) we calculated the spectral density functions for Ge-Si alloys. An examination of the optical modes of germanium[17] and silicon[18] in directions [100] and [110], obtained through neutron-scattering measurements by Ghose et.al.[17] and Dolling[18], respectively, shows that the opitcal phonons scale by numbers which lie between 0.58 and 0.61. This is reasonably close to $(M_{Si}/M_{Ge})^{1/2} = 0.62$. This encouraged us to take into account only the mass change in this calculation. The function $\rho(\omega')$ was taken from Dolling and Cowley's calculations[19] based on their neutron spectroscopic measurements for Ge and Si. The density of states was taken as a histogram of very closely spaced points and integration of (2.29) was done using Simpson's rule, with an initial approximate choice of $\tilde{\varepsilon}(\omega)$. Equation (2.28) was solved iteratively using Newton-Raphson's method applied to a function of a complex variable. Thereafter we calculated the spectral density function from (2.34) for $\vec{q} = 0$ optical modes of Si-Ge alloys.

3.1 Discussion of Results:

The peaks of the spectral density function for optical modes at $\vec{q} = 0$ give information about the zone-centre optical vibrations of alloys of Ge and Si, either

of the two taken as the host crystal. For low concentrations of Ge in Si, one of these may be identified as being due to the heavy defect resonance and the other is near the optical frequency of Si. In our calculations we find that the spectral function shows two distinct peaks. In the impurity band region the spectral function is not sharply peaked, and peaks are too broad to be called peaks. As the defect concentration increases, the weaker peak becomes merely a shoulder on the larger peak (cf.Fig.3). At any concentration, the more prominent peak is attributed to the majority atoms. With Ge taken as host lattice, when Si is added in small quantity it gives rise to a very weak and broad resonance, but this resonance gains prominence as more and more Si is added. At the middle of the concentration range, the two peaks are of comparable prominence, and as more Si is added the lower peak gradually loses prominence while the upper peak becomes narrower. Eventually the lower peak appears only as a shoulder to the upper peak, which approaches optical frequency of pure Si. When Si is taken as host and Ge is added to it, the similar structure of peaks is seen throughout the composition range with a shift in the frequency scale. The peaks at all compositions are shifted to slightly higher frequencies and the amount of shift remains almost constant. This shift may be attributed to the changes of force constants that accompany the alloying process. In our calculations we

did not consider these changes in force constants. When Ge is taken as host we assume that the force constants for the alloy are the same as those for pure Ge. Similarly, with Si we take the alloy force constants to be identical to those of Si. In order to take into account in an approximate manner the force-constant changes due to alloying, we did all calculations by first taking Ge as a host, then taking Si as a host lattice, and finally taking the average of the two values after weighting them with the concentration of that constituent which was regarded as host in that calculation. This appears to be reasonable and has the appearances of a virtual crystal approximation for force constants.

The variation of the frequencies assigned to the peak in the spectral function with the variation of the Si concentration is shown in Fig.4. The lower peak shows only slight variation with composition. The frequency decreases as the Si content increases. The maximum variation, was observed to be 16 cm^{-1}, when Ge was host and it was 20 cm^{-1} when Si was host. These variations for the frequency of the upper peak were 76 and 74 cm^{-1}, respectively in the two cases. The slight decrease in the lower frequency with increasing Si content obtained in our calculations does not agree with the experimental results of Chang, Lacina and Pershan[20], but is in agreement with the observations of Feldman et.al.[13] and Renucci et.al.[14]. At 33 at % Si the calculated downward shift is about 7%.

of the Ge optical-mode frequency. Xinh[21] has treated Raman scattering of light by crystals of the diamond structure containing substitutional random mass defects and no force constant changes. He obtained theoretical expressions for the Raman scattering using a self-energy calculated to lowest order in the concentration of the minority atoms.[22] His results should be valid, therefore, only for small concentrations. These results, when applied to Si in Ge, show that the Raman-active localized mode frequency for small finite concentrations is slightly higher than the localized-mode frequency for a single mass defect. The theory also predicts that the peak in the Raman spectra of the disordered crystal which corresponds to the optical mode ($\vec{q} \approx o$) of the perfect Ge crystal should shift to lower frequencies with increasing Si concentration.

As may be seen from Fig.4, the upper peaks obtained by Renucci et.al., which they assign to be Si-Si nearest neighbour vibrations, are very close to the upper peaks obtained by us taking Si as host, i.e. assuming atoms to be joined by the Si-Si force constant in the alloy. Similarly, the socalled Ge-Ge peaks of Renucci et.al.fall very close to our peaks obtained by taking Ge as host where Ge-Ge force constants are assumed to prevail in the whole lattice. The upper peaks obtained by taking weighted averages fall close to the upper peaks obtained with Ge base at small concentrations of Si and move close to the upper peaks obtained with Si base as the Si concentration

increases. Similar behaviour is seen with the lower peaks also. The averaged behaviour in both cases is pretty well in agreement with the behaviour obtained experimentally by Renucci et.al..

It is also worth noticing that many of the peaks have characteristic asymmetry; they are sharp on the high frequency side and broader at lower frequencies. This is consistent with the CPA theory. The CPA gives the sharp edges of the bands of the density of states, consequently lopsided spectral functions for the phonons belonging to the $\vec{q}$ values at these edges.[7] We are concerned with the top of the optical band; hence the peaks obtained by us are sharp at the high frequency side.

Feldman et.al. and Renucci et.al have assigned the three peaks to the vibrations of the pairs Ge-Ge, Ge-Si and Si-Si. Our calculation was based on the CPA, which is only the single-site approximation treated self-consistently. This approximation by its nature smooths out the structures due to pairs or clusters, so we did not assign the peaks in our results to the pair vibrations. The nature of upper and lower peaks is in correspondence with the upper and lower peaks obtained in references 13 and 14. Some other experimental data on Si-Ge alloys may be had from references 23 to 28.

To conclude this chapter we wish to indicate some limitations of CPA. The complexities involved in solving

the self-consistent equations in CPA require the use of a single band model. One has to further assume that the density of states curves (phononic or electronic) for constituents in their pure phases should have the same form and width and should only be displaced with respect to each other along the energy axis. This is far from reality because the density of states curves for the two constituents are usually devoid of any such similarity. The inability of CPA to take this effect into account limits its application to model systems only. Another complication with the realistic systems is that instead of a single non-degenerate band they have several sub-bands generated from the crystal field split atomic levels. Besides this the single site nature of the CPA and the inclusion of only diagonal disorder prove to be inadequate. The single site nature assumes that the environment of each site is identical whereas there are always good chances that the clusters of like atoms appear. The neglect of off-diagonal disorder is a highly simplifying assumption; in the case of electrons it means that the constituents have the same transfer integral and in the case of phonons it means that the constituents have the same force constants. In the succeeding two chapters we have attempted to extend CPA to account for these ingredients in two classes.

(a) Retaining the single-site nature of CPA, with the help of a technique using pseudopotentials we impute the

effect due to the different shapes and band widths of the constituent densities of states. This is equivalent to roughly take into account the effect of off-diagonal disorder. We also generalize this technique to account for the several sub-bands generated from the crystal field split atomic levels.

(b) Breaking the single-site nature of the CPA, we include the effects due to clusters. We explicitly calculate the effects due to pairs embedded into an effective medium and take into account both the diagonal and off-diagonal disorders. We test it for a simple cubic lattice.

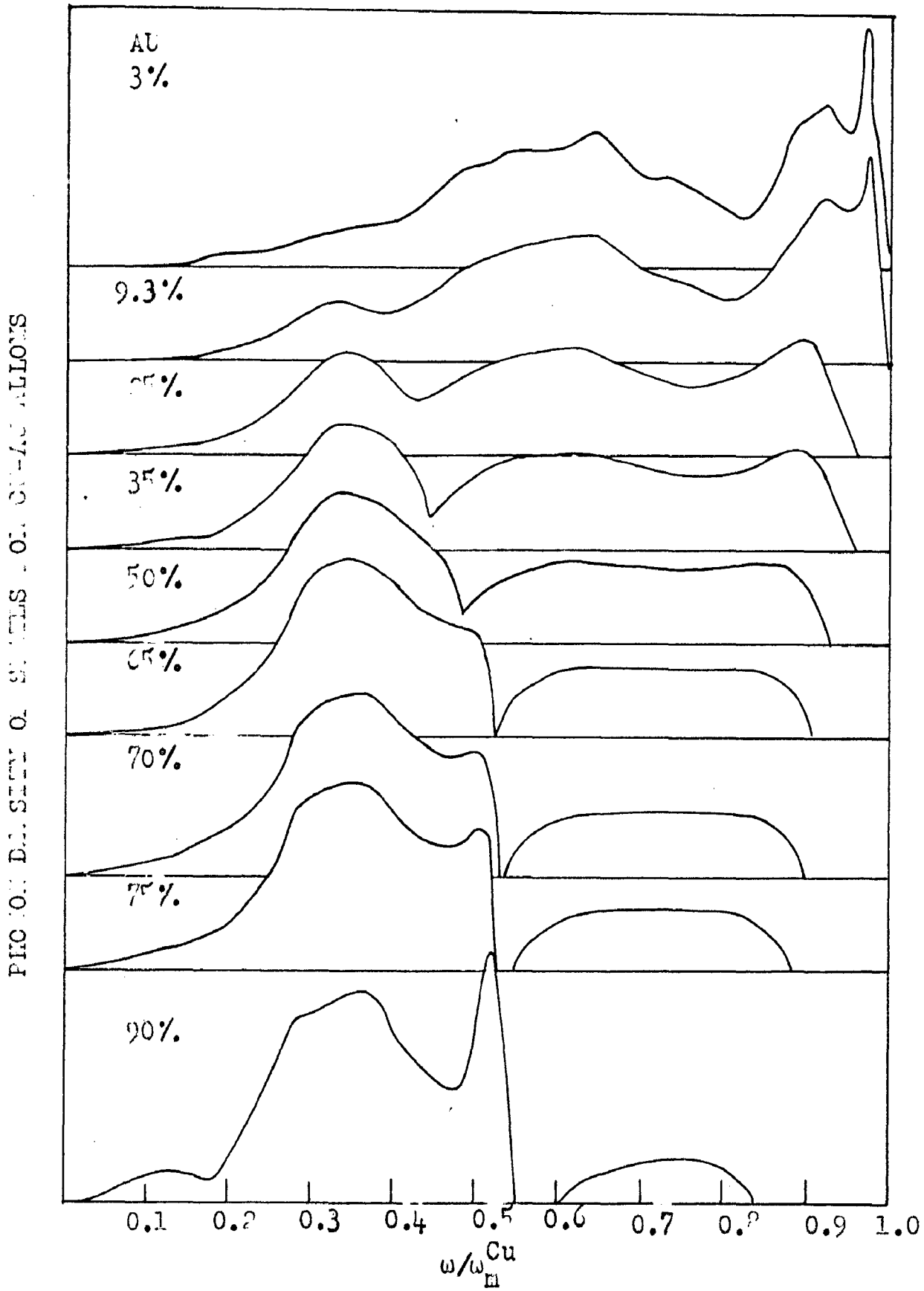

Fig.1. Plots of density of phonon states versus ω/ω_m^{Cu} for Cu-Au alloys obtained in CPA. The Au content increases from 3 at.% to 90 at.%.

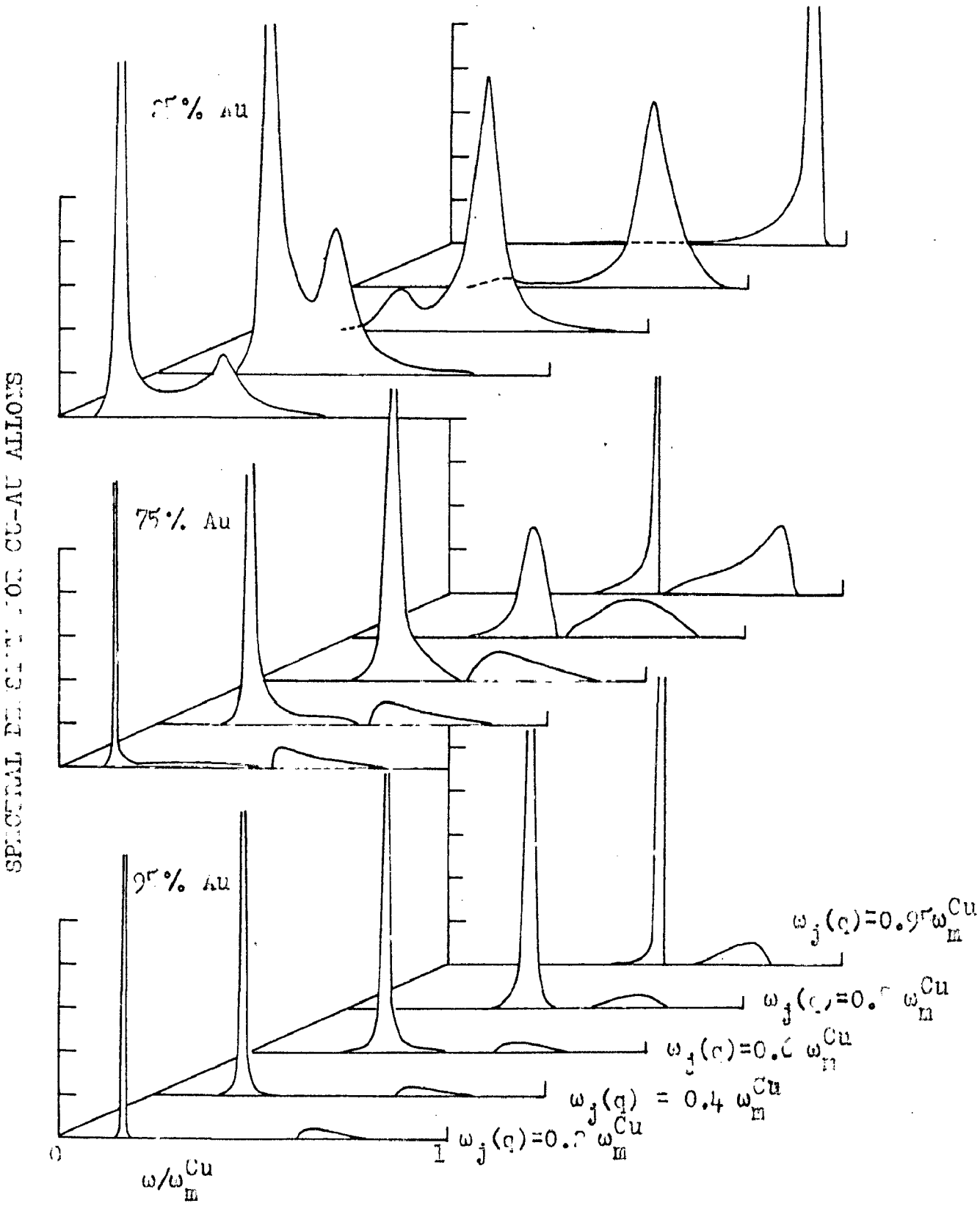

Fig. 3. Spectral density of phonon states versus ω/ω_m^{Cu} for Cu-Au alloys obtained in CPA. The Au contents are 25 at.%, 75 at.% and 95 at.%.

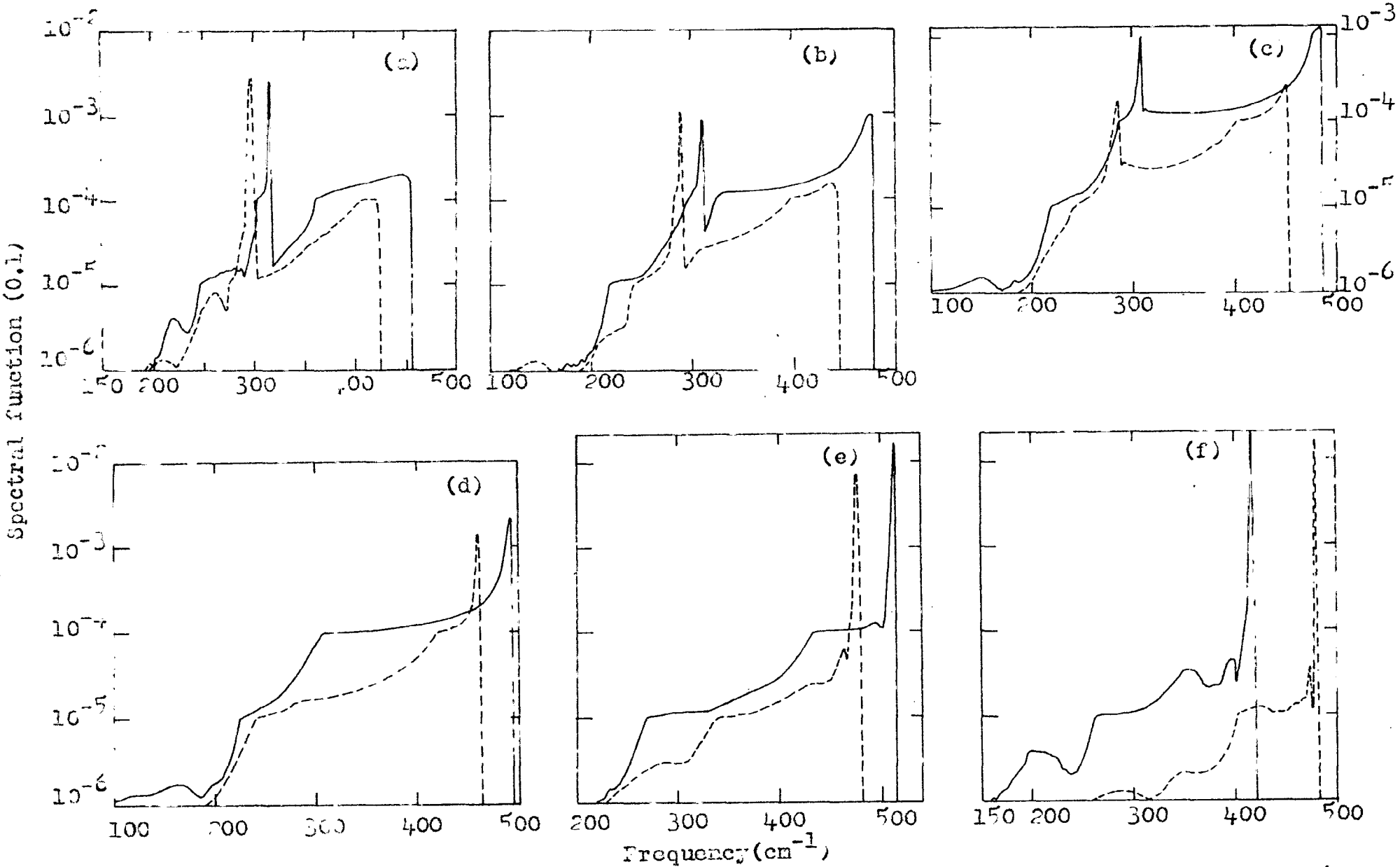

14.3. Spectral density function versus frequency for Si-Ge alloys with (a) 10 at.% Si, (b) [illegible] at.% Si, (c) 35 at.% Si, (d) 54 at.% Si, (e) [illegible] at.% Si and (f) [illegible] at.% Si (Solid line denotes Si as host and broken line denotes Ge as host).

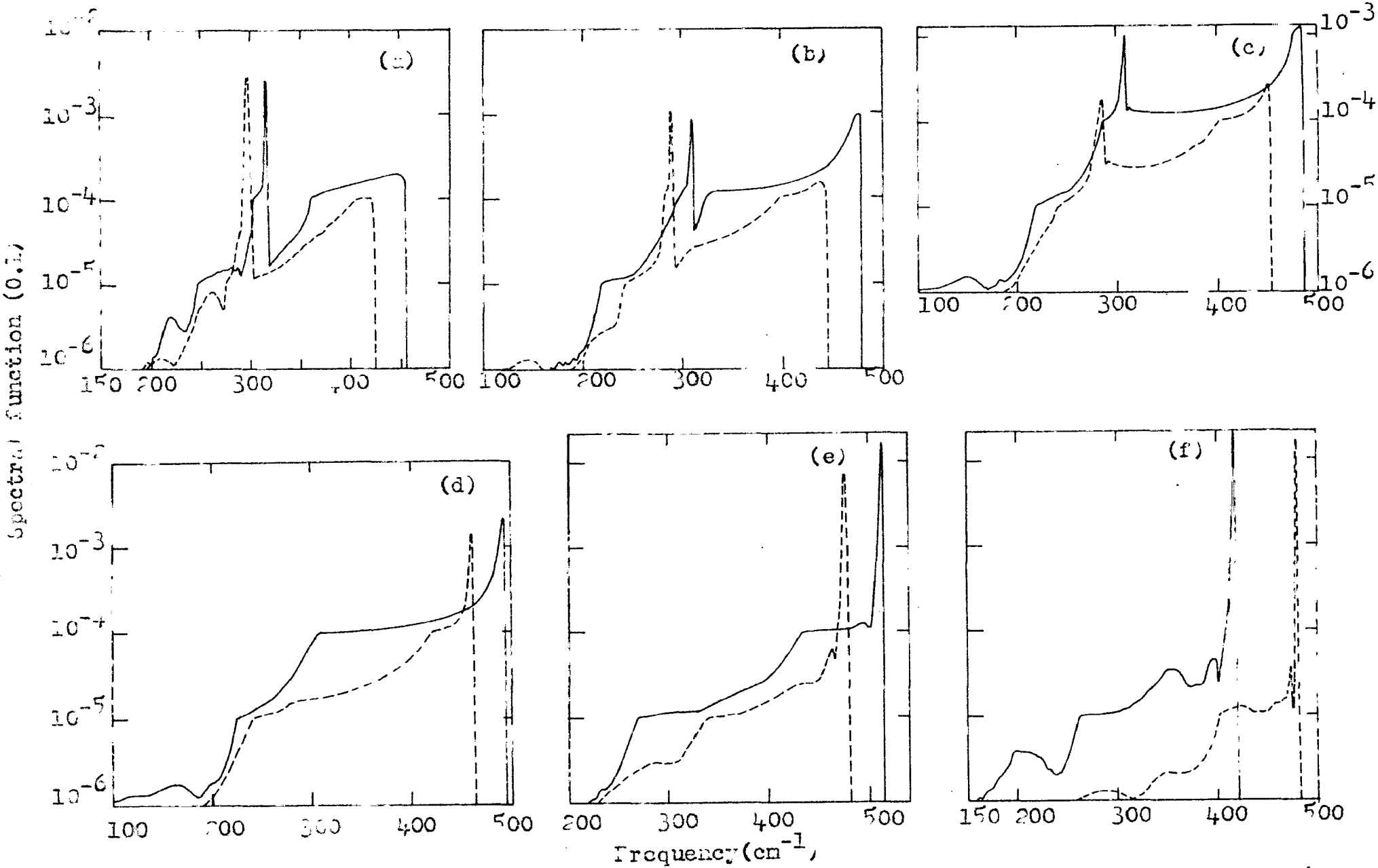

11.3. Spectral density function versus frequency for Si-Ge alloys with (a) 10 at.% Si, (b) 25 at.% Si, (c) 35 at.% Si, (d) 54 at.% Si, (e) 75 at.% Si and (f) 95 at.% Si

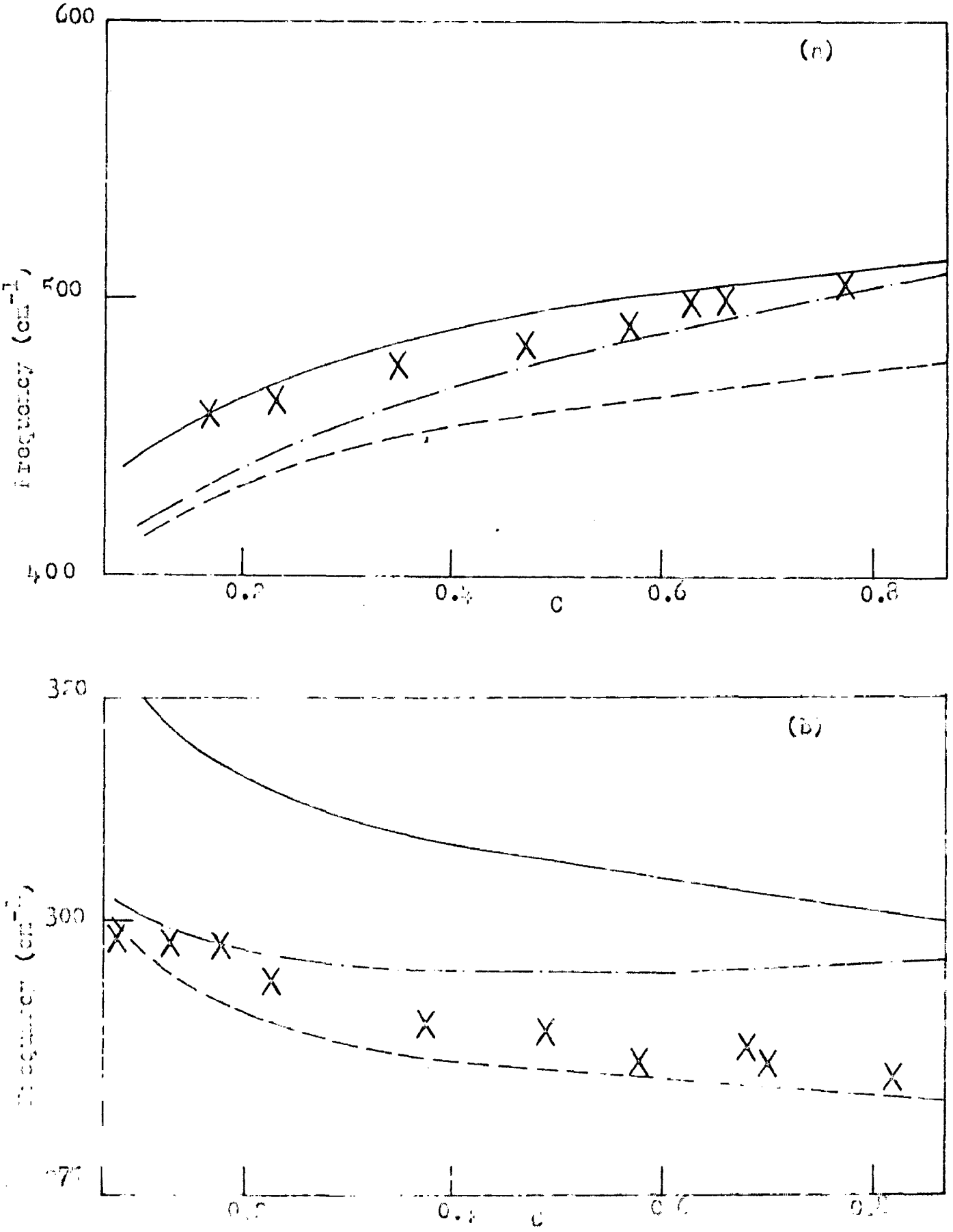
600
500
400
(a)
Frequency (cm⁻¹)
0.2
0.4
0.6
0.8
c
300
(b)

CHAPTER 3

Coherent Pseudopotential Approximation

In the concluding remarks of the preceding chapter we pointed out that for CPA calculations the constituents should have identical (in all respects) densities of states, merely shifted on energy scale. This is understandable for model systems only. Recently attempts have been made to improve upon these constraints. Following are the attempts within single-site approximation. Soven[29], Gyorffy[30] and Bansil et.al.[31] do it by using muffin-tin form for the alloy potential. Clark and Dawber[32] have attempted to improve upon the constraints using a simple pseudopotential scheme.

The basic idea behind our technique[33,34] of handling the problem is the following. In an AB alloy, starting from the electronic density of states, $\rho(E)$, of pure A constituent, one can arrive at the $\rho(E)$ for pure B constituent by putting an energy dependent pseudopotential, $V(E)$, on all the A sites. $V(E)$ can be determined from the knowledge of densities of states of both the constituents of the alloy, and thus acts as an energy dependent parameter completely determined from the one-to-one correspondence for the densities of states of the two constituents. This idea has been generalized for the case where there are many sub-bands, a situation which we always face in real systems. The density of states for each sub-band is allowed to have arbitrary shape.

We apply this generalized formulation to the Cu-Ni system. This system is a good example of a continuous solid

solution having f.c.c. lattice. The lattice constant changes by only 2.5% between pure Ni and pure Cu.[35] There is evidence for clustering of like atoms in a CuNi sample of roughly equal concentrations[36], but the clustering observed is slight and the clusters are small in size. The electronic band structures of the constituents, pure Ni[37] and pure Cu[38,39] are well known. Comparison of the essential features of the band structure of Ni and Cu reveals that the s-p bands are very similar in two and the two differ substantially in the location of d-bands with respect to the Fermi level. A lot of experimental information for this alloy system is available from the measurements of soft-x-ray spectra,[40-43] and photoemission spectra.[14,45] The electronic density of states of this alloy for a range of concentrations has also been previously calculated by Kirkpatrick et.al.[46] (hereafter referred as KVE) and Stocks et.al.[47] (hereafter referred as SWF), using the CPA. We can, therefore, compare our calculation with the existing ones and examine the effects of improvement of the model.

1. MODEL

1.1 Generalisation of CPA for Systems with Many Sub-Bands:

Within the single site approximation we have from eqn.(1.20) of Chapter 2, the CPA condition

$$\langle t_n \rangle = 0 \qquad \ldots (1.1)$$

We now take up the generalization of this condition for

a case where there are many subbands.

Single-Site, Single-Band Approximation:

If the system has F-fold orbital degeneracy(F = number of sub-bands), the single-site self-energy would become a FxF matrix, and FxF simultaneous equations would be required to find the elements of the matrix. It would simplify the matter a great deal if we assume F bands to be non-interacting. The perturbations with respect to the reference medium are assumed to be localized with respect to sites as well as sub-bands i.e.,

$$\text{Perturbation} = H_{eff} - \tilde{H} = \sum_{n} P_n = \sum_{nf} P_{nf}, \qquad \ldots (1.2)$$

where H_{eff} is the Hamiltonian of the averaged medium, $\tilde{H}$ is the Hamiltonian of a reference medium, P_n is the contribution of n^{th} site to the total perturbation, and P_{nf} is the contribution of the f^{th} band to P_n. This approximation yields,

$$t_n = \frac{P_n}{1-P_n\tilde{G}},$$

$$= \frac{\sum_f P_{nf}}{1-(\sum_f P_{nf})\tilde{G}},$$

$$= \sum_f t_{nf} \frac{1}{1-\frac{(\sum'_{f'} P_{nf'})\tilde{G}}{1-P_{nf}\tilde{G}}}, \qquad \ldots (1.3)$$

where, $t_{nf} = \frac{P_{nf}}{1-P_{nf}\tilde{G}}$, $\qquad \ldots (1.4)$

and $\sum_f'$ implies the sum over all the sub-bands excluding the f^{th} one. We can approximate t_n as a sum of t_{nf}'s

$$t_n \simeq \sum_f t_{nf} \quad , \qquad \ldots (1.5)$$

if $P_{nf} \ll 1$ for all f's. $\ldots (1.6)$

The approximation (1.6) is the same as introduced by KVE[46] in their eqn.(4.26) and was found to be reasonable for Ni-rich alloys. Later, it has been shown by SWF[47] that the limitations imposed by (1.6) are not severe for the whole range of composition in Cu-Ni system. Introduction of (1.5) into the well-known relation (1.19) of Chapter 2,

$$H_{eff} = \tilde{H} + \sum_n \left[\langle t_n \rangle \, (1+\tilde{G}\langle t_n \rangle)^{-1} \right], \qquad \ldots (1.7)$$

yields,

$$H_{eff} = \tilde{H} + \sum_n \left[\left(\sum_f \langle t_{nf} \rangle \right) \left\{ 1+\tilde{G}\left(\sum_f t_{nf} \right) \right\}^{-1} \right] \qquad \ldots (1.8)$$

1.2 Model Hamiltonian for Cu-Ni:

The Cu-Ni alloys have the nearly ideal substitutional nature. Mossbauer isomer shift data of Love et.al.[42] show that the nuclear contact density at the Ni nucleus does not depend on the concentration of Cu. This indicates that there is no charge transfer in Cu-Ni system. The s-p bands of pure Cu and Ni are identical and this band is assumed to remain unaffected on alloying Ni and Cu. One then has to examine the effects of alloying on the d-bands. In the Wannier representation, the d-d block of the model Hamiltonian takes the form,

$$H_{dd} = \sum_{n,f} |nf\rangle \varepsilon_{nf} \langle nf| + \sum_{\substack{n \neq n' \\ f,f'}} |nf\rangle t_{nf,n'f'} \langle n'f'|, \qquad \ldots (1.9)$$

where f represents the sub-band and n denotes the lattice sites. For an AB alloy ε_{nf} takes on values ε_{Af} or ε_{Bf} depending on the site n being occupied by A or B respectively. We simplify the problem by assuming $t_{nf,n'f'}$ to be translationally invariant and independent of the randomness of ε_{nf}. Calling the off-diagonal part to be W, we can choose the reference Hamiltonian in two ways:

$$\text{(a)} \quad H_{dd} = \sum_{n,f} |nf\rangle \sigma_f \langle nf| + W. \qquad \ldots (1.10a)$$

we assign a separate σ_f to each sub-band.

$$\text{(b)} \quad H_{dd} = \sum_{n,f} |nf\rangle \sigma \langle nf| + W. \qquad \ldots (1.10b)$$

Here a single σ is common for all sub-bands.

We discuss below the use of these two schemes to solve (1.8) to determine the self-energy non-self-consistently as well as self-consistently and we shall use coherent pseudopotential model.[32]

1.3 Coherent Pseudopotential Method

We consider an alloy $A_{1-c}B_c$, where c is the fractional concentration of B. In general pure A would have a band structure quite different from that of pure B. We can relate the band structure of pure B to the band

structure of pure A in an approximate manner by writing:

$$H^B = H^A + \sum_{\ell,f} V_f^{\ell}(E). \qquad \ldots (1.11)$$

H^B and H^A are the Hamiltonians of pure B and pure A respectively. We have introduced an energy dependent pseudopotential $V_f^{\ell}(E)$ to represent a B atom replacing an A atom on the site ℓ for the sub-band f. $V_f(E)$ is assumed to be diagonal in site in the basis of Wannier functions,

$$V_{f,nm}^{\ell}(E) = \delta_{n\ell}\delta_{m\ell}V_f(E). \qquad \ldots (1.12)$$

A reference system may now be introduced with Hamiltonian,

$$\tilde{H} = H^A + c\sum_{\ell,f} V_f^{\ell}(E). \qquad \ldots (1.13)$$

$\tilde{H}$ becomes H^A and H^B in the two limits (0 and 1) of c.

With the help of eqns.(1.10a), (1.10b), and (1.13), eqn.(1.8) is solved as follows.

Non-Self-Consistent Method:

We write

$$t_{nf} = |nf\rangle\, \tau_{nf}\langle nf| \text{ and } \tilde{G} = |nf\rangle \tilde{F}_{nf}\langle nf|. \qquad \ldots (1.14)$$

Then we can write eqn.(1.8) as,

$$H_{eff}(E) = W + \sum_n |nf\rangle\Big[\sigma_f + \sum_f \langle\tau_{nf}\rangle \left(1 + \tilde{F}_{nf}\sum_f \langle\tau_{nf}\rangle\right)^{-1}\Big]\langle nf| \qquad \ldots (1.15)$$

If we now transform to k-representation, we obtain for the self-energy of the effective medium:

$$\Sigma_f(k,E) = \Sigma_f(E) = \sigma_f + \frac{\sum_f \langle \tau_{nf} \rangle}{1 + \tilde{F}_{nf} \sum_f \langle \tau_{nf} \rangle} \quad \ldots (1.16)$$

For the reference medium the Green's function is given by[46],

$$\tilde{F}_{nf}(E) = \tilde{F}_f(E) = \int \frac{\rho_{Af}(\varepsilon)d\varepsilon}{E-\varepsilon-c\ V_f(E)} \quad \ldots (1.17)$$

In the alloy $A_{1-c}B_c$, for the sub-band f, the fluctuation with respect to the reference medium is $-c\ V_f(E)$ at sites occupied by A atoms (A sites) and is $(1-c)\ V_f(E)$ at B sites. τ_{nf}'s can therefore be calculated. An initial choice of σ_f and $\varepsilon_{Af} + c\ V_f(E)$, then enables one to solve (1.16), with τ_{Af} and τ_{Bf} given by,

$$\tau_{Af} = \frac{-c\ V_f(E)}{1 + c\ V_f(E)\ \tilde{F}_f}, \quad \ldots (1.18a)$$

and

$$\tau_{Bf} = \frac{(1-c)\ V_f(E)}{1-(1-c)\ V_f(E)\tilde{F}_f}. \quad \ldots (1.18b)$$

Having obtained $\Sigma_f(E)$, a new choice of the reference medium is made by replacing $cV_f(E)$ in eqn.(1.13) by $\Sigma_f(E) - \varepsilon_{Af}$ and as before we again calculate $\Sigma_f(E)$. This procedure is repeated till two values of $\Sigma_f(E)$ in consecutive cycles come close together within a tolerance.

Self-Consistent Method

With the help of equations (1.1),(1.5), (1.10a) and (1.10b), eqn.(1.16) may be solved self-consistently in two ways,

(I) $\langle t_{nf} \rangle = 0$, ... (1.19)

which follows when we write H_{dd} as in (1.10a).

(II) $\langle \sum_f t_{nf} \rangle = 0$, ... (1.20)

which corresponds to H_{dd} given by eqn.(1.10b).

The self-consistency condition (1.19) yields,

$$\sigma_f = \varepsilon_f - (\varepsilon_{Af} - \sigma_f)\tilde{F}_f(\varepsilon_{Bf} - \sigma_f), \quad \ldots (1.21)$$

where,

$$\langle \varepsilon_f \rangle = (1-c)\varepsilon_{Af} + c\varepsilon_{Bf}(E), \quad \ldots (1.22)$$

$$\varepsilon_{Bf}(E) = \varepsilon_{Af} + V_f(E), \quad \ldots (1.23)$$

and $$\tilde{F}_f = \int \frac{\rho_{Af}(\varepsilon)d\varepsilon}{E-\varepsilon-\sigma_f+\varepsilon_{Af}}, \quad \ldots (1.24)$$

ρ_{Af} is the density of states of the sub-band f of pure A system.

The self-consistency condition (1.20) yields,

$$\sum_f \left[(1-c)\frac{\varepsilon_{Af}-\sigma}{1-(\varepsilon_{Af}-\sigma)\tilde{F}_f} + c\frac{\varepsilon_{Bf}-\sigma}{1-(\varepsilon_{Bf}-\sigma)\tilde{F}_f}\right] = 0. \quad \ldots (1.25)$$

Here $\tilde{F}_f$ is given by,

$$\tilde{F}_f = \int \frac{\rho_{Af}(\varepsilon)d\varepsilon}{E-\varepsilon-\sigma+\varepsilon_{Af}}. \quad \ldots (1.26)$$

1.4 Calculation of Pseudopotential:

If a system has a Hamiltonian involving an energy

dependent potential, we follow Soven[48] to derive the expression for the densities of states. The out-going Green function, G in this case is given by $[E+iS-E_n'(E)]^{-1}$, where $E_n'(E)$ is the formal eigenvalue of the energy dependent Hamiltonian. The potentials are chosen to ensure $E_n'(E_n)=E_n$. Explicitly we want the quantity $\sum_n \delta(E-E_n)$ while we actually calculate $\sum_n \delta(E-E_n'(E))$. But since $E_n'(E_n)= E_n$, with the use of the identity.

$$\delta(f(E))\,|f'(E)|_{E=E_o} = \delta(E-E_o), \qquad \ldots (1.27)$$

where E_o is the zero of $f(E)$ (i.e. $f(E_o)=0$), we have,

$$\delta(E-E_n) = \delta(E-E_n'(E))\left(1-\frac{\partial E_n'}{\partial E}\right). \qquad \ldots (1.28)$$

The density of states is, therefore, given by,

$$\begin{aligned}\rho(E) &= \sum_n \delta(E-E_n) = -\frac{1}{\pi}\sum_n \mathrm{Im}\,[E+iS-E_n'(E)]^{-1}\left(1-\frac{\partial E_n'}{\partial E}\right)\\ &= -\pi^{-1}\mathrm{Im}\,\mathrm{Tr}G\left(1-\frac{\partial E_n'}{\partial E}\right). \qquad \ldots (1.29)\end{aligned}$$

Using similar arguments we establish a relation between the density of states for each sub-band of pure A and pure B crystals. We have a pure A crystal Hamiltonian, $H^A(\vec{r})$, and the Bloch eigenstates $\phi_{\vec{k}f}(\vec{r})$, satisfying the Schrödinger equation,

$$H^A(\vec{r})\phi_{\vec{k}f}(\vec{r}) = \varepsilon_{\vec{k}f}\phi_{\vec{k}f}(\vec{r}). \qquad \ldots (1.30)$$

The pseudopotential $V_f(E)$ is diagonal in Bloch representation. So the eigenstates of crystal B are the same Bloch

functions as those of crystal A but their energies are changed.

$$H^B(\vec{r})\phi_{\vec{k}f}(\vec{r}) = (H^A(\vec{r})+V_f(E))\phi_{\vec{k}f}(\vec{r})$$
$$= (\varepsilon_{\vec{k}f}+V_f(E))\phi_{\vec{k}f}(\vec{r})$$
$$= E_{\vec{k}f}\phi_{\vec{k}f}(\vec{r}). \quad \ldots (1.31)$$

The eigenvalues of pure B crystal, $E_{\vec{k}f}$ are thus related to the eigenvalues of crystal A by the relation,

$$E_{\vec{k}f} - V_f(E_{\vec{k}f}) = \varepsilon_{\vec{k}f}. \quad \ldots (1.32)$$

Now the pure A and pure B densities of states are defined as,

$$\rho_{Af}(E) = \sum_{\vec{k}} \delta(E-\varepsilon_{\vec{k}f}), \quad \ldots (1.33a)$$

$$\rho_{Bf}(E) = \sum_{\vec{k}} \delta(E-E_{\vec{k}f}). \quad \ldots (1.33b)$$

Making use of the identity (1.27), we can write,

$$\rho_{Bf}(E) = \sum_{\vec{k}} \delta(E-E_{\vec{k}f})$$
$$= \sum_{\vec{k}} \delta(E-\varepsilon_{\vec{k}f}-V_f(E))\left(1-\frac{\partial V_f(E)}{\partial E}\right), \quad \ldots (1.34)$$

where $E_{\vec{k}f}$'s are the zeros of the function $f(E) = E-\varepsilon_{\vec{k}f}-V_f(E)$. Using the definition (1.33a), we have from (1.34),

$$\rho_{Bf}(E) = \rho_{Af}(E-V_f(E))\left(1-\frac{\partial V_f(E)}{\partial E}\right). \quad \ldots (1.35)$$

Substituting $X = E-V_f(E)$ in (1.35) and integrating from

$-\infty$ to $+\infty$,

$$\int_{-\infty}^{\infty} \rho_{Bf}(E)dE = \int_{-\infty}^{\infty} \rho_{Af}(X)dX. \qquad \ldots (1.36)$$

If the bottoms of A and B bands are respectively at E_{Af} and E_{Bf},

$$V_f(o) = E_{Bf} - E_{Af}. \qquad \ldots (1.37)$$

Other values of $V_f(E)$ are then obtained as,

$$\int_{E_{Bf}}^{E} \rho_{Bf}(E)dE = \int_{E_{Af}}^{E-V_f(E)} \rho_{Af}(X)dX. \qquad \ldots (1.38)$$

$V_f(E)$ is thus completely determined from the knowledge of the electronic densities of states of the two constituents. For all the energy measurements we assume the energy zero at the bottom of the s-band, which we take as common for both A and B.

2.5 Total and Partial Densities of States:

We shall adopt two approaches to calculate the total densities of states.

(i) In the first approach (hereafter referred to as approach(i)) we calculate the contribution from each individual sub-band to the total density of states. For an averaged medium, eqn.(1.29) enables us to write the alloy density of states for the f^{th} sub-band as,

$$\rho_f(E) = -(\pi N)^{-1} \, \mathrm{Im}\mathrm{Tr} \left\langle G(E)\left(1 - \frac{\partial V_f(E)}{\partial E}\right)\right\rangle. \qquad \ldots (1.39)$$

Decoupling of the configurational average simplifies it,

$$\rho_f(E) = -(\pi N)^{-1} \mathrm{Im\ Tr} \langle G(E) \rangle \langle 1 - \frac{\partial V_f(E)}{\partial E} \rangle . \quad \ldots (1.40)$$

Our mean crystal consists of a potential $\varepsilon_A + cV_f(E)$ on every site, so that (1.40) may be written as,

$$\rho_f(E) = -(\pi N)^{-1} \mathrm{Im} \sum_n \langle nf | \langle G(E) \rangle | nf \rangle (1 - c \frac{\partial V_f(E)}{\partial E}) . \quad \ldots (1.41)$$

$\langle G(E) \rangle$ is approximated by $\tilde{G}$ introduced in Eq.(1.14). We can then write Eq.(1.41) as

$$\rho_f(E) = -(\pi N)^{-1} \mathrm{Im}\ \tilde{F}_f (1 - c \frac{\partial V_f(E)}{\partial E}) , \quad \ldots (1.42)$$

where N is the total number of states in the system. The validity of the decoupling employed above depends upon the magnitude of $|\partial V_f(E)/\partial E|$. It is valid if $|\partial V_f(E)/\partial E|$, is much smaller than 1.

(ii) In the second approach (hereafter referred as approach (ii)) we calculate the contributions of A and B to $\rho_f(E)$. For calculating the partial (component) densities of states we define $\mathcal{H}^A$ and $\mathcal{H}^B$ as the Hamiltonians of the systems in which in an otherwise averaged medium one site, say 0^{th}, is occupied by an A or a B atom. In our formalism the two are related by

$$\mathcal{H}^B = \mathcal{H}^A + V(E) .$$

If $\mathcal{H}_f^{A(B)}$ be the projections of $\mathcal{H}^{A(B)}$ on the f^{th} sub-band,

they would satisfy the relation,

$$\mathcal{H}_f^B = \mathcal{H}_f^A + V_f(E)$$

The partial densities of states are given by,

$$\rho_f^{(A)} = -\frac{m}{\pi}(1-c)\,\mathrm{Im}\langle 0|(E+iS-\mathcal{H}_f^A)^{-1}|0\rangle , \quad \ldots (1.43a)$$

$$\rho_f^{(B)} = -\frac{m}{\pi}\,c\,\mathrm{Im}\langle 0|(E+iS-\mathcal{H}_f^B)^{-1}|0\rangle \left(1-\frac{\partial V_f(E)}{\partial E}\right), \quad \ldots (1.43b)$$

where m indicates the m-fold degeneracy of the f^{th} sub-band. For Cu-Ni systems m is 3 for t_{2g} symmetry and 2 for e_g symmetry. These partial densities of states may be evaluated in two ways. In the first method as shown by VKE,[7] we write for A-component:

$$\rho_f^{(A)} = -\frac{m}{\pi}(1-c)\,\mathrm{Im}\,\frac{\tilde{F}_f}{1-(\varepsilon_f^A - \sigma_f)\tilde{F}_f}. \quad \ldots (1.44)$$

In the other method we borrow the following expression from KVE,[46]

$$\rho_f^{(A)} = -\frac{m}{\pi}(\varepsilon_f^A - \varepsilon_f^B)^{-1}\,\mathrm{Im}\left[(\sigma_f-\varepsilon_f^B)\tilde{F}_f\right]. \quad \ldots (1.45)$$

Both formulae may be used in any single site theory but they yield different results and only (1.45) satisfies the natural condition,

$$\rho_f = \rho_f^{(A)} + \rho_f^{(B)}. \quad \ldots (1.46)$$

With the help of eqn.(1.43b) and the analogy with eqns.(1.44) and (1.45), the corresponding formulae, for the partial density of states for the B-component according to these first and second methods are respectively

$$\rho_f^{(B)} = -\frac{m}{\pi}\,c\,\mathrm{Im}\left\{\frac{\tilde{F}_f}{1-(\varepsilon_f^B - \sigma_f)\tilde{F}_f}\right\}\left(1-\frac{\partial V_f(E)}{\partial E}\right), \quad \ldots (1.47)$$

and

$$\rho_f^{(B)} = -\frac{m}{\pi}(\varepsilon_f^A-\varepsilon_f^B)^{-1}\,\mathrm{Im}\left[(\sigma_f-\varepsilon_f^A)\tilde{F}_f\right]\left(1-\frac{\partial V_f(E)}{\partial E}\right). \quad \ldots (1.48)$$

When we use σ from eqns.(1.21) and (1.25) based on the two self-consistent methods, the formulae written above for the two methods become identical. So either of the two may be used in the present calculations.

After having calculated ρ_f's either through (1.42) or through (1.45), (1.48) and (1.46), it is important to examine which of the two procedures is more rigorous for calculating the total density of states,

$$\rho = \sum_f \rho_f \quad \ldots (1.49)$$

Calculations through (1.42) involve a decoupling in averaging, whereas, the calculations through the approach (ii) [eqns.(1.45), (1.48) and (1.46)] do not involve any such approximation. Obviously the approach (ii) should be preferred. Denoting $\rho_f^{(A)}$'s, calculated from the approach (i) and approach (ii) by, $\rho_f^{(A)}(i)$ and $\rho_f^{(A)}(ii)$, we find the difference in their magnitudes as,

$$\rho_f^{(A)}(ii) - \rho_f^{(A)}(i) = -\frac{m}{\pi}c\,\frac{\partial V_f(E)}{\partial E}\left[(1-c)\left\{\mathrm{Im}\,\frac{\tilde{F}_f}{1-(\varepsilon_f^A-\sigma_f)\tilde{F}_f} + \mathrm{Im}\,\frac{\tilde{F}_f}{1-(\varepsilon_f^B-\sigma_f)\tilde{F}_f}\right\}\right]. \quad \ldots (1.50)$$

For CPA this difference is zero. CPA does not distinguish between the two approaches as it does not deal with an energy dependent part and we do not have to introduce the

decoupling approximation of the type used in eqn.(1.42).

2. COMPUTATION AND DISCUSSION OF RESULTS

We studied the density of states for CuNi alloys using the model Hamiltonian for the d-d block derived in Section 1.2 . This model for the d-bands incorporates the effects of hybridization and takes into account the orbital degeneracy. For this system in Eq.(1.9) f describes the d-orbital symmetry which is t_{2g} for f = 1,2,3 and e_g for f = 4,5. The inputs for the calculations are based on the data provided by the calculations of SWF.[47]. The components of Cu and Ni densities of states have been illustrated in Figs.5(a) and 5(b). As mentioned before we assume that the s-p band remains unaffected by alloying, and we dwell here on the total and component densities of states for the d-band only, of the alloy. The input parameters for Cu and Ni have been tabulated in Table 1. The e_g and t_{2g} sub-bands have common atomic potentials for both Cu and Ni.

The pseudopotentials belonging to each sub-band are calculated from eqn.(1.36). The mesh for Cu-densities of states consists of 77 points spread at a regular interval of 0.0061 Ryd. and for Ni it consists of 103 points spread at an interval of 0.0050 Ryd. The pseudopotentials for the t_{2g} and e_g sub-bands have been shown in Fig.6 by broken and full lines respectively. In order to evaluate the derivatives of $V_f(E)$, we use their values

available to us at points at intervals of E equal to 0.0061 Ryd. For calculating the derivative at a certain energy point E, a second order polynomial is fitted at three points: the point E under consideration and its two nearest neighbours. In order to make sure that we have a fairly reasonable value of the derivative by this method, we calculated the derivative at a few points by using points successively upto nearest, upto next nearest and upto next-next nearest neighbourhood and found that the values of the derivative differ only at the third place of decimal.

Having obtained $V_f(E)$ for t_{2g} and e_g bands, the self-consistent equations (1.21) and (1.25) are solved with the help of eqns.(1.22), (1.23), (1.24) and (1.26). The difference in the value of ε_{Ni} for the two sub-bands is sufficiently small[47], so that we take it to be the same for both t_{2g} and e_g bands and obtain two sets of ε_{Cu}'s with the help of eqn.(1.23). For calculating $\tilde{F}_f$'s from (1.24) and (1.26) we use $\rho_{Nif}(\varepsilon)$'s for Ni rich alloys and $\rho_{Cuf}(\varepsilon)$'s for Cu rich alloys. In order to take proper account of the degeneracy of t_{2g} and e_g bands we normalize the corresponding electronic densities of states to 3 and 2 respectively. The areas enclosed by the t_{2g} and e_g densities of states curves of Cu and Ni are given in the table 1. In Sec.1.3 we had discussed the two self-consistent methods to evaluate the self-energies. In one we obtain σ_f's from (1.21) and in the

other eqn.(1.25) is used to calculate σ. The self-consistent equations (1.21) and (1.25) have been solved iteratively using Newton-Raphson's method (for complex variables here). The integrals (1.24) and (1.26) are evaluated by Simpson's rule. The iterations are seen to converge quite rapidly. These self-energies are then used to calculate the t_{2g} and e_g components of the density of states from (1.42) and also the partial densities of states for the sub-bands using (1.45) and (1.48). Then use is made of (1.46) and (1.49) for calculating the total d-band densities of states. Figures 7-12 show the results of our calculations of the total and partial densities of states for d-bands, $\rho(E)$, $\rho^{(Cu)}(E)$ and $\rho^{(Ni)}(E)$, through the two self-consistent methods discussed above for the alloy systems possessing the following atomic percentages of Ni : 13% Ni, 23% Ni, 38% Ni, 61% Ni, 81% Ni and 89% Ni. The $\rho(E)$'s displayed in these figures were calculated from the partial densities of states [i.e. the approach (ii)] and not from (1.42). We have compared the density of states curves calculated by us with CPA calculations of SWF[47] and the experimental results of Seib and Spicer[44,45]. In all the figures $\rho(E)$ is given by the the full line, $\rho^{(Cu)}(E)$ by the dashed line and $\rho^{(Ni)}(E)$ by the dotted line. The CPA results of KVE and SWF follow as a special case of our formalism in which all the $V_f(E)$'s reduce to a constant value, the δ-parameter ($\delta=\varepsilon_A-\varepsilon_B$). We did verify this by replacing $V_f(E)$'s by 0.1340 Ryd. and

then calculating the density of states for 13% Ni composition. The results based on the two self-consistent methods are shown in Fig.13. The results from the first method (Eqn.(1.19)) are almost the same as thoseof SWF. The second method, which uses the same σ for both the sub-bands t_{2g} and e_g shows slight differences in the structure of the curve and the peak positions are shifted to the lower energies by a small amount (about 0.0095 Ryd.).

Comparison of our results for densities of states and those of SWF reveals that the shapes of $\rho(E)$ curves from these two calculations, are different specially for the majority bands of Cu-rich alloys.Our calculations show lot of structure whereas the density of states curves calculated by SWF are comparatively smooth. But the densities of states curves calculated here for Ni-rich alloys, 81 at.% Ni and 89 at. % Ni are almost similar to those from calculations of SWF, only that the structures are a bit more pronounced in $\rho(E)$ calculated by us. This may be understood from the conclusions reached by SWF in their analysis that Cu-rich alloys are very sensitive to change in δ, as $\delta\left[=\varepsilon_{Ni}-\varepsilon_{Cu}\right]$ increases from 0.0, and this is not the case for Ni-rich alloys. The Stater-Koster[49] criterion for the formation of an impurity level leads us to see that the values of δ required to split off an impurity level from the bottom of the Ni d-band and the corresponding value to split off an impurity level from the top of the Cu d-band are 0.42 Ryd. and 0.07 Ryd respectively. Our energy dependent V(E)

(corresponding to δ) assumes the values in the range of 0.02 Ryd.—0.14 Ryd. One could, therefore, expect the structures shown for Cu-rich alloys and their sensitivity to V(E).

Both the self-consistent methods lead to quite the same structures in densities of states. In the second method (Eq.(1.25)) the structures are not as sharp as in the first one (eqn.(1.21)). This relative rounding off of the structures in the second method becomes less noticeable with increasing Ni-concentration. The peak positions in the two methods are nearly the same. The second method based on a common self-energy for both the sub-bands is simpler to implement compared to the first method where we assign a separate self-energy to each sub-band. The likeness of the curves in the two methods is interesting in the light of the fact that computer time required for calculating ρ(E) for the second method is almost half of that required for the first.

An important difference between SWF and our calculations for 13 at.% Ni and 23 at .% Ni alloys (Figs.7 and 8 respectively) is that in SWF calculations the three main peaks of the host band (marked 2,3 and 4 on the graphs) follow descending order for their heights, whereas our calculations show just the reverse for both the Ni concentrations. Also the height of the 4th peak in the host band is almost double in our case as compared to the SWF calculations. The impurity band in our case is

slightly broader than in SWF calculations. In our calculations with the second method (eqn.(1.25)) some structures show up in the impurity band and these are absent when we use the first method (eqn.(1.21)). These structures appear near the top edge of the impurity band and may be suggestive of the trend to build up the top peak in the pure Ni density of states.

These features regarding the differences in structures in densities of states calculated by us and SWF, may be qualitatively understood with the help of the imaginary part of self-energy. For 13 at.% Ni alloy, the imaginary part of self-energy has been plotted in Fig.14. Figure 14(a) shows it for the present coherent pseudo-potential approximation and Fig.14(b) shows it for the CPA. The solid line curves belong to the first method with dotted line curves and dash and dot line curves showing respectively the e_g and t_{2g} band contributions to the total self-energy. The broken line curves belong to the second method (an average self-energy for each sub-band). The $\mathrm{Im}\sigma$ is proportional to the life time of the electronic states in disordered systems. Comparison of Figs.14(a) and 14(b) show that in the region where $\mathrm{Im}\sigma$ is significantly large, it is larger in CPA than in our case by almost a factor of 2. This implies that compared to our calculation, CPA should show more of the rounding off of critical point singularities in the density of states. The two methods, eqns.(1.21) and (1.25), show little difference in $\mathrm{Im}\sigma$ for

CPA in the region where impurity band occurs. This feature also showed up as additional structures in the impurity band obtained through eqn.(1.25) as compared to that obtained through eqn.(1.21).

Our calculation takes into account the forms and the widths of the densities of states of both the constituents based on band-structure calculations. The input densities of states used here are shown in Figs.5(a) and 5(b) instead of densities of states in Fig.5(c) which were inputs of SWF calculation. Almost complete independence of the location of high energy edge in the majority band on Ni concentration in Cu rich alloys is conspicuous both in our case as well as SWF calculations and also in experiments. The gradual erosion of the high energy peak in the Cu band as Ni is added is seen in SWF and also in our calculations with the difference that for 13 at. % Ni alloy this peak is very prominent in our case whereas in SWF calculations it is not so prominent.

For comparison the optical density of states (ODS) plots calculated from the electron distribution curves (EDC) of Seib and Spicer[44,45] using a non-direct transition model, have been given for 13 at. % Ni and 23 at. % Ni alloys. For the rest of alloys EDC's[44,45] have been reported. The EDC for 38 at. % Ni alloy is for an incident photon energy of 10.2 eV and the rest are for an incident photon energy of 10.0 eV. The peak positions of the prominent peaks deduced from the experimental, SWF and our

calculated curves have been displayed in table 2. The peaks have been numbered as 1,2,3,4 and 5, and this identification is shown in figures. This assignment is arbitrary and has been made to locate only those structures in calculated density of states which appear to correspond to the structures in the experimental curves. The disagreements among the calculated and measured curves should be taken in the light of the fact that the interpretation of photomission measurements is not very clear. In particular the relationship of EDC's with density of states is quite ambiguous. In general the agreement of the peak positions from our calculations with the experiment is good except for a few peaks. Of all the alloy compositions, the SWF calculation for $\rho(E)$ for the alloy 61 at .% Ni (Fig.10) shows worst correlation with the structures in the experimental EDC. On the other hand the three main peaks in EDC for this alloy are in good agreement with those obtained in our calculations. This is expected because SWF and KVE calculations incorporate as input only Cu density of states for Cu rich alloys and Ni density of states for Ni rich alloys, so that the calculations tend to become inaccurate as the two constituents appear in comparable compositions. In our case the use of the energy dependent pseudopotential enables us to incorporate the change in density of states as we go from pure A to pure B(through Eqn.(1.38)), our calculation should be much better than SWF or KVE calculation for alloys

having 50 at.%Ni. As stated earlier we automatically go from pure Cu to pure Ni density of states in our calculation when we change Ni concentration in the alloy from 0 to 100 at. % . This has not been done in an ad hoc basis as in earlier CPA calculations.

Figure 15 shows the total density of states and its t_{2g} and e_g components for 77 at. % Cu, 23 at. % Ni alloy calculated through the approach (i) mentioned in Sec. 2.5. Comparison of Fig.15 with Fig.6 shows a major difference in the impurity band. In Sec.1.5 it has been proved that the method involved in the Fig.15 is less accurate than that involved in Fig.6 and this is revealed in the calculations plotted in Fig.15. There the height of the impurity band appears to be underestimated by a factor of about 2, though the width remains the same. Figure 16 compares the t_{2g} component of total density of states for 23 at..% Ni alloy as calculated through approaches (i) and (ii) within the schemes represented by eqns.(1.21) and (1.25).

Recently, House et.al.[50] have completed a CPA calculation for a cluster of muffin tin wells by applying the methods of scattering theory. With a 13-atom cluster they calculate the densities of states for pure Cu; 10 at. % Ni, 90 at. % Cu and 10 at.% Zn, 90 at.% Cu alloys. Their density of states for Cu is shifted downwards on the energy scale by about 0.05 Ryd. as compared to the density

of states calculated by Stocks et.al.,[47] shown in Fig.5. Consequently their alloy density of states is also shifted downwards on the energy scale by about the same amount as compared to the density of states functions for 13 at.% Ni alloy reported in this work . For comparison their 10 at.% Ni alloy calculations have been shown with our 13 at.% Ni alloy calculations in Fig.17. Their plot has been pulled to the higher energy so that the major peak in the main band falls around 0.5 Ryd. The agreement is good and a significant feature is that the high energy peak (~ 0.5 Ryd.) in Cu is enhanced in magnitude by about 25% when 10 at.% Ni is added. Our calculations also exhibit this feature, whereas CPA shows a damping of the same peak by an amount of 25 % . The ratio of the intensities of the impurity peak and the high energy peak of the main band is 1/8 in cluster calculations as compared to 1/5 in our calculations.

Above discussion suggests that the method requires a precise calculation of V(E)'s done with a reliable integration scheme and that too using extrapolation of densities of states at a narrow grid of energy. The Simpson's rule (for integration) used by us with the grids of 0.0061 Ryd. and 0.0050 Ryd. for Cu and Ni respectively may not be very reliable in the regions where steep rise and fall are occurring in the densities of states. In the light of this weakness of our calculations, the good agreement with experiments indicated in table 2 indicates

that the method is promising.

To sum-up the Chapter we indicate that within the coherent pseudopotential scheme we can have three self-consistency requirements in order of austerity. In a F-band formulation, a single-site, single-band approximation yields,

(i) $\langle t_{nf} \rangle = 0$ (each sub-band has a separate self-energy)

(ii) $\langle \sum_f t_{nf} \rangle = 0$ (all subbands have a common self-energy)

And in a single-band formulation, a single-site approximation requires,

(iii) $\langle t_n \rangle = 0$ (this is within pseudopotential scheme, hence different from CPA).

In addition to the calculations using (i) and (ii), we also performed calculations using (iii)[51] and found that if one is interested in the essential features of the density of states, it is not necessary to complicate the calculation by incorporating subbands. The experimentally found density of states (photo-emission) available for comparison with calculations, possess extremely rounded-off structures and depict only roughly the peak positions. As long as this requirement goes, (iii) yields as good results as those obtained from (i) and (ii). This finding is important in the light of the fact that the computer time required for (ii) is almost half of that required for (i) and for (iii) it is again almost half of that required for (ii). For comparison we have plotted in fig.18 the pseudopotentials

for e_g and t_{2g} subbands and within the single band theory. The densities of states for 62 at.% Cu, 38 at.% Ni alloy obtained through method (iii) are shown in fig.19(a), along with the same obtained through (i) and (ii) as shown in fig.19(b). The main features are retained in all the methods with negligible changes in peak positions.

CPA follows as a special case of our method [replacing V(E)'s by -0.134 Ry.(= $\varepsilon^{Cu}-\varepsilon^{Ni}$)]. With this replacement in CPA also we have three self-consistent methods parallel to (i), (ii) and (iii). The densities of states in CPA for 87 at.% Cu, 13 at.% Ni are shown in fig.20. [(a) gives those obtained through (i) and (ii)]. This leads to the same conclusion as made in the preceding paragraph. However, the comparison of our method with CPA shows that the effects of the difference in the shapes of the densities of states of the constituents are more important.

TABLE 1 Parameters relevant for calculations

Parameters	Copper	Nickle
ε	0.4418 Ryd.	0.5760 Ryd.
E_F	0.6740 Ryd.	0.6800 Ryd.
AREA(e_g)	1.97 States/atom.	1.72 States/atom
AREA (t_{2g})	2.91 States/atom	2.65 States/atom

TABLE 2. Positions of the prominent peaks in the densities for six alloy systems. Comparison has been made for results based on calculations with eqns. (1.21) and (1.25) (indicated as methods I and II respectivel), CPA and the photo-emission experiments of Seib and Spicer.[44,45]

Composition	Method	Peak Positions (Rydbergs)				
		1st	2nd	3rd	4th	5th
87 at.% Cu, 13 at.% Ni,	I	0.4000	0.4427	0.4732	0.4976	0.6074
	II	0.3939	0.4427	0.4732	0.4976	0.6074
	CPA	0.3923	0.4533	0.4771	0.5229	0.6045
	EXPT.	0.36	0.43	0.49	0.51	0.61
77 at.% Cu, 23 at.%	I	0.4122	0.4424	0.4610	0.4915	0.6071
	II	0.4183	0.4485	0.4671	0.4976	0.6071
	CPA	0.3995	-	0.4624	0.4941	0.6241
	EXPT	0.38	-	0.44	0.50	0.62
62 at.% Cu, 38 at.% Ni	I	0.4183	-	0.4671	0.4970	0.6196
	II	0.4183	-	0.4671	0.4909	0.6257
	CPA	0.4076,	-	0.4757	-	0.6400
	EXPT.	0.43	-	0.49	-	0.62
39 at.% Cu, 61 at.% Ni	I	0.4000	-	0.4671	-	0.6623
	II	0.4000	-	0.4610	-	0.6684
	CPA	0.3694	-	0.5523	-	0.6489
	EXPT.	0.37	-	0.52	-	0.66
19 at.% Cu, 81 at.% Ni	I	0.4183	0.5525	-	0.6074	0.6562
	II	0.4183	0.5586	-	0.6134	0.6623
	CPA	0.3923	0.5617	-	0.6136	0.6648
	EXPT.	-	0.52	-	-	0.66
11 at.% Cu, 89 at.% Ni	I	0.4122	0.5403	-	0.6196	0.6745
	II	0.4183	0.5464	-	0.6074	0.6684
	CPA	0.3910	0.5502	-	0.6045	0.6631
	EXPT	0.39	0.51	-	-	0.67

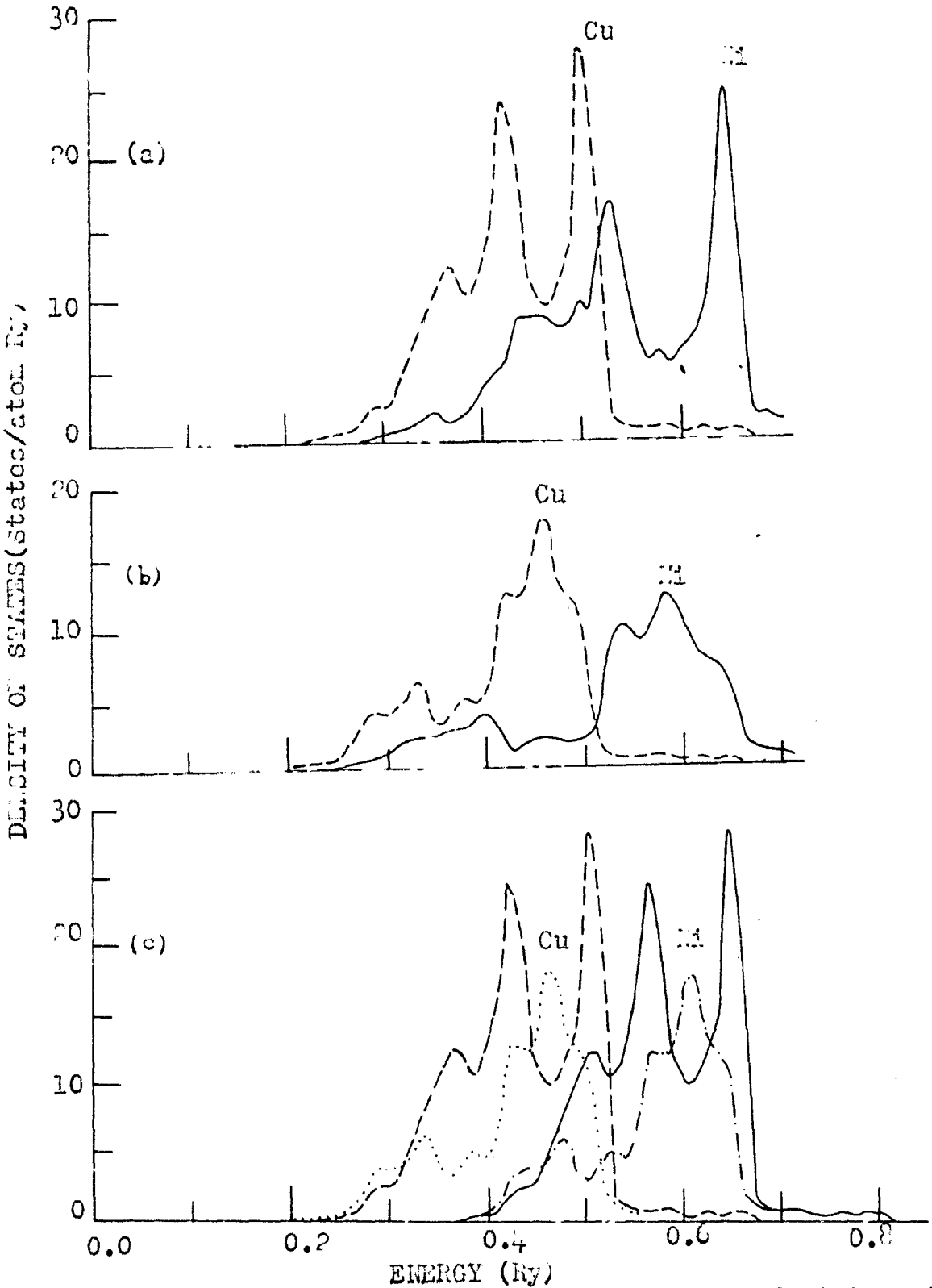

Fig.5(a) The t_{2g} component of the unperturbed densities of states of Cu(------) and Ni(————). (b) The e_g component of the unperturbed densities of states of Cu(-----) and Ni(———). (c) The model used in CPA calculations. Cu and Ni have identical forms, merely shifted by δ on energy scale. (·····) and (-----) are e_g and t_{2g} components of Cu density of states respectively; and (-·-·-·) and (-——) denote the same for Ni.

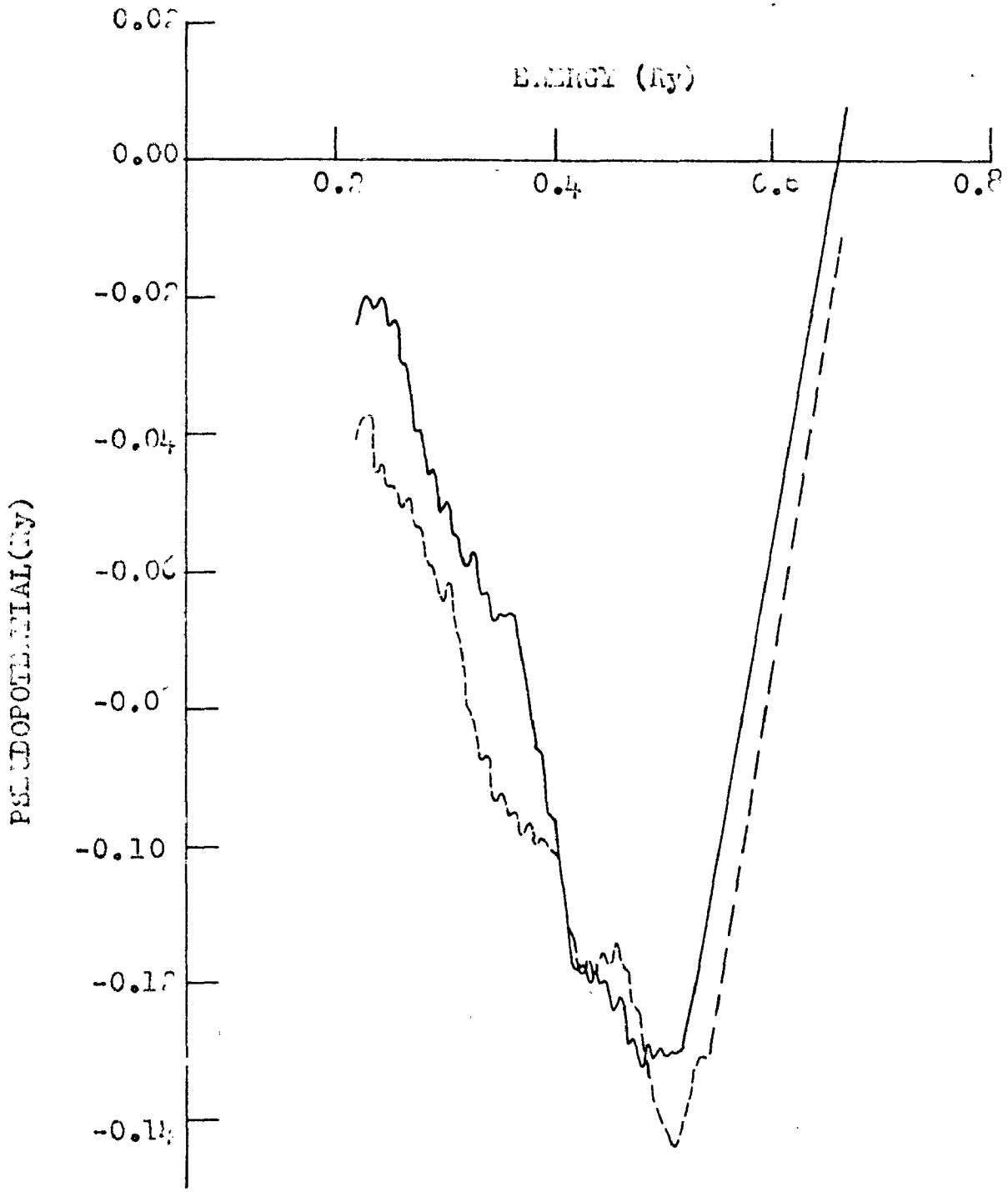

Fig.6. Plots of the pseudopotentials versus energy:
(-----) belongs to the t_{2g} symmetry, $V_{t_{2g}}(r)$; and
(———) belongs to the e_g symmetry, $V_{e_g}(r)$.

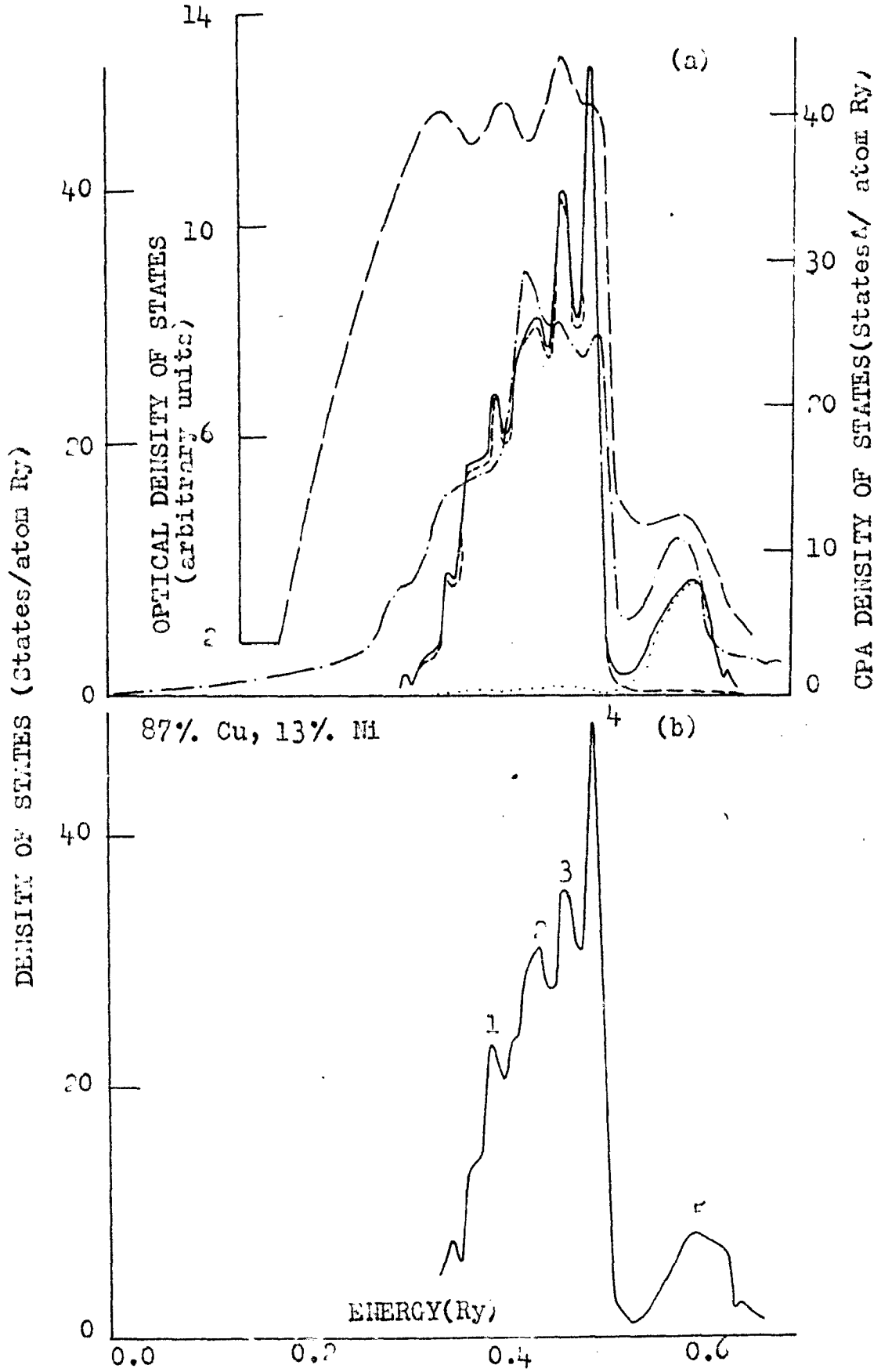

Fig.7. Densities of states for a 87 at.% Cu,13 at.% Ni alloy. (———) denotes $\rho(E)$, (----) denotes $\rho^{Cu}(E)$, and (·····) denotes $\rho^{Ni}(E)$. (—— ——)denotes the experimental ODS (Ref. ++,+), and (—·—·—) the CPA calculation (47). (a) gives the calculations done using the self-consistent equation (1.21) and (b) gives the same using the eqn.(1.[illegible]). The zero of the energy scale is the bottom of the s-band.

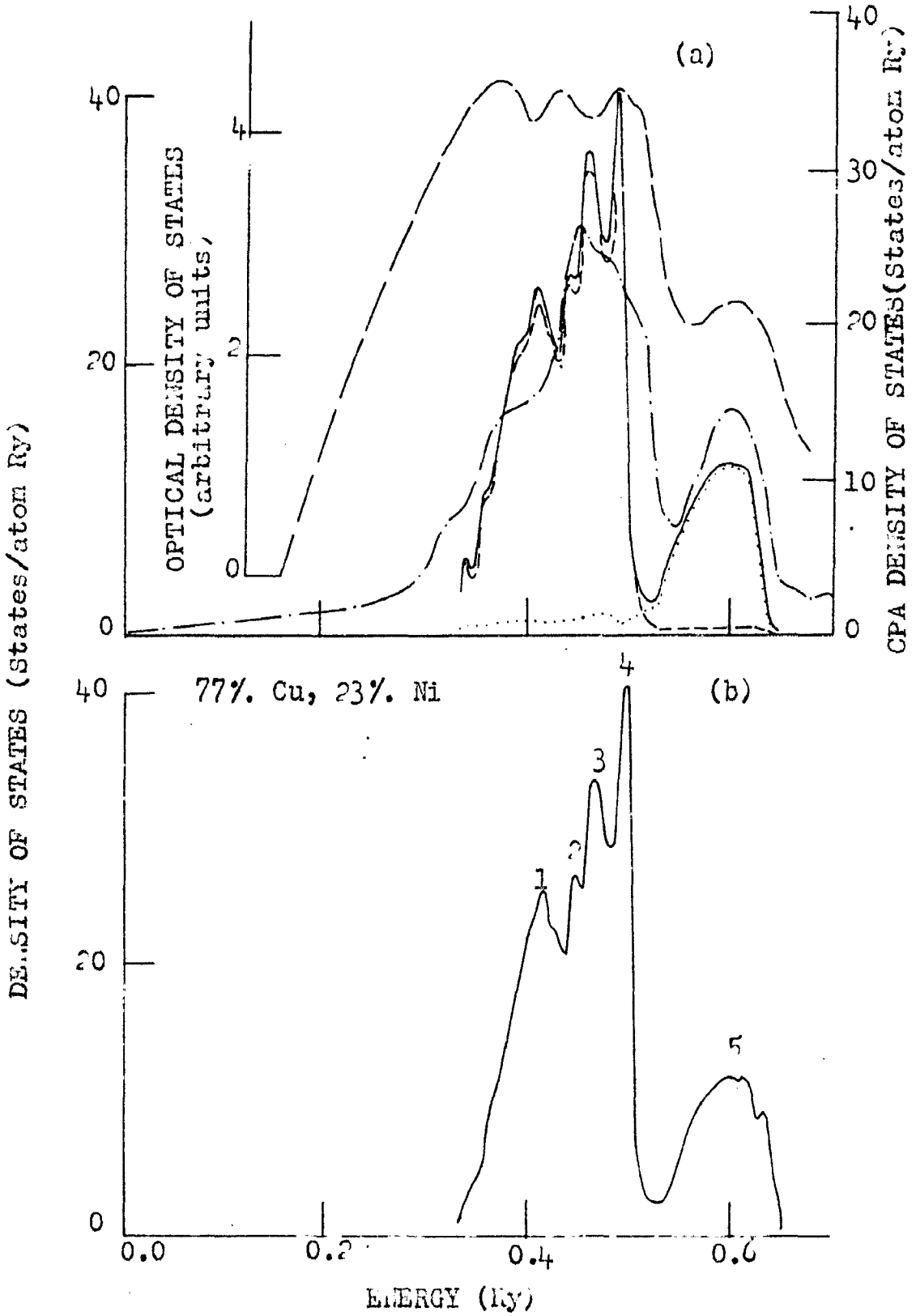

Fig.8. Densities of states for a 77 at.% Cu, 23 at.% Ni alloy. The notation is as in Fig.7.

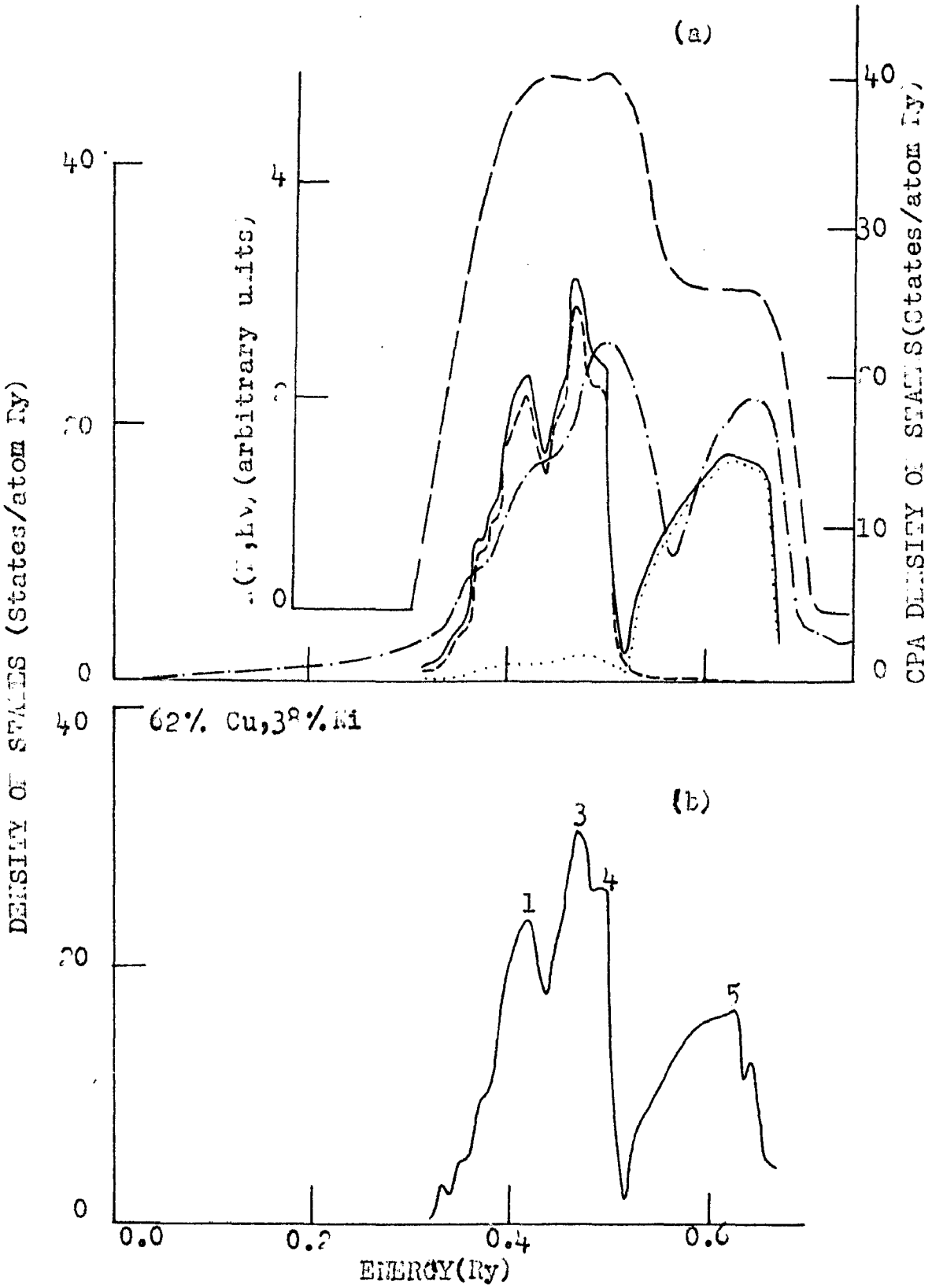

Fig.9. Densities of states for a 62 at.% Cu , 38 at.% Ni alloy. For theoretical curves the notation is as in Fig.7. The experimental curve is the electron distribution curve taken from the photoemission work of Spicer and Spicer. The CDC is for an incident photon energy of 10.2 eV.

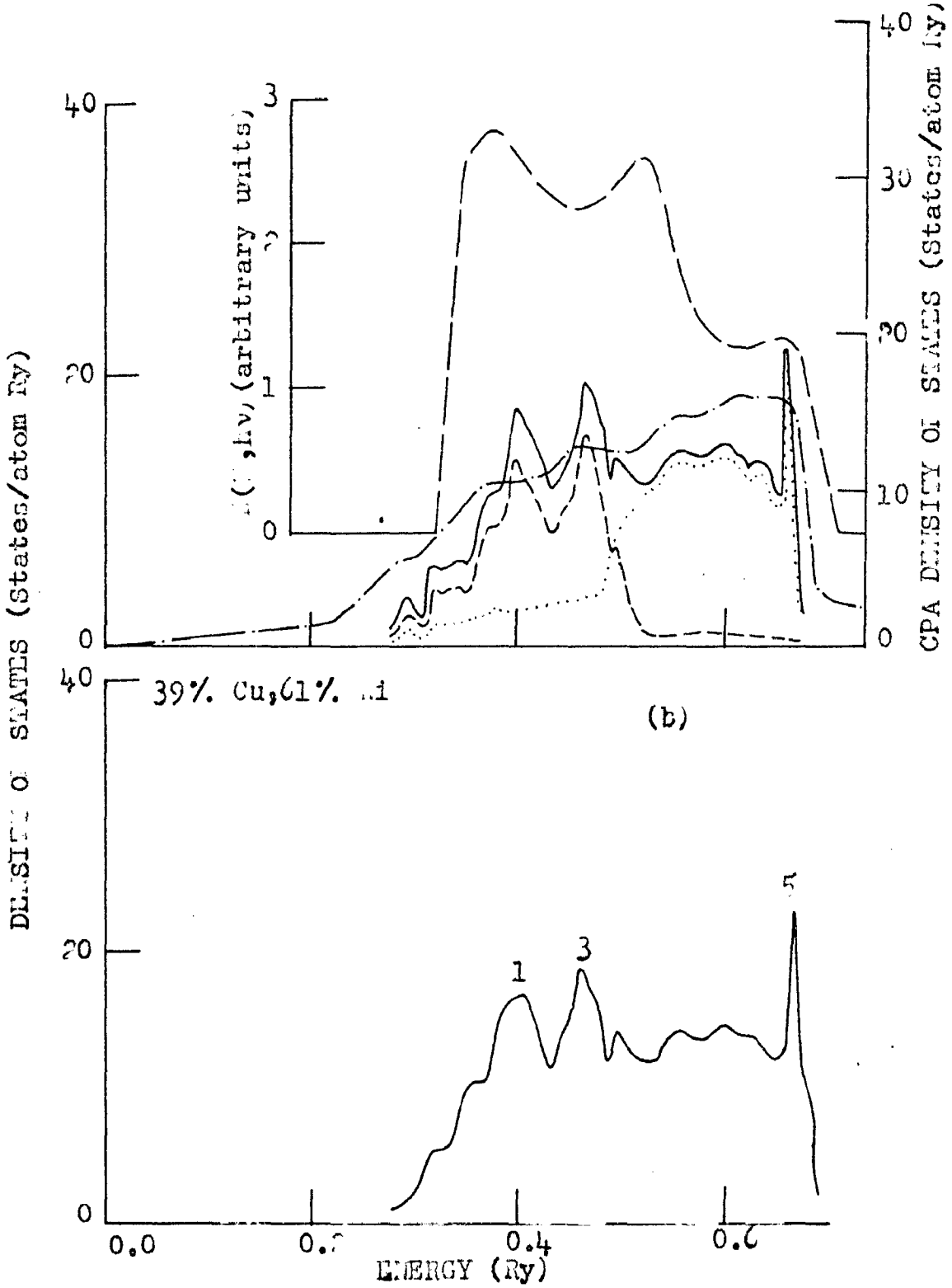

Fig.10. Densities of states for a 39 at.% Cu, 61 at.% Ni alloy. The notation is as in Fig.9. The EDC is for an incident photon energy of 10.0 eV.

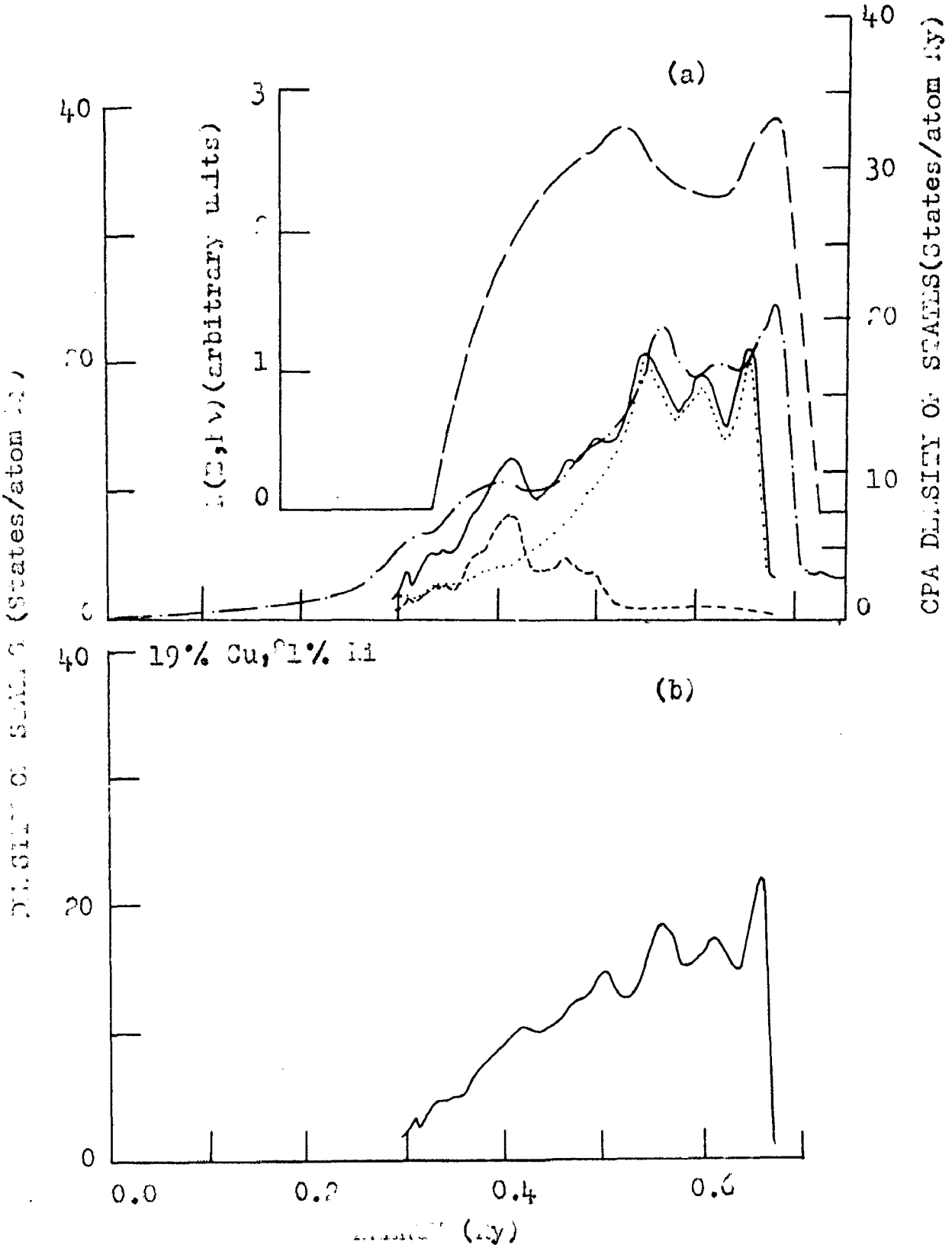

Fig.11. Densities of states for a 19 at.% Cu, 81 at.% Ni alloy. The notation is as in Fig.9.

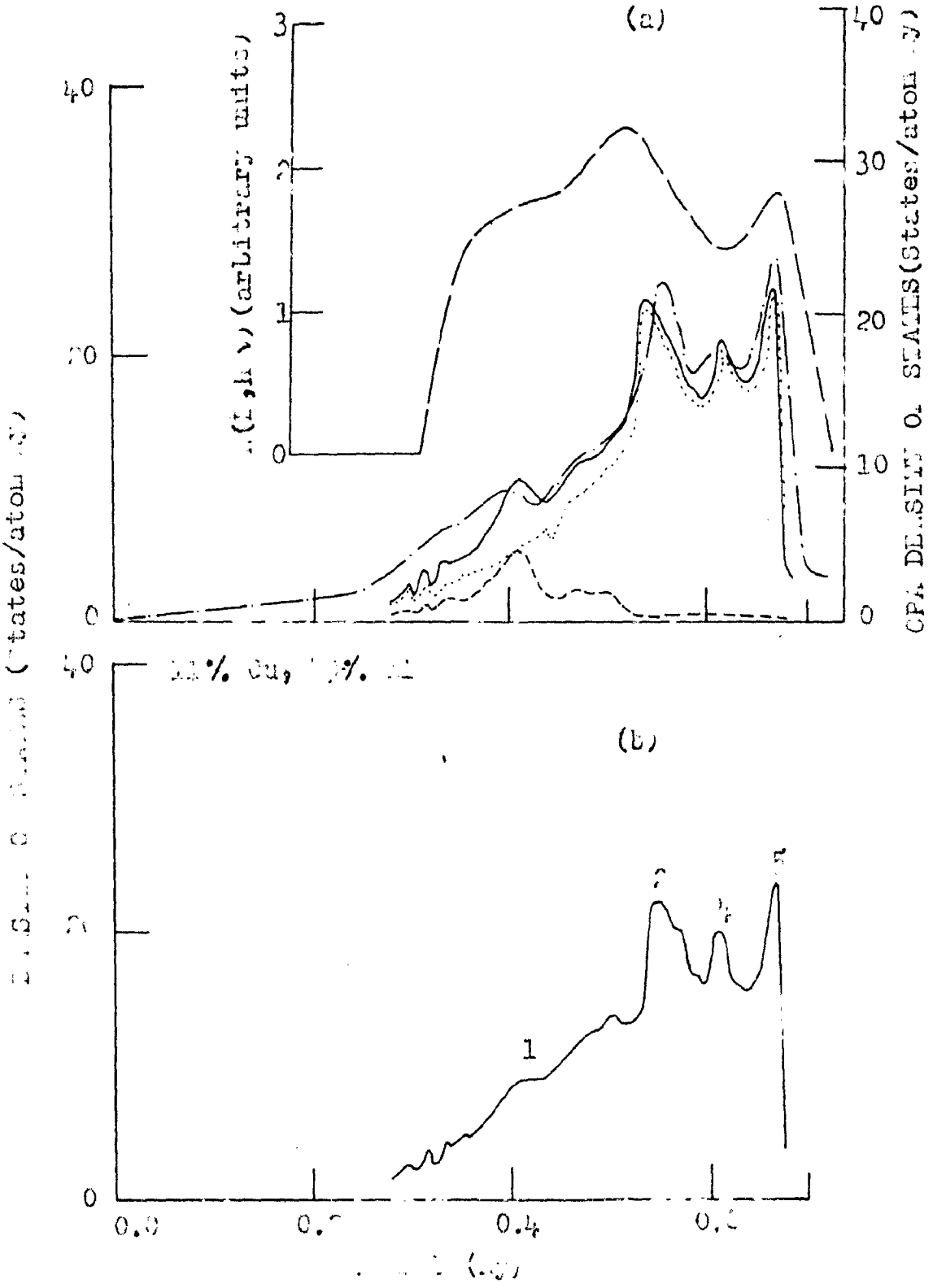

Fig.17. Densities of states for a 11 at.% [illegible], 39 at.% [illegible] alloy. The notation is as in Fig.6.

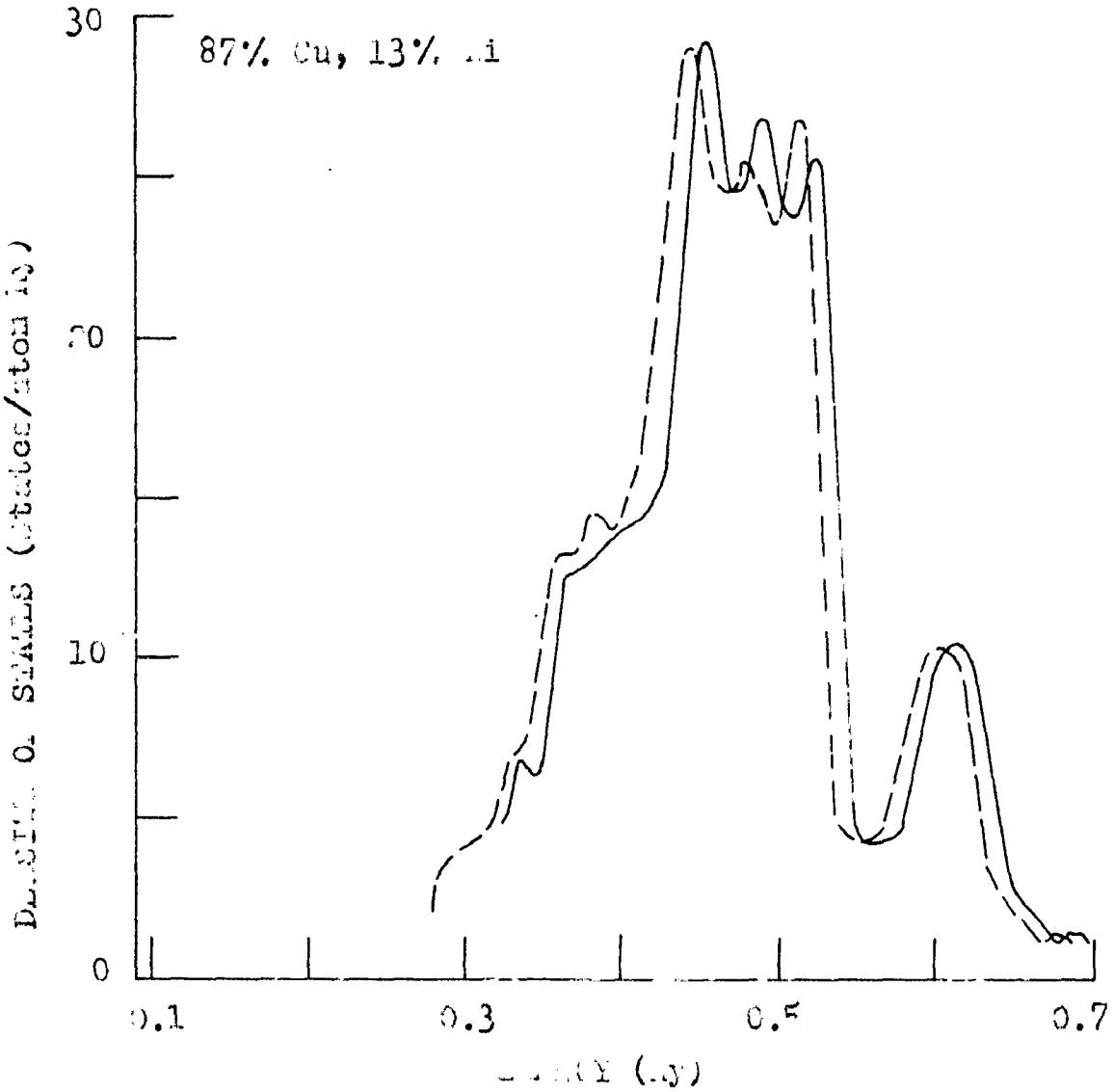

Fig.13. Densities of states calculated using the CPA:(——, through eqn.(1.7), and (----, through eqn.(2.5),.

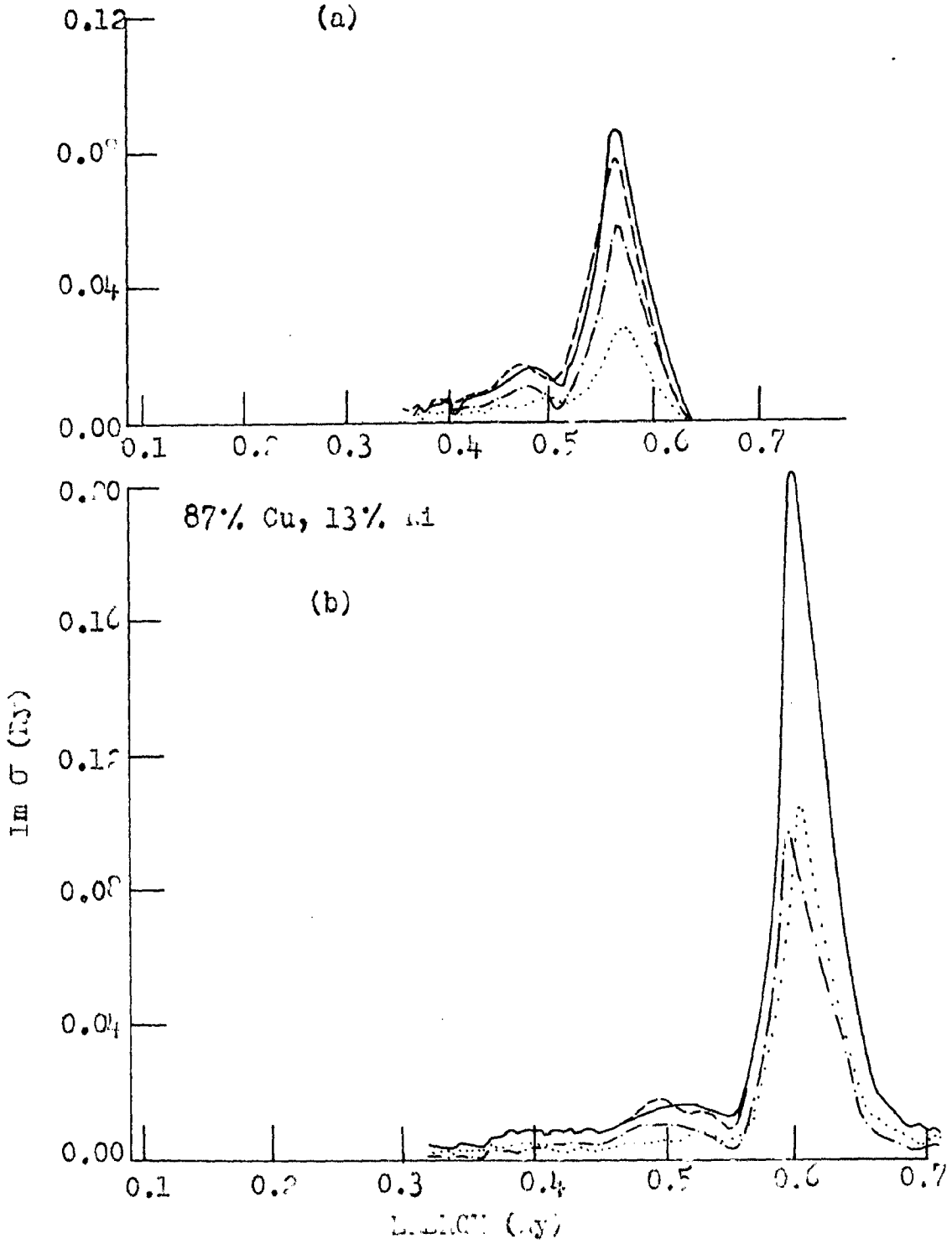

Fig.4. The Im $\sigma(E)$ versus energy plots calculated with methods employing eqn.(1.21) (——) and eqn.(1.25) (----). (a) shows the same for coherent pseudopotential method and (b) shows them for CPA. (.....) and (—·—·—) respectively belong to the e_g and t_{2g} contributions to the total Im σ obtained through eqn.(1.21).

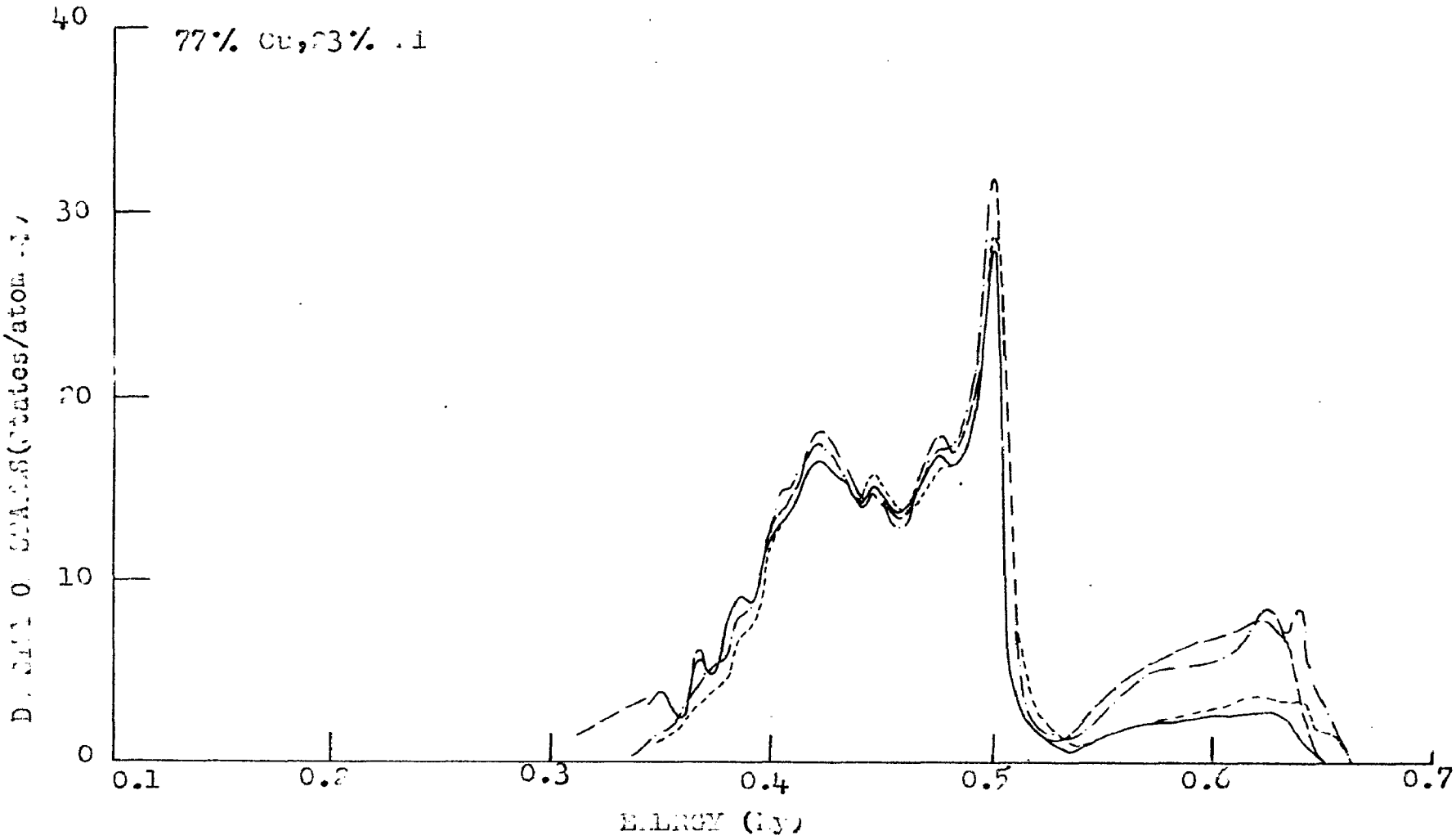

Fig.1[illegible] The t_{2g} component of the densities of states calculated through the approaches (i) and (ii), given respectively by eqn.(1.47) and by (1.45), (1.46) and (1.48), with the two self-consistent methods given by eqn.(1.21) and (1.25). (——) and (- - -) show $\rho_{t_{2g}}$ obtained from (i), and (----) and (·—·) are obtained from (ii).

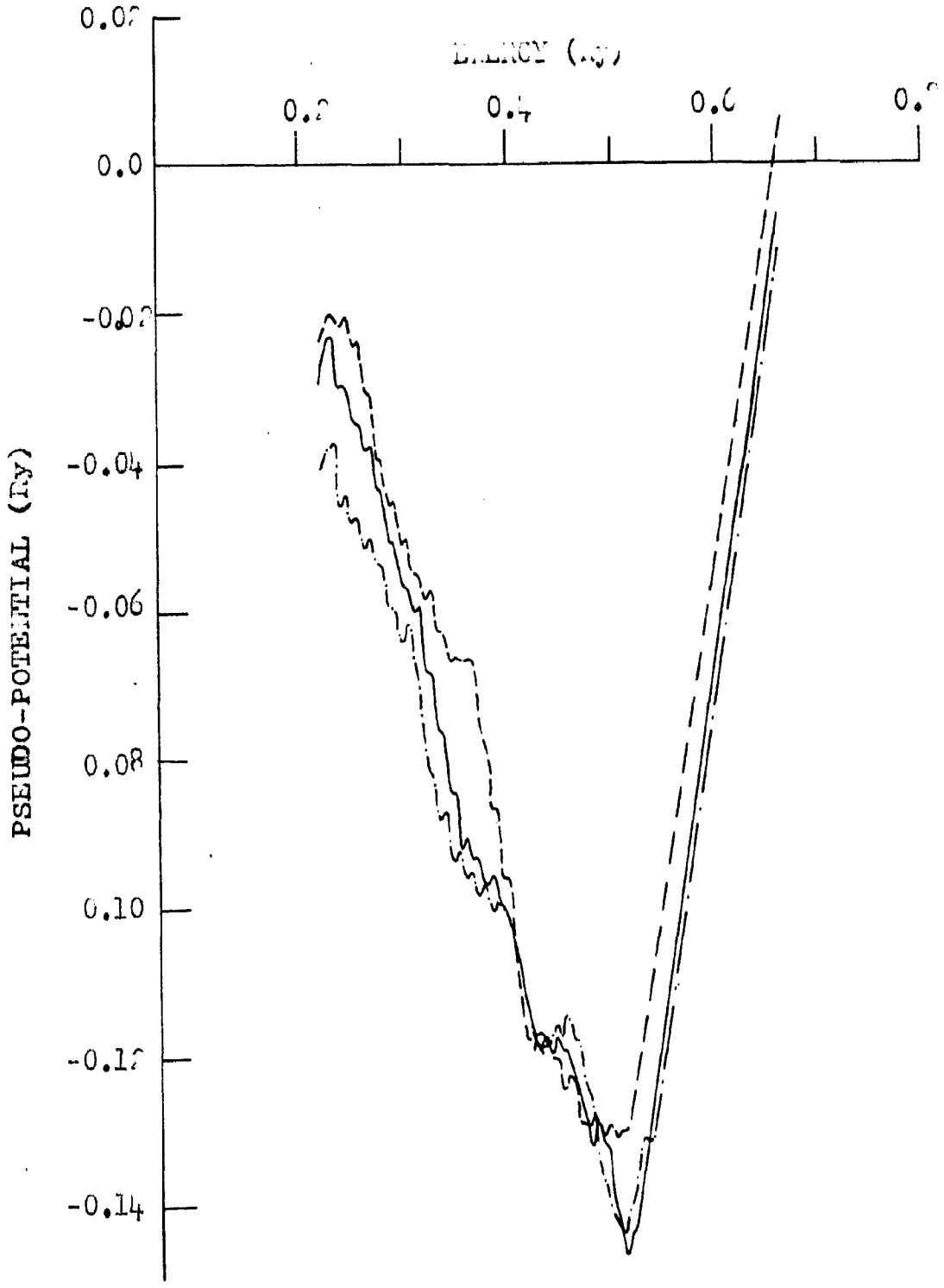

Fig.18. Plots of the pseudopotential versus energy: (——) shows V(E) from method (iii) and (----) and (—·—·—) respectively belong to the $V_{eg}(E)$ and $V_{t_2g}(E)$ shown earlier in Fig.5.

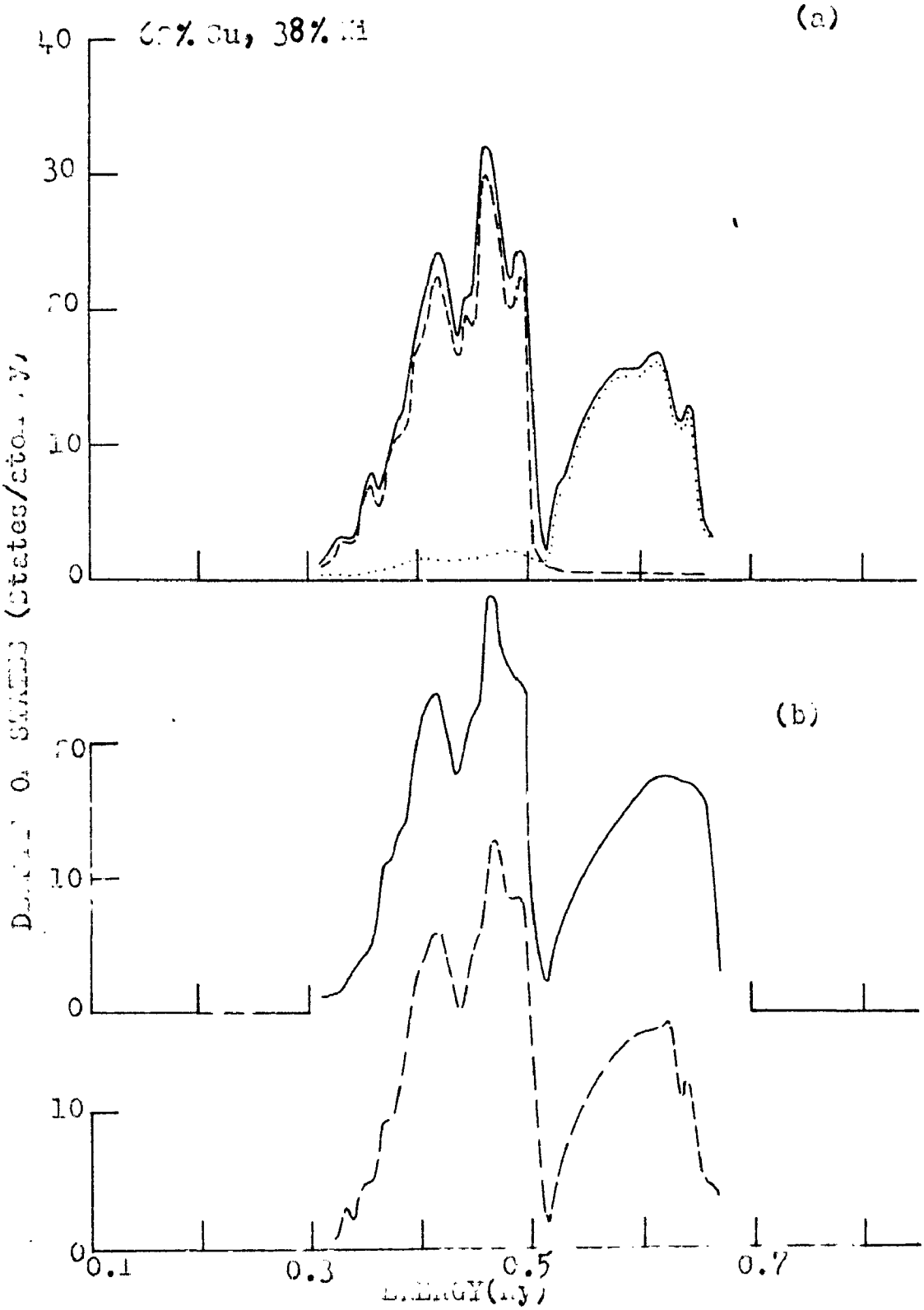

Fig.19. Densities of states calculated in CPPA.

(a) Calculations with method (iii):(——) denotes the total density of states, and (– – – –) and (• • • • •) denote $\rho^{(Cu)}(E)$ and $\rho^{(Ni)}(E)$, respectively.

(b) Calculations with methods (i) and (ii), shown respectively by (– – – –) and (— —).

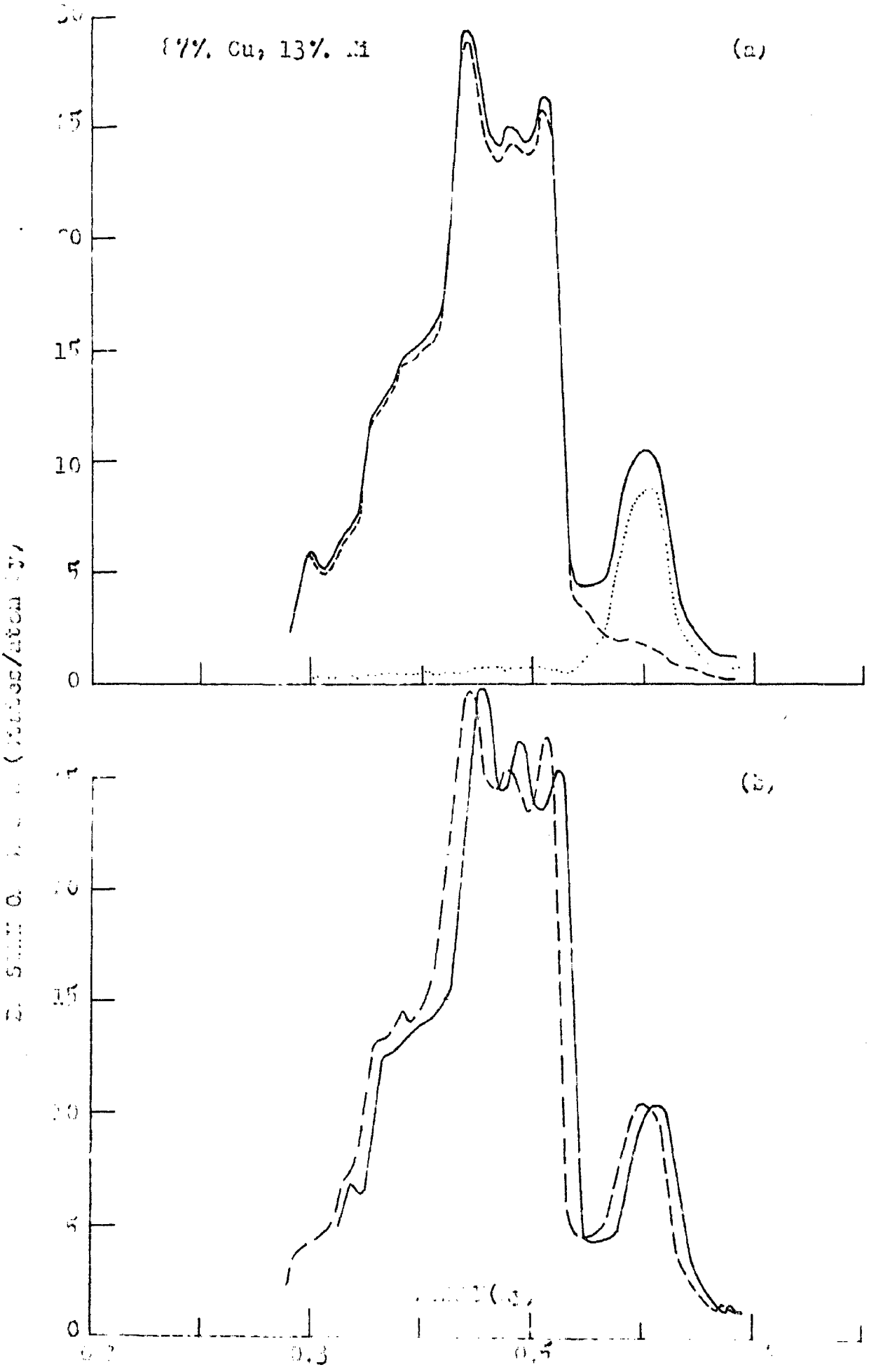
87% Cu, 13% Ni
(a)
(b)
0
5
10
15
20
0.3
0.5

CHAPTER 4

Cluster Effects in Disordered Systems

This chapter is concerned with the generalizations of coherent potential approximation to include the effects due to clusters, as indicated in Chapter 2. The CPA has been generalized in numerous ways[52] to include self-consistently the two or many site scatterings. The methods involving multiple scattering theory are due to Cyrot-Lackmann and Ducastelle[53], Schwartz and Ehrenreich[54], Cyrot-Lackmann and Cyrot[55], Vipin and Joshi[56], Foo et.al.,[57,58] Horiguchi et.al.[59] and Čàpek.[60] A method involving generalized mean field theory has been given by Ducastelle.[61,62] A diagram technique has been introduced by Aiyer et.al.[63] and Nickel and Krumhansl.[64] Some other attempts have been given in references 65-71. There are also some attempts due to Brouers et.al.[72,73] and Butler[74] which treat clusters in the spirit of single site approximation centring attention on a single site and taking local environmental effects of the nearest neighbour sites.

The CPA treatment is the unique self-consistent single site method. But there is no unique way to generalize it for clusters. We have made a critical study of this non-uniqueness, to examine the subtle differences in their derivations, in the decoupling schemes involved in them, their calculational details and finally how all these methods may be linked together. This helps in seeing how the calculations in a method may be made tractable by taking clues from alternative approaches. For the sake of simplicity we look at the case of pairs only. All the arguments can be

generalized for higher order clusters.

1. GENERALISATION OF CPA

The properties of a disordered system represented by a Hamiltonian $\underline{H}$ are determined by replacing it by an ordered system (reference) of Hamiltonian $\underline{\tilde{H}}$ and then treating the difference between the two as perturbation. The reference medium is the one in which at every site a self-energy matrix $\underline{\Sigma}(Z)$ is placed. The scattering in the system is governed by a scattering matrix

$$\underline{T} = \frac{\underline{V}}{\underline{I}-\underline{V}\,\underline{G}} , \qquad \ldots (1.1)$$

$$\underline{G} = (Z\underline{I}-\underline{H})^{-1}, \quad \underline{V} = \underline{H}-\underline{\tilde{H}} \equiv \sum_n \underline{V}_n \qquad \ldots (1.2)$$

The aim is to solve the Dyson equation,

$$\langle \underline{G} \rangle = \underline{\tilde{G}} + \underline{\tilde{G}}\,\underline{\Sigma}\langle \underline{G} \rangle , \qquad \ldots (1.3)$$

i.e. to determine $\underline{\Sigma}$, which, as we have seen in Chapter 2, is done self-consistently by putting

$$\langle \underline{T} \rangle = 0 .$$

The problem becomes convenient in momentum representation so that one must go back and forth from coordinate to momentum representation according to,

$$\underline{\Sigma}_{\vec{k}} = \underline{\Sigma}^{(1)}(n) + \sum_m{}' \underline{\Sigma}^{(2)}_m(nn) + \sum_p{}' \sum_m{}' \tfrac{1}{2} \underline{\Sigma}^{(3)}_{p,m}(nn) + \ldots .$$
$$+ \sum_m{}' e^{i\vec{k}\cdot\vec{R}_{nm}} \left[\underline{\Sigma}^{(2)}(nm) + \sum_p{}' \underline{\Sigma}^{(3)}_p(nm) + \ldots \right], \qquad \ldots (1.5)$$

$$\text{and } \langle G_{nm} \rangle = \frac{1}{(2\pi)^3} \int d^3k \, \frac{e^{-i\vec{k}.\vec{R}_{nm}}}{\tilde{G}_k^{-1} - \Sigma_{\vec{k}}} \, . \qquad \ldots (1.6)$$

The various terms on the right hand side describe the contributions from single site, two sites, three sites etc. and will be described in more detail later. The primes on the lattice sums indicate that no two indices be the same.

It is impossible to solve (1.4) exactly using all the terms of (1.5). $\underline{T}$ is therefore expanded in terms of the single site contributions to it (cf. eqn.(1.12) of chapter 2),

$$\underline{T} \equiv \sum_n \underline{T}_n = \sum_n \underline{t}_n + \sum_n \underline{t}_n \tilde{\underline{G}} \sum_{m \neq n} \underline{t}_m + \ldots \, . \qquad \ldots (1.7).$$

Vanishing of $\langle T \rangle$ implies $\langle \underline{T}_n \rangle = 0$, which in the SSA decoupling scheme reduces to $\langle \underline{t}_n \rangle = 0$ (the CPA condition). In CPA $\underline{\Sigma}$ is taken to be cell localized (i.e. (1.5) is truncated at the very first stage, $\underline{\Sigma} = \sum_n \underline{\Sigma}^{(1)}(n)$, where $\underline{\Sigma}^{(1)}(n)$ is site diagonal), so that $\underline{V}_n$ is cell localized and consequently $\underline{t}_n$ is site diagonal.

To extend CPA, $\underline{\Sigma}$ should be taken to be non-diagonal. Restricting to the case of pairs only, the self-energy $\Sigma_{\vec{k}}$ can be broken in terms of the various contributions to it in two ways.

(A) Contributions from single sites and from pairs of various separations, i.e.

$$\Sigma_{\vec{k}} = \Sigma(nn) + \sum_m{}' \Sigma^{(2)}(nm) \, e^{i\vec{k}.\vec{R}_{nm}} \, . \qquad \ldots (1.8)$$

(B) $\sum(nn)$ may be further broken in two parts, one giving the contribution when electron comes at n and gets immediately reflected and the other belongs to the case in which electron comes at n and goes out of n after suffering intermediate scatterings between n and all other m's , i.e.

$$\sum_{\vec{k}} = \sum^{(1)}(n) + \sum_{m}{}' \sum_{m}^{(2)}(nn) + \sum_{m}{}' \sum^{(2)}(nm) e^{i\vec{k}.\vec{R}_{nm}} \qquad \ldots (1.9)$$

If in a system there are (N-1) pairs of different separations, then for the evaluation of the effective medium, (A) has N and (B) has (2N-1) unknown variables. The self-consistent equations for their calculation are obtained as follows. We will briefly review three main approaches to the problem.

(a) Multiple Scattering Approach:

The t-matrix expansion (1.7) is written so as to involve one site explicitly as

$$\underline{T}_n = \underline{t}_n + \underline{t}_n \underline{\tilde{G}} \sum_{m \neq n} \underline{T}_m, \qquad \ldots (1.10)$$

and two sites explicitly as

$$\underline{T}_n = \underline{t}_n + \underline{t}_n \underline{\tilde{G}} \underline{T}_m + \underline{t}_n \underline{\tilde{G}} \sum_{\ell \neq m,n} \underline{T}_\ell, \qquad \ldots (1.11a)$$

$$\underline{T}_m = \underline{t}_m + \underline{t}_m \underline{\tilde{G}} \underline{T}_n + \underline{t}_m \underline{\tilde{G}} \sum_{\ell \neq m,n} \underline{T}_\ell. \qquad \ldots (1.11b)$$

In (1.10) the influences of all $m(\neq n)$ over n have been summed and we will call it the 'single site framework', In (1.11) the influences of all $\ell(\neq m,n)$ over the pair of sites

m-n have been summed and we will call it the 'two site framework'. We will derive two self-consistency conditions within these frameworks.

(i) Two site framework: The solution of the coupled equations (1.11a) and (1.11b) is

$$\underline{T}_n = \underline{t}_n^{(2)}(m)\ (\underline{I} + \underline{\tilde{G}} \sum_{\ell \neq m,n} \underline{T}_\ell), \quad , \qquad \ldots (1.12a)$$

where
$$\underline{t}_n^{(2)}(m) \equiv \underline{t}_n(\underline{I}+\underline{\tilde{G}}\,\underline{t}_m)(\underline{I}-\underline{t}_n\underline{\tilde{G}}\,\underline{t}_m\underline{\tilde{G}})^{-1}$$
$$= \underline{t}_n+\underline{t}_n\underline{\tilde{G}}\underline{t}_m+\underline{t}_n\underline{\tilde{G}}\,\underline{t}_m\underline{\tilde{G}}\,\underline{t}_n+ \ldots . \qquad \ldots (1.12b)$$

If (1.12a) be averaged over all configurations of n and m and the average on the right hand side be decoupled to isolate the pair scattering matrix from the effective wave incident on the pair, then the general self-consistency requirement ($\langle T_n \rangle = 0$) yields,[56]

$$\langle \underline{t}_n^{(2)}(m) \rangle = 0 \quad \text{for all n and m,} \qquad \ldots (1.13)$$

i.e. on the average the scattering from n and all the multiple scatterings between n and m of an electron entering either through n or m but emerging out of n only, together go to zero. This is required for all pairs of any separation. Since we can discriminate between the situations in which electron enters at n, or m for each specified pair, (1.13) should be capable of calculating the corresponding contributions, $\Sigma_m^{(2)}(nn)$ and $\Sigma^{(2)}(nm)$ separately. The (2N-1) elements of (1.9) are calculated from the following equations,

$$\langle\langle n|\underline{t}_n+\underline{t}_n\tilde{\underline{G}}\underline{t}_m+\underline{t}_n\tilde{\underline{G}}\,\underline{t}_m\tilde{\underline{G}}\underline{t}_n+\ldots|n\rangle\rangle = 0 \quad [(N-1) \text{ eqns.}], \quad \ldots (1.14a)$$

$$\langle\langle n|\underline{t}_n+\underline{t}_n\tilde{\underline{G}}\underline{t}_m+\underline{t}_n\tilde{\underline{G}}\,\underline{t}_m\tilde{\underline{G}}\,\underline{t}_n+\underline{t}_n\tilde{\underline{G}}\,\underline{t}_m\tilde{\underline{G}}\,\underline{t}_n\tilde{\underline{G}}\,\underline{t}_m+\ldots|m\rangle\rangle = 0$$
$$[(N-1) \text{ eqns.}], \quad \ldots (1.14b)$$

$$\langle\langle n|\underline{t}_n(n)\rangle\rangle = 0 \qquad [1 \text{ eqn.}] \qquad \ldots (1.14c)$$

Equation (1.14c) is obtained as a special case of (1.13) in which n and m are infinitely distant. The atomic t-matrix, $\underline{t}_n$, is defined as,

$$\underline{t}_n = \frac{\underline{\varepsilon}_n - \underline{\Sigma}}{\underline{I} - (\underline{\varepsilon}_n - \underline{\Sigma})\tilde{\underline{G}}}, \qquad \ldots (1.15)$$

and is different from the one used in CPA because now the site n is influenced by the other specified site m. The information of all m's is contained in $\tilde{\underline{G}}$, which is a functional of full $\underline{\Sigma}_k$. $\underline{\varepsilon}_n$ is the site energy matrix. This method yields 12 exact moments of density of states.[62]

(ii) Single-Site Framework: Instead of treating each pair individually, if we introduce (1.12a) into (1.10), we get

$$\underline{T}_n = (\underline{t}_n+\underline{t}_n\tilde{\underline{G}}\sum_{m\neq n}\underline{t}_m^{(2)}(n))(\underline{I}+\tilde{\underline{G}}\sum_{\ell\neq m,n}\underline{T}_\ell), \qquad \ldots (1.16)$$

which after usual operations yields a self-consistency condition,

$$\langle \underline{t}_n + \underline{t}_n\tilde{\underline{G}}\sum_{m\neq n}\underline{t}_m^{(2)}(n)\rangle = 0, \qquad \ldots (1.17a)$$

$$\text{or } \langle \underline{t}_n + \sum_{m\neq n}\underline{t}_n\tilde{\underline{G}}\,\underline{t}_m+\underline{t}_n\tilde{\underline{G}}\,\underline{t}_m\tilde{\underline{G}}\,\underline{t}_n+\ldots\rangle = 0, \qquad \ldots (1.17b)$$

i.e. the scattering from n and multiple scattering corrections due to all m($\neq$n) in the system go to zero on the average. By the nature of (1.17) it is clear that if the electron is incident at n, then before it goes out of n, the multiple scattering corrections due to individual m(= n) can not be distinguished. Hence the contributions $\sum_m^{(2)}$ (nn) due to individual m can not be sieved out, and all such scatterings together contribute a single term, $\tilde{\sum}$(nn) (= $\sum^{(1)}$(n) + $\sum_m{}'\tilde{\sum}_m$(nn)). But if the electron is incident on m, then the multiple scatterings before it leaves through n can be distinguished. It follows from the fact that $\langle n|\sum_{\ell=m,n} \underline{t}_n \tilde{\underline{G}}\, \underline{t}_\ell |m\rangle = 0$, because with n fixed, (1.17b) allows multiple scatterings only between n and all other m's and not between $\ell(\neq n)$ and m's. Therefore $\tilde{\underline{G}}$ is a functional of N elements in (Λ), which are determined from the following equations,

$$\left\langle\!\left\langle n\left|\underline{t}_n + \sum_{m\neq n} (\underline{t}_n \tilde{\underline{G}}\, \underline{t}_m + \underline{t}_n \tilde{\underline{G}}\, \underline{t}_m \tilde{\underline{G}}\, \underline{t}_n + \ldots)\right|n\right\rangle\!\right\rangle = 0 \quad [\text{I eqn.}], \qquad \ldots (1.18a)$$

$$\left\langle\!\left\langle n\left|\underline{t}_n + \underline{t}_n \tilde{\underline{G}}\, \underline{t}_m + \underline{t}_n \tilde{\underline{G}}\, \underline{t}_m \tilde{\underline{G}}\, \underline{t}_n + \ldots\right|m\right\rangle\!\right\rangle = 0 \quad [(N-1)\text{eqns.}] \qquad \ldots (1.18b)$$

This method yields 11 exact moments of density of states.[62]

Cyrot-Lackmann and Cyrot[55] have made a remark on (1.17) that it does not treat all the pairs in the system equivalently because an atom being fixed at n, all possible pairs n-m are properly taken into account but pairs m-ℓ, with $\ell\neq$n, are not correctly described. We see that this argument is not right. The choice of n is random and in (1.17),

the sum has been taken over pairs of all possible separations from n. It is only the different separations between the two sites of the pair that give rise to the various contributions to $\underline{\Sigma}$. Rather it seems that the sites of the pair are not treated equivalently while considering the scattering from the pair in both (i) and (ii). One of the two sites is given special treatment by requiring the effective wave to emerge out of it only. This incongruity is trivial from numerical calculational point of view. However, it is simple to avoid it also. Adding expressions for $\underline{T}_n$ and $\underline{T}_m$ of the type (1.12a),

$$\begin{aligned}\underline{T}_n+\underline{T}_m &= (\underline{t}_n^{(2)}(m)+\underline{t}_m^{(2)}(n))(\underline{I}+\underline{\tilde{G}}\sum_{\ell\neq m,n}\underline{T}_\ell), \\ &\equiv \underline{t}^{(2)}(n,m)(\underline{I}+\underline{\tilde{G}}\sum_{\ell\neq m,n}\underline{T}_\ell). \qquad \ldots (1.19)\end{aligned}$$

To elaborate a little further, (1.19) can be written in a symmetrical form as

$$\underline{T}_n+\underline{T}_m = \underline{t}^{(2)}(n,m)(\underline{I}+\underline{\tilde{G}}\sum_{\substack{\ell,p\\(\neq n,m)}}(\underline{T}_\ell+\underline{T}_p)), \qquad \ldots (1.20)$$

the sum extends over half the sites because a pair n-m (or ℓ-p) got specified would mean that fixing n(or ℓ) would fix m(or p) also. The eqn.(1.20) is thus in terms of identical and disjoint pairs. Averaging (1.20) and then decoupling of the average gives the self-consistency condition,

$$\langle \underline{t}^{(2)}(n,m)\rangle = 0 \quad \text{for all n and m.} \qquad \ldots (1.21)$$

$\underline{t}^{(2)}(n,m)$ is the pair t-matrix and includes all the multiple scattering terms in which the effective wave exits through n as well as m after being incident on n as well as m. Sites n and m are therefore treated symmetrically. If (1.20) be iterated we get the standard multiple scattering series with atomic t-matrices replaced by pair t-matrices,

$$\underline{T}_n+\underline{T}_m = \underline{t}^{(2)}(n,m) + \underline{t}^{(2)}(n,m)\,\underline{\tilde{G}} \sum_{\ell p\neq(n,m)} \underline{t}^{(2)}(\ell,p)$$

$$+ \underline{t}^{(2)}(n,m)\underline{\tilde{G}} \sum_{\ell,p\neq(n,m)} \underline{t}^{(2)}(\ell,p)\underline{\tilde{G}} \sum_{q,s\neq(p,\ell)} \underline{t}^{(2)}(q,s)+\ldots$$

$$\ldots \quad (1.22)$$

It is not possible to get such a series from (1.12a). Conditions (1.13) and (1.21) are formally the same and make no difference in calculations.

(b) Diagram Method

For a particular pair the self-energy is broken as

$$\underline{\zeta} = \underline{\Sigma}^{(1)} + \underline{\Sigma}^{(2)}$$

$$\begin{pmatrix} \Sigma^{(1)}(n) & 0 \\ 0 & \Sigma^{(1)}(m) \end{pmatrix} + \begin{pmatrix} \Sigma_m^{(2)}(nn) & \Sigma^{(2)}(nm) \\ \Sigma^{(2)}(mn) & \Sigma_n^{(2)}(mm) \end{pmatrix}$$

$$\ldots \quad (1.23)$$

and following equations are solved simultaneously,

$$\Sigma^{(1)}(n) \equiv \Sigma^{(1)}(n)\,\{\langle G_{nn}\rangle\}, \qquad \ldots \quad (1.24a)$$

and

$$\underline{\zeta} \equiv \underline{\zeta}\,\{\langle \underline{G}\rangle\}\,. \qquad \ldots \quad (1.24b)$$

Equation (1.24b) is solved for all pairs in the system whereas (1.24a) is the simple CPA condition. This method is essentially the same as (i) and the differences between

the two may be noted from the following. The self energy in (1.23) is broken as in (B), but it follows from the text of Nickel and Krumhansl[64] that when (1.24b) is solved for a particular pair, $\sum_m^{(2)}(nn)$'s and $\sum^{(2)}(nm)$'s belonging to other pairs are completely ignored i.e. taken to be zero. Thus the Green's function is a functional of six elements of self-energy whereas in (i) it is a functional of full self-energy matrix. Because of this reason (1.24a) is different from (1.14c) contrary to the statement by Cyrot-Lackmann and Cyrot[55] that they are the same. These are the subtle differences between this method and multiple scattering method and not the one pointed out by Leath[75] that the two methods involve self energy respectively like (B) and (A). Both, (b) and (i) take self energy in the form (B).

(c) Generalized Mean Field Method:

This method goes parallel with the diagram method and ane assumes $\underline{\Sigma}^{(2)}$ [$\underline{\Sigma}_m^{(2)}(nn) = \langle n|\,\underline{\Sigma}^{(2)}\,|n\rangle$, $\underline{\Sigma}^{(2)}(nm) = \langle n|\,\underline{\Sigma}^{(2)}\,|m\rangle$] to be the same for all p's $\neq$ m when going from H_{eff} to H_{eff}^{nm} [H^{nm} is the Hamiltonian of the system in which n and m sites have been excluded from averaging] What $\underline{\Sigma}^{(2)}$ is to be taken for all the pairs but the one under consideration, is free to be chosen and choosing it to be zero like in (b), is a special case of this method. In fact using some approximate suitable value for these terms is necessary because it is not strictly speaking possible to disconnect a single pair from the others and

the information belonging to these other pairs should be contained in an approximate way in $\underset{\sim}{G}$.

It is important to state Leath's theorem[75] at this stage. The theorem bridges the generalized CPA obtained through Bloch state expansion [i.e. (a)] and locator expansion, and provides an interpolation formula from the virtual crystal to the atomic limit (not the split band limit as stated by Leath[75]). The theorem states: the self energy as a matrix should be cluster diagonal, i.e. it does not have any non-zero elements $\Sigma(n,\ell)$ connecting a site n within the nxn cluster to another site ℓ outside the cluster. Besides merging the locator approach into the multiple scattering approach, we see that it further merges (c) into (b) and also (i) into (b). Thus all the methods that use Σ_K of the kind (B) merge to yield a single method, i.e. (b). The method (ii), that uses Σ_K of the kind (A), is greatly simplified with the use of Leath's theorem, which eradicates the sums of the type $\sum_{p}{}' {}'_{n,m}$ hidden in (1.18a) and (1.18b) because of the specified m deciding (1.18b). However, (ii) does not merge into (b), contrary to what Leath[75] has stated.

So eventually we are left with two methods, (ii) [simplified form] and (b), respectively based upon Σ_K of the kinds (A) and (B). It will be discussed in the next section that to make the numerical calculations tractable one has to take into account only the pairs of nearest neighbours. Then the formulation outlined under (ii) takes into account simultaneously all the Z nearest neighbours

of a pair, where Z is the coordination number, and (b) type formulations take into account only one such pair embedded into an averaged medium. It should be interesting to compare the detailed nature of density of states obtained through the two methods. Ducastelle's observation[62] that (ii) has 11 exact moments of density of states whereas (b) has 12 , makes it more interesting although a priorily (ii) looks to be firmer than (b). Using the approach of the type (ii) originally due to Cyrot-Lackmann and Ducastelle[53], Moorjani et.al.[78] have done density of states calculation for body-centred cubic lattice. We have attempted to do the three dimensional calculations using the (b) type approach for simple cubic lattice.

1.1 Simplifications For Numerical Calculation:

The calculations are still too tedius to be tractable if done for all pairs of all separations. However, since $\underline{\Sigma}^{(2)}$ decays asymptotically as $(\langle G_{nm} \rangle)^3$, one can expect only small R_{nm} to contribute except possibly at isolated energies near band edges. So one can further simplify the calculations by doing them for few pairs of small spatial separations, and thus truncating the self-energy matrix after few neighbours. We have seen that the calculations for a single pair lead to heavy computation, so doing it for few pairs would multiply the amount of computation accordingly. It can be guessed from the fact that following

the methodology discussed here, only one dimensional calculations have been done[57,76,77] so far. We report the results obtained by assuming a pair of nearest neighbour atoms embedded in an effective medium. Our aim is not to analyse the fine structures of the effective medium but to see the behaviour of diagonal part of Green's function. Therefore, we do not isolate $\sum^{(1)}(n)$ from $\sum_m^{(2)}(nn)$ and consider the sum of the two ($\sum(nn) = \sum^{(1)}(n) + \sum^{(2)}(nn)$) as the diagonal part of self-energy. This removes the need of solving (1.14c). We have to solve only two equations (1.14a) and (1.14b). The elaborated calculation of these two equations is discussed below. We consider both, diagonal and off-diagonal randomness. Among the other attempts to consider the off-diagonal randomness, two are due to Brouers and Van der Rest[78] and Blackman et.al.[80,81] (hereafter referred as BEB). They cast the off-diagonal disorder problem in a form suitable for single site averages. The two sets of authors respectively work within multiple scattering and locator approaches.

To conclude this section we remark that for three dimensional systems there is no calculation for clusters consisting of more than two sites. All big cluster calculations done so far are in the spirit of single site approximation. Ducastelle[82] has reduced the problem discussed in the preceding text by further neglecting the off-diagonal matrix elements of the self-energy within a cluster, and

keeps a single scalar self-consistent equation. He reduces the Molecular CPA(MCPA) condition $\langle t_c \rangle = 0$ [equivalent to $\langle\langle \underline{G} \rangle_c\rangle = \tilde{\underline{G}}$] to $\langle\langle G_{oo} \rangle_c\rangle = \tilde{G}_{oo}$ only, where 'o' is the central site of the cluster 'c'. This approximation is called the central site approximation and has also been used by Butler[66], Brouers et.al.,[72,73] and Tsukada.[77] This approximation yields good results after calculations. Butler[76] has discovered that if the above thing is done for a site at the boundary of the cluster rather than for the central site, then in one dimension, the single self-consistent equation obtained in this way is exactly equivalent to the MCPA.

2. PAIR CALCULATION

The alloy effective medium may be written in terms of the diagonal (Σ_1) and off-diagonal (Σ_2) parts of the self-energy discussed in (1.8),

$$\underline{H}_{eff} = \Sigma_1(E) \sum_n |n\rangle\langle n| + \Sigma_2(E) \sum_{\substack{n,m \\ n\neq m}} |n\rangle\langle m| \qquad \ldots (2.1)$$

Here $|n\rangle$ and $|m\rangle$ are the Wannier orbitals at the n^{th} and m^{th} lattice sites. Naming two nearest neighbour sites constituting the pair as 1 and 2, the perturbation equation(1.1) is expanded to yield T_{11} and T_{21} as follows,

$$T_{11} = \frac{V_{11} + \dfrac{V_{21}(V_{11}G_{12}+V_{12}G_{22})}{1-(V_{21}G_{12}+V_{22}G_{22})}}{1-(V_{11}G_{11}+V_{12}G_{21}) - \dfrac{(V_{11}G_{12}+V_{12}G_{22})(V_{21}G_{11}+V_{22}G_{21})}{1-(V_{21}G_{12}+V_{22}G_{22})}}$$

$$\equiv \frac{V_{11}+N}{D}, \qquad \ldots (22)$$

$$T_{21} = \frac{V_{21}+(V_{21}G_{11}+V_{22}G_{21})T_{11}}{1-(V_{21}G_{12}+V_{22}G_{22})},$$

$$\equiv \frac{V_{21}+A}{B} . \qquad \ldots (2.3)$$

T_{11} and T_{21} are diagonal and off-diagonal parts of $\underline{t}_n^{(2)}(m)$. The expansion of (1.1) takes the terms belonging to n and m other than 1 and 2 to be zero. The diagonal and off-diagonal perturbations with respect to the effective medium parameters Σ_1 and $\tilde{h}(1-\Sigma_2)$ are given as

$$V_{11} = \varepsilon_1-\Sigma_1 , \qquad \ldots (2.4)$$

$$V_{22} = \varepsilon_2-\Sigma_1 , \qquad \ldots (2.5)$$

$$V_{12} = V_{21} = h-\tilde{h}(1-\Sigma_2). \qquad \ldots (2.6)$$

ε_1 and ε_2 are allowed to take two values ε^A and ε^B and h, the hopping integral can be h_{AA}, h_{BB} and $h_{AB}=h_{BA}=\frac{1}{2}(h_{AA}+h_{BB})$ depending upon the occupancy of the sites of the pair. The particular form of h_{AB} is a simplification, not a requirement.

The self-consistency requirements $\langle T_{11}\rangle = 0$ and $\langle T_{21}\rangle = 0$, yield two coupled equations in Σ_1 and Σ_2 to be satisfied simultaneously,

$$\Sigma_1 = \frac{\langle \frac{\varepsilon_1}{D}\rangle + \langle \frac{N}{D}\rangle}{\langle 1/D\rangle}, \qquad \ldots (2.7)$$

$$\Sigma_2 = 1- \frac{\langle h/B\rangle + \langle A/B\rangle}{\tilde{h}\langle 1/B\rangle}. \qquad \ldots (2.8)$$

The averaging is done over the occupancy of the pair 1-2. The pairs A-A, A-B, B-A and B-B occur respectively with the probabilities c^2, $c(1-c)$, $(1-c)c$ and $(1-c)^2$, where c is the concentration of A atoms. The diagonal and off-diagonal contributions to the medium Green's function are obtained as follows. The diagonal part is

$$G_{11} = G_{22} = \sum_k \frac{1}{E - \Sigma_1(E) - \tilde{h}Zs(k)\left[1-\Sigma_2(E)\right]}$$

$$= \frac{1}{1-\Sigma_2} \sum_k \frac{1}{\frac{E-\Sigma_1}{1-\Sigma_2} - \tilde{w}s(k)}, \qquad \ldots (2.9)$$

$\tilde{w} = Z\tilde{h}$, where Z is the number of nearest neighbours. For convenience if we take $\tilde{h} = h_{AA}$, then the 'integral' form of (2.9) can be written as

$$G_{11} = \frac{1}{1-\Sigma_2} \int \frac{\rho^A(E')}{\frac{E-\Sigma_1}{1-\Sigma_2} - E' + \varepsilon^A} dE'. \qquad \ldots (2.10)$$

$\rho^A(E')$ is the unperturbed density of states of pure A system and the integral runs between the band edges of $\rho^A(E)$. For deriving the off-diagonal part of Green's function, we proceed as in the localor formulation,

$$G_{11} = g_{11} + \sum_2 g_{11} W_{12} G_{21}, \qquad \ldots (2.11$$

where $g_{11} = (E-\Sigma_1)^{-1}$, $W_{12} = \tilde{h}(1-\Sigma_2)$ and 2 denotes the nearest neighbours of 1. So we easily get,

$$G_{12} = G_{21} = \frac{(E-\Sigma_1)G_{11}-1}{Zh_{AA}(1-\Sigma_2)} . \qquad \ldots (2.12)$$

Having obtained Σ_1 and Σ_2 from (2.7) and (2.8), the alloy density of states is given by

$$\rho(E) = -\pi^{-1}\mathrm{Im}G_{11}(E+i0) \qquad \ldots (2.13)$$

2.1 Component Density of States

The partial density of states $\rho_{A(B)}(E)$ can be derived by defining the conditional averaged Green's functions,

$$\begin{aligned}\langle 1|\underline{G}^{(A)}(Z)|1\rangle &\equiv G_{11}^{(A)}(Z) \\ &= \langle 1|\{Z-\underline{H}_{eff}-(\varepsilon^A-\Sigma_{11}^A)|1\rangle\langle 1| \\ &\quad -[\underline{h}-h_{AA}(1-\Sigma_2)]\sum_{2\neq 1}|1\rangle\langle 2|\}|1\rangle \end{aligned} \qquad \ldots (2.14)$$

and a similar expression for $G_{11}^{(B)}(Z)$, $Z \equiv E+i0$.

After some transformations this can be rewritten,

$$G_{11}^{(A)}(Z) = \frac{G_{11}(Z)}{(Z-\varepsilon^A)G_{11}(Z)-\{(Z-\Sigma_1)G_{11}(Z)-1\}/(1-\Sigma_2)} , \qquad \ldots (2.15a)$$

$$G_{11}^{(B)}(Z) = \frac{G_{11}(Z)}{(Z-\varepsilon^B)G_{11}(Z)-h_{BB}\{(Z-\Sigma_1)G_{11}(Z)-1\}/\{h_{AA}(1-\Sigma_2)\}} \qquad \ldots (2.15b)$$

The partial densities of states are given by,

$$\rho_A(E) = -\pi^{-1}\mathrm{Im}G_{11}^{(A)}(E+i0), \qquad \ldots (2.16a)$$

and $\rho_B(E) = -\pi^{-1}\mathrm{Im}\, G_{11}^{(B)}(E+i0)$. ... (2.16b)

These quantities satisfy the natural identity

$$\rho(E) = c\rho_A(E)+(1-c)\rho_B(E). \quad \ldots (2.17)$$

2.2 Computation and Discussion of Results:

The self-consistent simultaneous equations (2.7) and (2.8) have been solved with the required components calculated from eqns.(2.10),(2.12) and (2.2)-(2.6). Having obtained Σ_1 and Σ_2 iteratively from (2.7) and (2.8), component densities of states are obtained from (2.5a)-(2.6b) and finally the total density of states from eqn.(2.17). The parameters for which we performed the calculations are the following: $\delta = 0.4(=\epsilon_A-\epsilon_B)$, c_A(concentration of A atoms)= 0.6 ; and $\delta = 1$, $c_A = 0.1$. For $\delta = 0.4$, $c_A = 0.6$ we also studied the effect of off-diagonal randomness, taking $h_{AA} = 2h_{BB}/3$ and $3h_{BB}/2$.

For small $\delta(=0.4)$ we employed the simple iteration method to solve the twin equations in Σ_1 and Σ_2, but for larger $\delta(=1.0)$ we had to use the Newton Raphson's method for iteration. Although the latter method gives convergence at places where the former fails but the amount of computation per iteration increases enormously. Besides this, in the impurity band region the convergence becomes very tough. About 45 to 50 iterations are needed even at very close interval of energy. The calculation is thus very time taking,

even on the IBM 360/44 computer. Another type of convergence difficulty arises in the minority band region. At certain energies two different solutions are obtained depending on whether these energies are approached from higher or lower energy side. Similar difficulty has also been reported by Moorjani et.al..[78]

Figures 21 and 22 show the density of states respectively for $c_A = 0.6$, $\delta = 0.4$ and $C_A = 0.1, \delta = 1.0$. For $\delta = 0.4$, fig.21 shows very little and trivial difference between the pair calculation and the CPA result[81] (the BEB[81] method reduces to CPA for no off-diagonal disorder). Figure 23 quantifies the difference in terms of the off-diagonal coherent potential, Σ_2. Σ_2, which is zero for CPA, is only about 7% of Σ_1 (if the maximum values of the two be compared). For larger $\delta(=1)$, i.e. stronger scattering case, Σ_2 becomes very significant. Σ_1 and Σ_2 have comparable magnitudes, also Σ_1 reduces by a large magnitude as compared to its CPA value (cf.fig.24). The effect of large magnitude of Σ_2 is seen in the density of states plot in fig.22. CPA gives two split bands with a considerable gap between the host and impurity bands. The present pair calculation erodes this gap by pulling the top edge of host band and the bottom edge of impurity band towards each other by a sufficiently large amount. The convergence problem discussed earlier arises around E=0.32. While approaching higher energies from lower side, density of states decreases smoothly upto E=0.38 then a sudden increase occurs at E=0.39 and density of states

goes smoothly upto E=0.854. After this energy, convergence is not obtained even at the energy interval of 0.0005. Then we tried convergence from the top of the band with energy decreasing. The iterations did converge though at very small energy interval and very large number of iterations (around 45 to 50). The region between E = 0.854 and 0.39 was retraced and this time it kept decreasing smoothly and joined the main band at E = 0.32. The shape of the impurity band is quite different than that obtained from CPA. An anomaly is found: the density of states obtained by us does not seem to be conserved. We are trying to analyse this anomaly by doing the calculations again with a small imaginary part added to energy. However, it appears that the shape of the impurity band will not change much, only the magnitude of density of states may change in some energy regions. The shape obtained by us looks very much like that obtained from continued fraction methods.[83] The results of Moorjani et.al.[78] show distinct structures in the impurity band and are assigned to the bonding and anti-bonding states of a molecule embedded in an effective medium. Schwartz and Siggia[84] also obtained similar structure in the impurity band. The non-self consistent approach of Schwartz and Siggia[84] has been shown in its self-consistent form to be equivalent to the approach of the type (ii) discussed in Section 1. The approaches (ii) and (b), representatives of the two classes of pair-methods discussed in Section 1, thus lead to two types of impurity bands. The earlier shows

structures in the minority band, whereas the latter shows a smoothly varying pattern with a peak at the top of the band. It is interesting that the feature of $Im\Sigma_2$, that it changes sign within the minority band, has been found common with both the approaches. This feature has been discussed to be compatible with the dispersion relations and with interpretation of associating the side bands as originating from bonding and anti-bonding states of a molecule.[78]

3.2 Effects due to off-diagonal disorder:

We now discuss the effects when two elements with quite different band widths are alloyed. Figures 25 and 26 show the total and component densities of states for the cases when the bandwidths of A are respectively 3/2 and 2/3 times the bandwidth of B. The figures also show the corresponding results obtained by BEB.[81] The diagonal and off-diagonal self-energies for these cases are plotted in figures 27 and 28. The centers of gravity of pure A and pure B densities of states, ε_A and ε_B, are respectively at 0.2 and -0.2; i.e. $\delta = \varepsilon_A - \varepsilon_B = 0.4$. The concentration of A atoms is 60%.

The effect of narrower solute (B) band (cf.Fig.25) shows up in the negative energy portion of the total and partial densities of states (ρ, ρ_B and ρ_A). ρ and ρ_B have distinct peaks at almost the same energy and ρ_A has a shoulder (satellite peak) in the same region. The results of BEB[81] are almost like ours except that in our case the band width

is slightly larger than the BEB results. This shows that the larger band width of host(A) band plays more important role in our case. Both the peaks in ρ are indicated as kinks in the real and imaginary parts of Σ_1 and Σ_2. Both the coherent potentials have almost equal magnitudes at individual energies. Interestingly the plots of Σ_1 and Σ_2 look like mirror images of each other, the physical implication of which is unclear. The development of the satellite structure in the component density of states is of physical importance. The existence of the shoulder in ρ_A(A atoms being in majority) due to a narrower pure B-band, indicates that slightly more charge is concentrated about the A atoms (and slightly lesser about the B atoms) than would be inferred if the weight of the peak in ρ was attributed solely to a peak in ρ_B.

In the case of a narrower host (A)band the satellite peak is seen in the A-component density of states ρ_A and in the positive energy region (cf.fig.26). The total density of states in this case is quite different as compared to the same obtained by BEB. The solid and broken curves for ρ are respectively obtained through eqns. (2.17) and (2.13). Σ_2 in this case becomes much larger than Σ_1. Besides, $\mathrm{Im}\Sigma_1$ and $\mathrm{Im}\Sigma_2$ are peaked over a narrower range as compared to the earlier case (cf.figs.27 and 28). This can be understood as follows. The imaginary parts of self-energies indicate the width caused by disorder in the dispersion curves, hence they should be large in the energy region

where ρ_A and ρ_B are almost equal or have small ratio (i.e. both types of atoms contribute to ρ comparably). This region is obviously narrower in the latter case. Total span of allowed energies is much narrower when $h_{AA} = \frac{2}{3} h_{BB}$ than when $h_{AA} = \frac{3}{2} h_{BB}$ if $Zh_{BB} = w_B = 1$ (w_B = unperturbed bandwidth of B-band).

To sumup these results we make following remarks. Generalization of CPA for clusters is non-unique. The numerical computation for cluster-CPA is at the same time too tough to be feasible. The simplifications to make the calculations tractable for three dimensional solids categorise all the generalisations into two classes. The calculations through one of these two methods have been done by Moorjani et.al.[78], and results through the other method are obtained by us.[85] The case of most interest is when $\delta = 1.0$ and $c = 0.1$. The method used by Moorjani et al. would yield a well separated impurity band with lot of structures. Our method yields highly broadened and smoothly varying impurity band. No band gap is obtained. It is difficult to predict which of the two methods is better. Though the two methods respectively yield 11 and 12 exact moments of density of states, this can not be held as a reliable criterion for judgement. Only computer simulation results can be the best results for comparison. The so-called 'experimental' numerical results for crystalline semiconductors obtained using the moment technique[83] show the impurity band of the type we have obtained.

In the case of off-diagonal disorder, for small δ, although BEB's[81] results look like ours (BEB's method has first four moments of density of states exactly), but the very significant magnitude of Σ_2 indicates the necessity of employing pair-calculations rather than incorporating these effects in single-site theories.

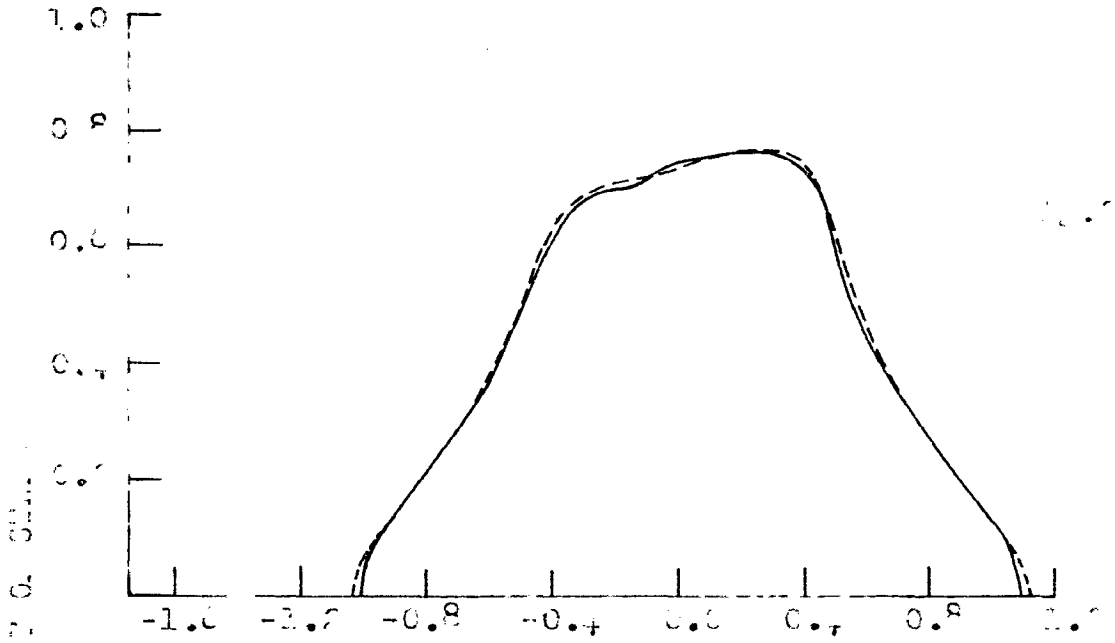

Fig. 11. Density of electronic states, $\rho(\epsilon)$, versus energy for $\delta = 2.4$, $c_A = 0.6$ and h_{AA}, h_{BB}. (— —) shows the results of pair calculation and (— —) shows the CPA results taken from Ref. [21]. The scales are in arbitrary units.

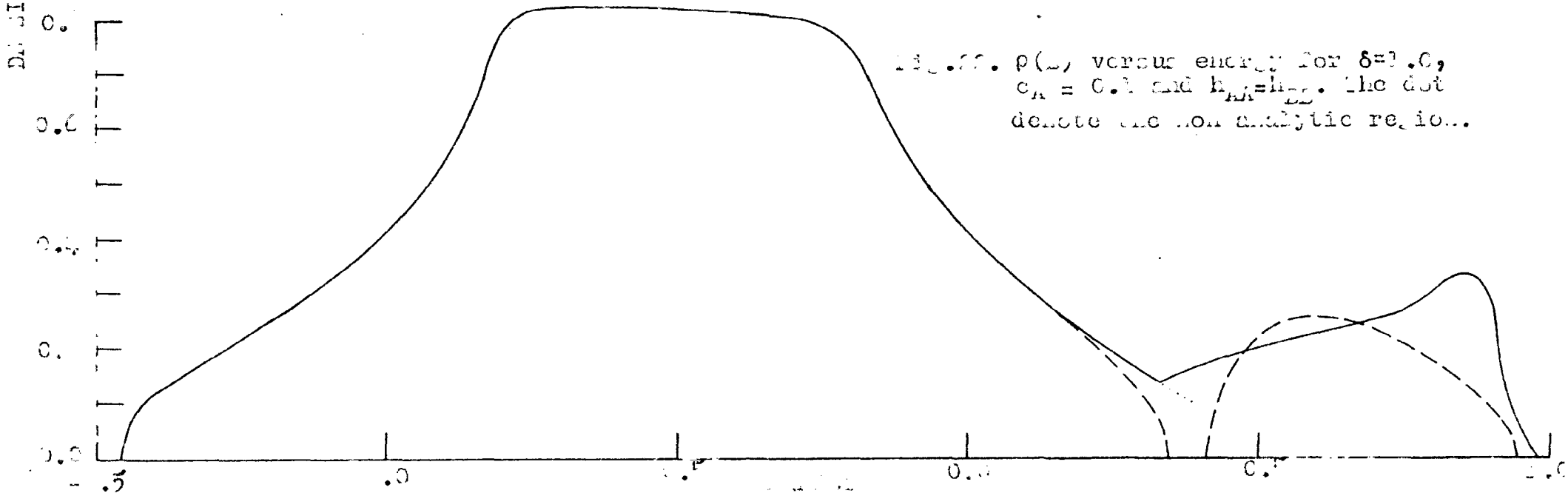

Fig. 12. $\rho(\epsilon)$ versus energy for $\delta = 1.0$, $c_A = 0.1$ and $h_{AA} = h_{BB}$. The dot denotes the non analytic region.

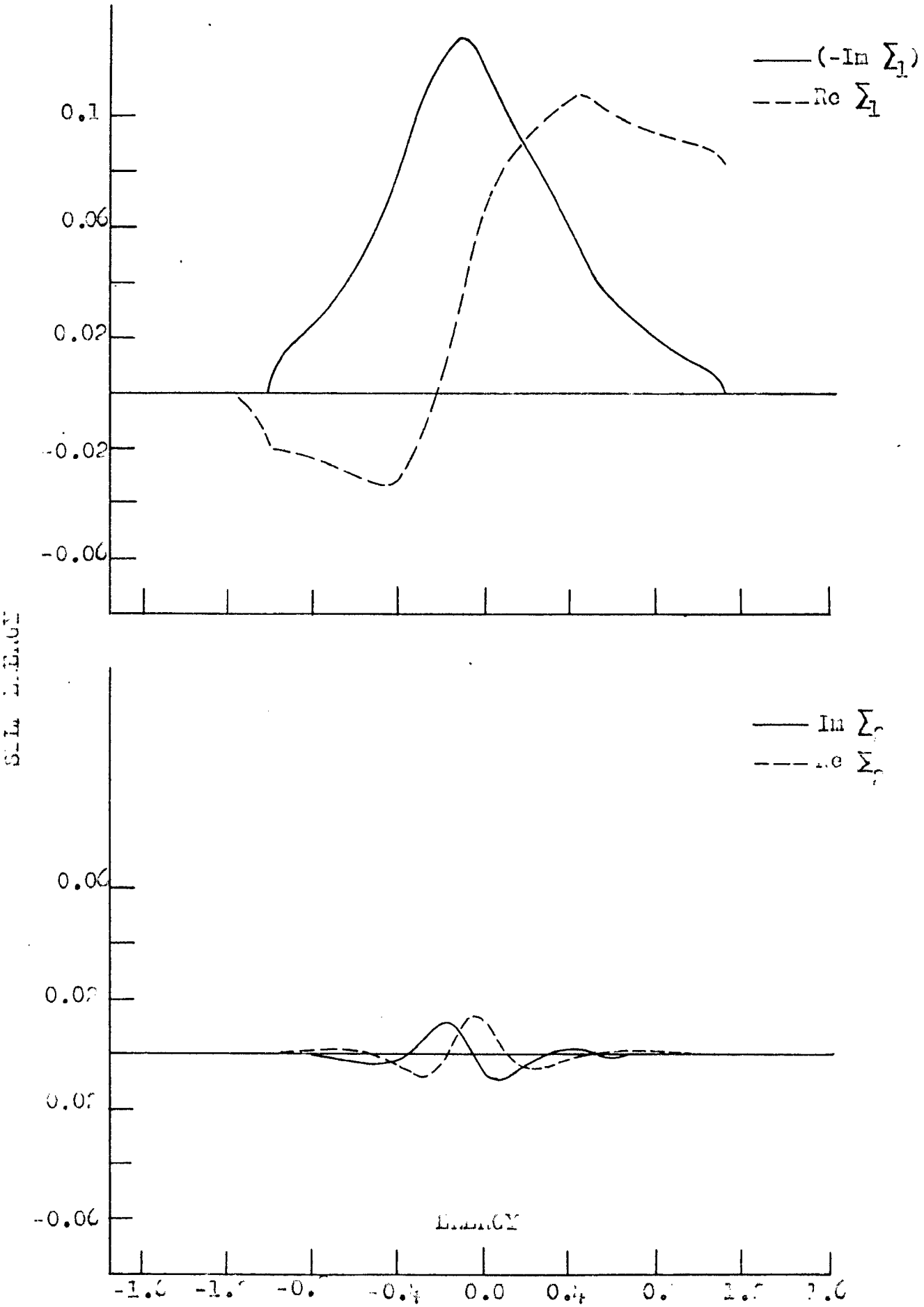

[illegible] real and imaginary parts of coherent potentials $\Sigma_1(E)$ and $\Sigma_2(E)$ versus E, for δ=0.4, c_A=0.5 and $t_{AA} = t_{BB}$. The scales are in arbitrary units.

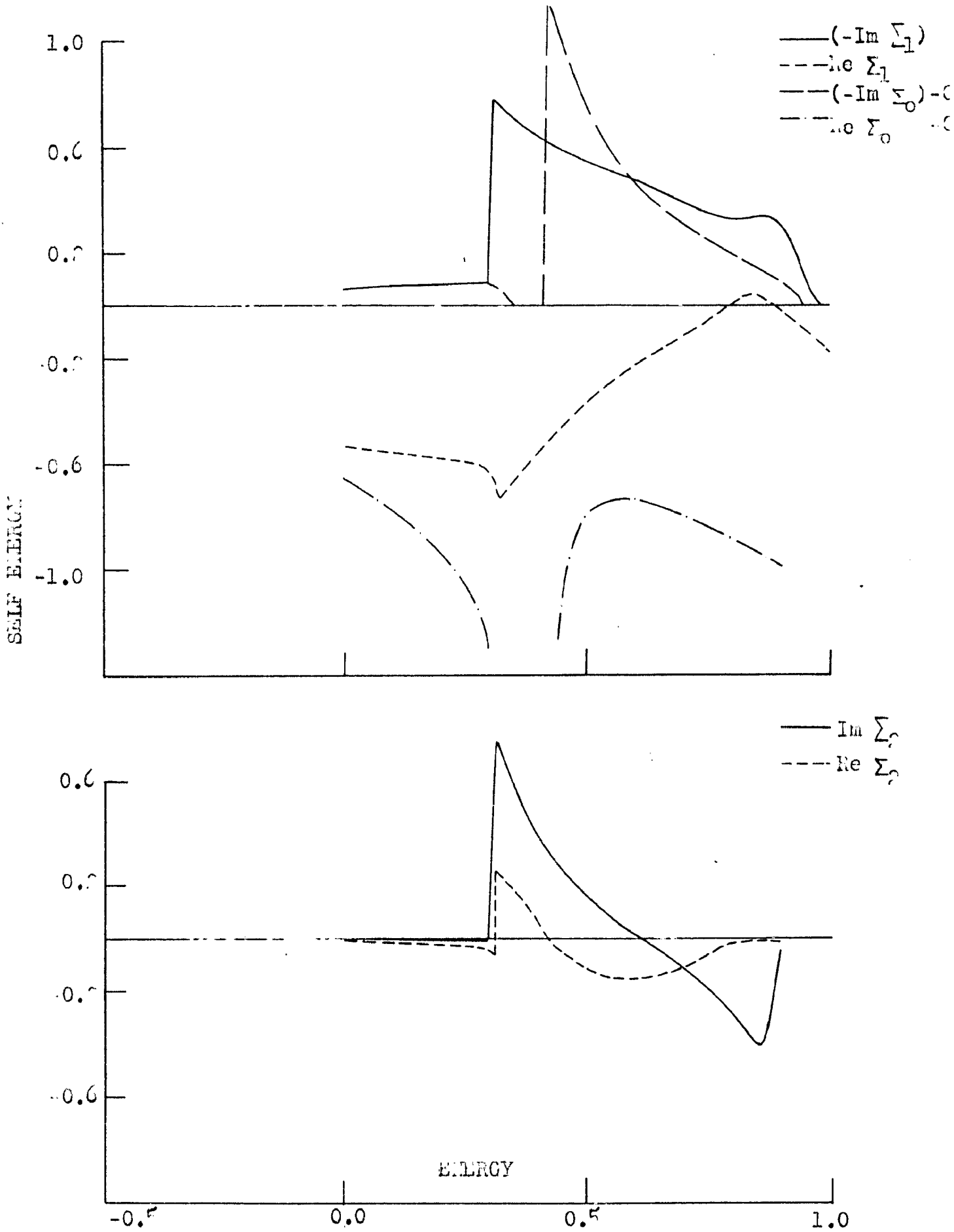

Fig. 7. Real and imaginary parts of coherent potentials $\Sigma_1(E)$ and $\Sigma_2(E)$ versus E for $\delta = 1.0$; $c_A = 0.1$ and $h_{AA} = h_{BB}$.

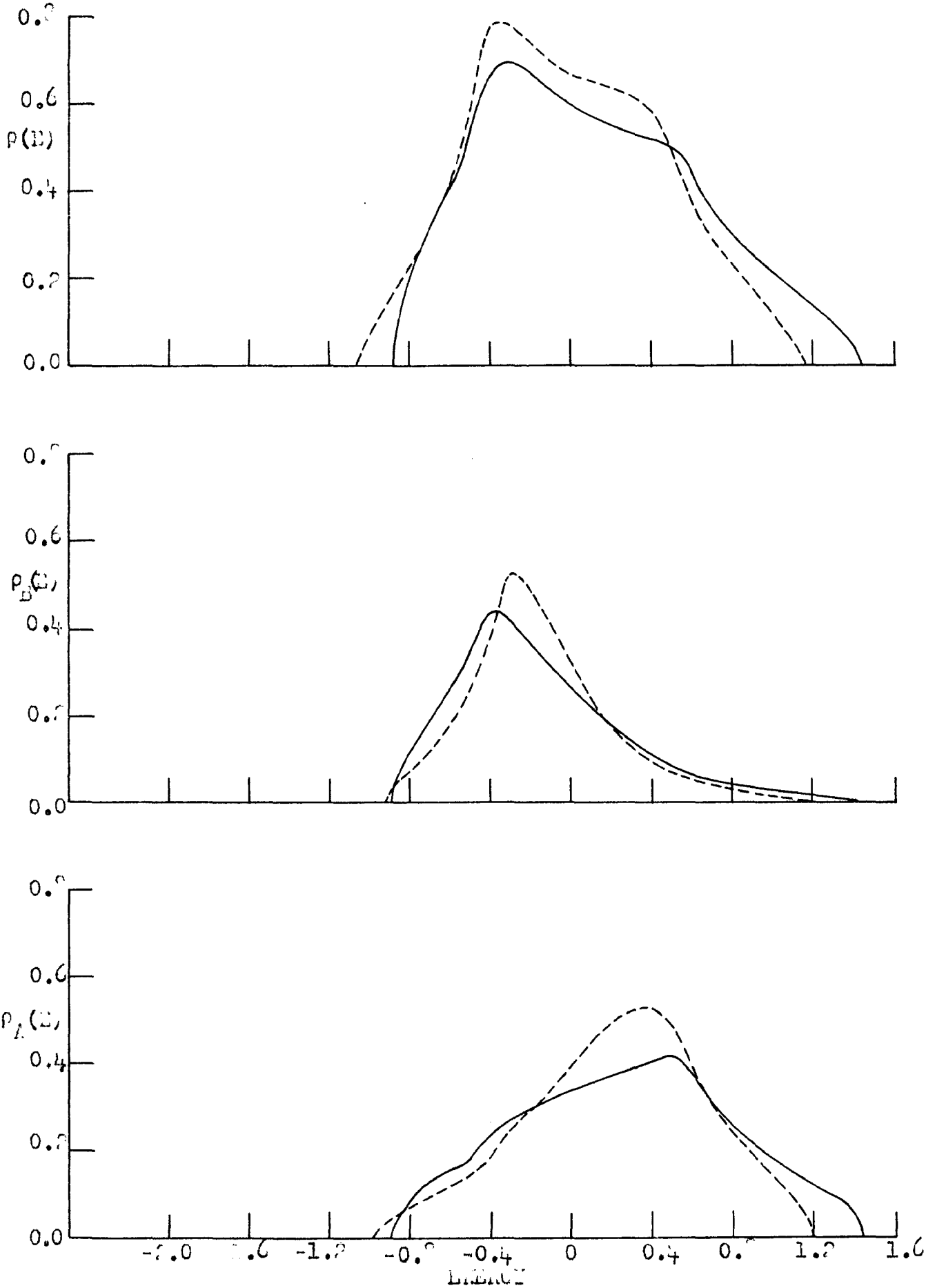

Fig. 5. $\rho(E)$, $\rho_A(E)$ and $\rho_B(E)$ versus E for $\delta = 0.4$, $\epsilon_A = 0.0$ and $h_{AA} = 3/2\ h_{BB}$. (——) shows the results of pair calculation, and (---) shows the results of BLD (Ref. 1).

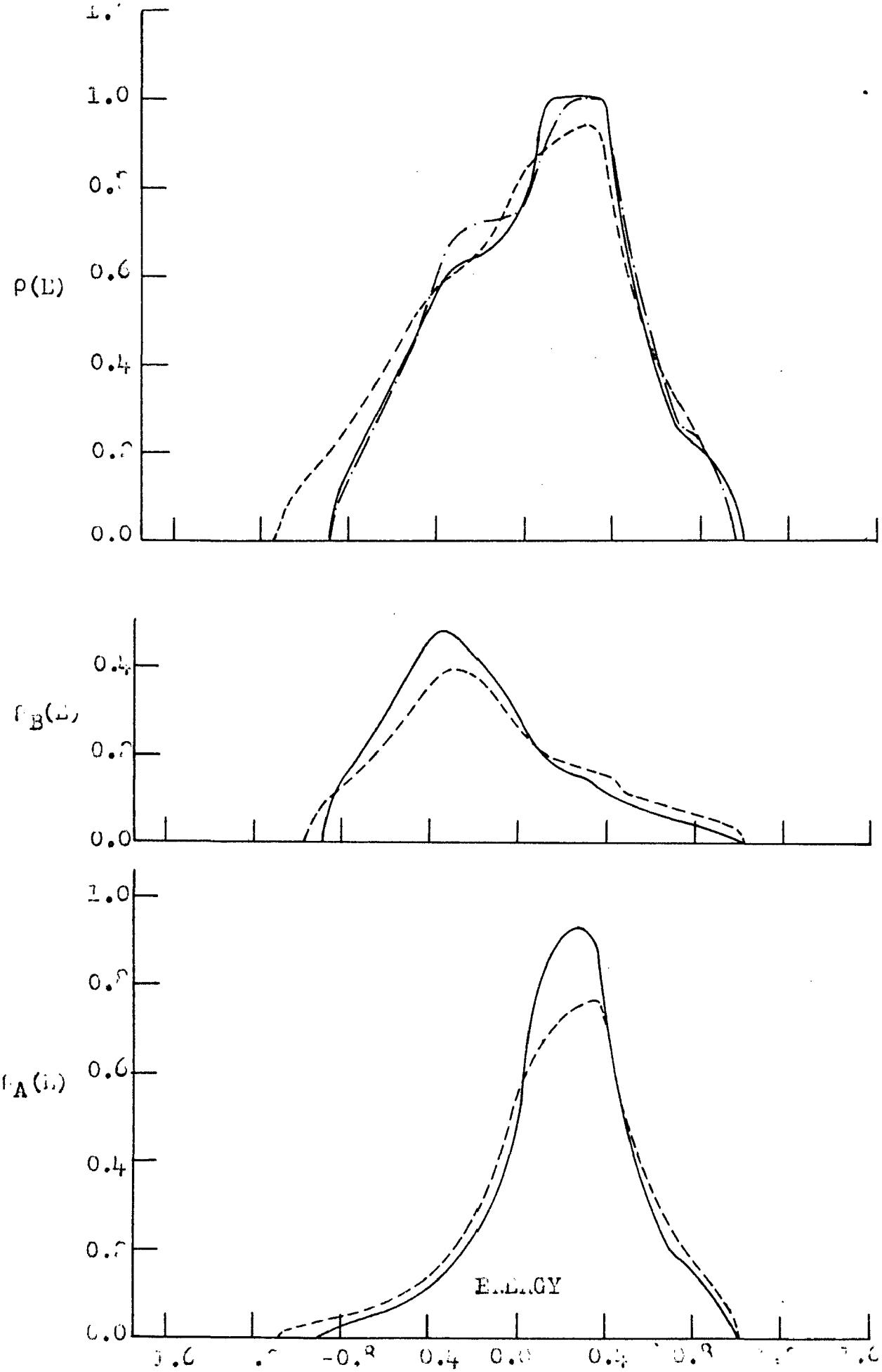

Fig. 6. $\rho(E)$, $\rho_A(E)$ and $\rho_B(E)$ versus E for $\delta = 0.1$, $c_A - 0.6$ and $h_{AA} = 2/3\ h_{BB}$. Notation is as in Fig. 5. (—·— curve has been described in the text.

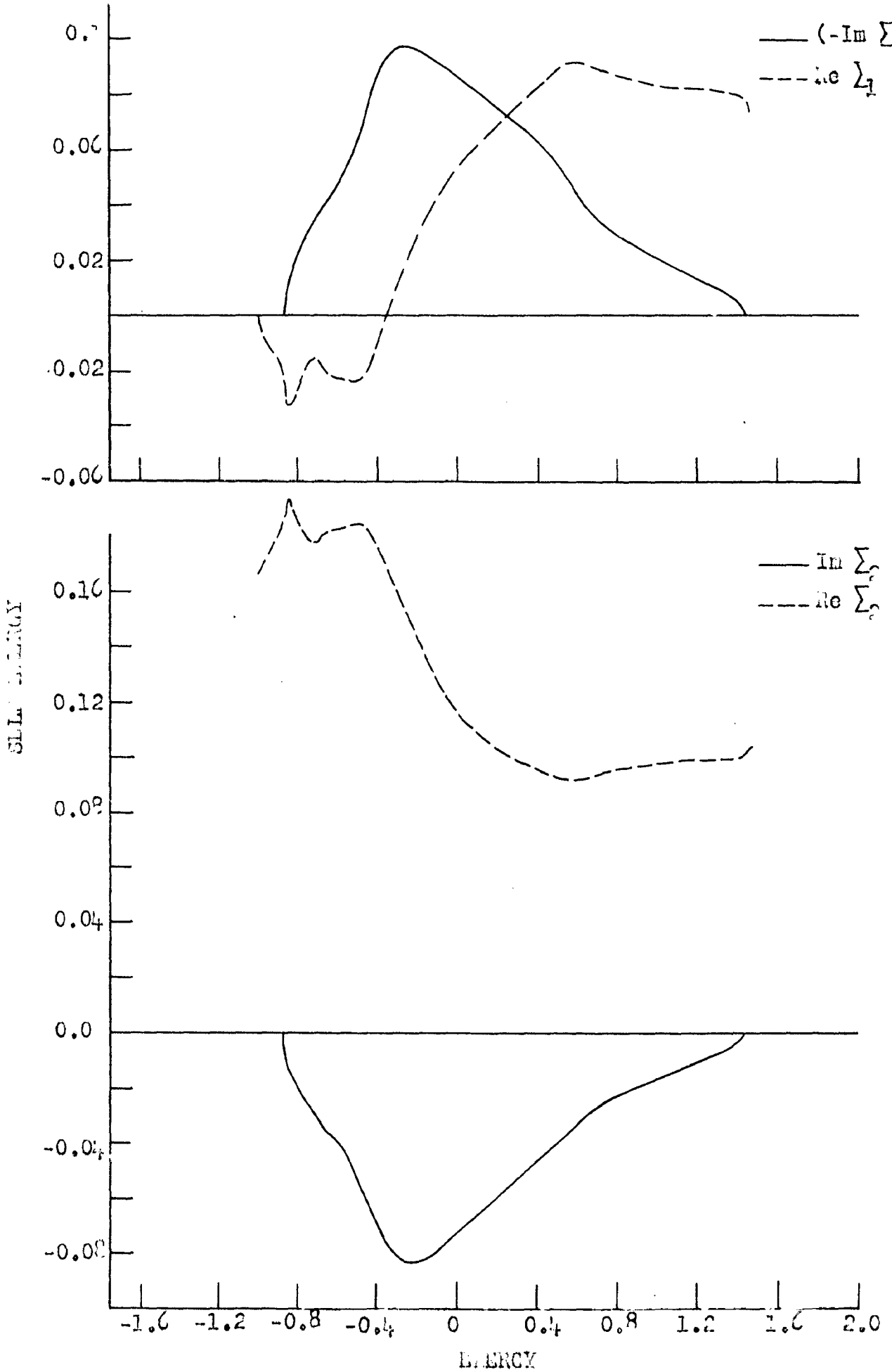

Fig. 7. Real and imaginary parts of $\Sigma_1(E)$ and $\Sigma_2(E)$ versus E for $\delta = 0.4$, $c_1 = 0.6$ and $h = 3h_{HF}$

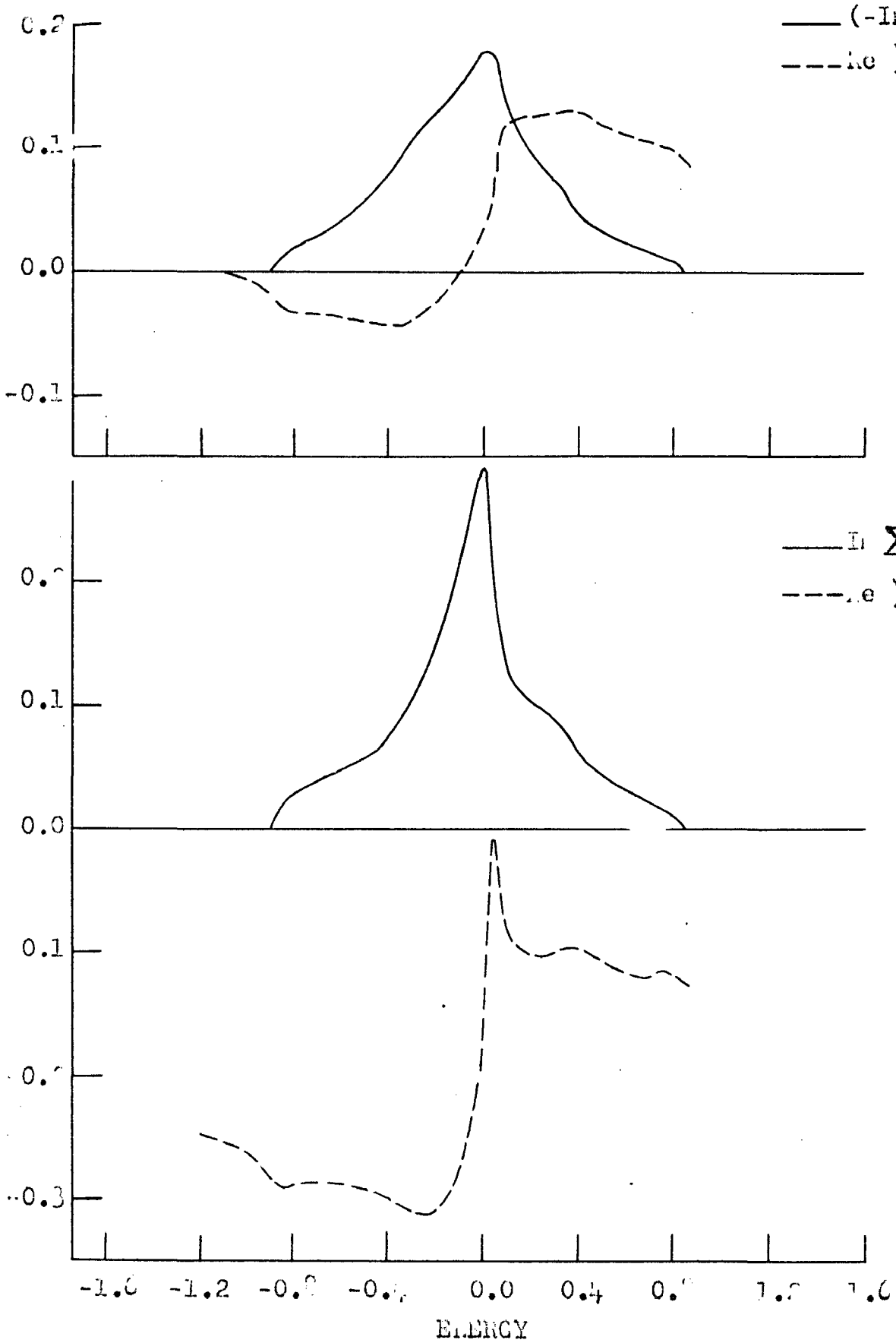

Fig. 2. Real and imaginary parts of $\Sigma_1(E)$ and $\Sigma_2(E)$ versus E for $\delta = 0.$, $\epsilon_A = 0.$ and $h_A = \frac{2}{3}H_{AB}$.

CHAPTER 5

Localisation

We finally turn to the most fascinating, yet controversial phenomenon in the study of disordered systems: exciton localization caused by disorder. Anderson[86] first suggested that under same conditions an electron cannot diffuse in a random lattice. Using a tight-binding model which goes under his name, Anderson presented the first quantitative estimates of the critical disorder which produces such localization.

There are two competing processes that must be accounted for: first, the potential fluctuations favouring localization; and secondly the fact that however deep the well the electron may experience, it can always quantum mechanically tunnel away with finite probability. The subtle balance between these two competing phenomena is the ultimate cause of localization. We can express the problem of wave propagation in a given system in terms of the wave amplitudes at fixed atomic sites. The wave equation takes the form of a set of coupled linear equations for those amplitudes. The propagating character of the wave is expressed mathematically through the existence of non-vanishing transfer matrix elements coupling the amplitudes at a given site with those of neighbouring sites. If the transfer matrix elements were zero, the eigenmodes of the system would be non-propagating oscillations associated with each atomic site. As the transfer matrix elements are turned on, an oscillation formerly associated with one specific site would propagate to neighbouring sites

and from them on giving thus rise to a wave propagating through the system. This propagation however does equally strongly depend on another factor, namely, the matching of eigenfrequencies of oscillations at the sites i and j. The closer the eigenfrequencies the easier the transfer of energy is. Thus the most favourable condition for propagation is achieved when all the eigenfrequencies are the same. The wave can then propagate through the whole medium without any scattering in the form of Bloch's solution. These states are extended throughout the space, with a perfectly horizontal envelope. When a little disorder is introduced, and we depart from the ideal condition of having all the eigenfrequencies the same, the wave is scattered, the wave function remains no longer periodic and has random sign and fluctuating amplitude across the system. We expect two possibilites: first., the wave function may remain extended with a horizontal envelope (in the sense that there is always a finite probability of the electron being somewhere in its neighbourhood.) These are the extended states of disordered system. Secondly, the wave may be attenuated in such a way that it would cease to propagate, thus giving rise to localized eigenmodes. The envelope of localized states is quite different in character; It becomes humped over the region of localization and falls off to zero far away. How the wave function falls away from the region of localization is a matter of conjecture. Mott defines it to fall off like $\exp(-Y|\vec{r}-\vec{r}_o|)$

from the centre $\vec{r}_o$ of the localized region. Thouless and Last[87] suggest that in addition to exponentially localized states there are also states localized by 'power laws'. Thus the existence or not of localized states depends on the strength of transfer matrix elements and the difference in the eigenfrequencies associated with each site. The more random the system, the larger the spread in eigenfrequencies is and consequently the more favourable the situation is for localization.

Localization can be defined in an alternative way in terms of conductivity. Mott defines an energy to be localized if the configuration averaged d.c. conductivity σ (E) vanishes for that energy, in an energy range where the density of states is finite.

We now introduce the model which we have used for our localization studies. We work within the Mott-CFO(after Cohen, Fritsche and Ovshinsky) model[88], which states that the extended states in the centre of the band and the localized states tailing deep into the band gap of the ordered system are separated by sharp mobility edges E_c. At a critical degree of disorder γ_c measured by the ratio of the spread in well-depths (caused by disorder) to the band width-suddenly the entire spectrum becomes localized. This transition is called Anderson transition.

Following Anderson[86] we adopt the following criterion for localization: let $P_{oo}(\infty)$ be the probability of re-discovering a particle at a particular Wannier state $|0\rangle$as

$t \to \infty$ if initially ($t=0$) the particle was at the state $|0\rangle$, then the existence of localized eigenstates overlapping with $|0\rangle$ is equivalent to $P_{oo}(\infty) \neq 0$.

1. GENERALY THEORY

The Hamiltonian in Anderson's model is expressed as,

$$\langle n|H|m\rangle = \varepsilon_n \delta_{nm} + V_{nm}, \qquad \ldots (1.1)$$

$$V_{nm} = V \quad \text{if n and m are nearest neighbours,}$$
$$= 0 \quad \text{otherwise.}$$

ε_n are distributed with a probability distribution $p(\varepsilon_n)$. Corresponding to H we define a resolvent as before, $G(Z) = (ZI-H)^{-1}$. For $t>0$, the wave function can be expressed in terms of the amplitudes at given sites,

$$\psi(t) = \sum_n C_n(t)|n\rangle , \qquad \ldots (1.2)$$

$$\text{then} \quad P_{oo}(t) = \lim_{t\to\infty} \frac{1}{t} \int_0^t |C_o(t')|^2 dt'. \qquad \ldots (1.3)$$

It can be shown[68] that,

$$P_{oo}(t) = \int_{-\infty}^{\infty} p_{oo}(E)\,dE, \qquad \ldots (1.4)$$

$$\text{where,} \quad p_{oo}(E) = \lim_{\delta \to o^+} \frac{\delta}{\pi} |G_{oo}(E+i\delta)|^2 .$$

G_{oo} is the diagonal element of Green's function, i.e. $G_{oo}(E+i\delta) = \langle 0|(E+i\delta-H)^{-1}|0\rangle$. It is clear from (1.4) that localization is related to the analytic properties of the Green's function. Introducing a self-energy $\sum_o(E)$ through the definition, $G_{oo}(E) = (E-\varepsilon_o-\sum_o)^{-1}$, we get p_{oo} in terms

of $\sum_o$ as,

$$p_{oo}(E) = \lim_{\delta \to 0^+} \frac{\delta}{\pi} \frac{\text{Im } G_{oo}(E+i\delta)}{2i\delta - [\sum_o(E+i\delta) - \sum_o(E-i\delta)]} . \quad \ldots (1.5)$$

Writing $\sum_o(Z) = E_o(Z) - i\Delta_o(Z)$ and $G_{oo}(Z) = G^R_{oo}(Z) - in_o(Z)$ in terms of real and imaginary parts, where $n_o(E) = \delta(E-\varepsilon_o-\sum_o)$, we get from (1.5),

$$p_{oo}(E) = \lim_{\delta \to 0^+} \left\{ \frac{n_o(E)}{1 + \frac{\Delta_o(E)}{\delta}} \right\} . \quad \ldots (1.6)$$

For an infinite disordered system, the complete spectrum of the Hamiltonian can be separated into two parts. (i) Extended part $\mathcal{E}$: this constitutes a true branch cut for $G_{oo}(Z)$ along the real axis. On it the spectral measure is absolutely continuous. $\Delta_o(Z) \to$ a finite quantity as $\delta \to 0^+$ on a set in $\mathcal{E}$ of finite measure. (ii) Localized part $\mathcal{L}$: this consists of a dense set which does not constitute a true branch cut. On it the spectral measure is singularly continuous and $\Delta_o(Z) \to 0$ as $\delta \to 0^+$ except on a set in $\mathcal{L}$ of measure zero. Whenever $E \in \mathcal{E}$, we have $\lim_{\delta \to 0^+} \frac{\Delta_o}{\delta} \to \infty$, so $p_{oo}(E) = 0$. This is what we expect. p_{oo} can also vanish because of the poles of $\sum_o$. But Economou and Cohen[68] have shown that the poles of $\sum_o(Z)$ coincide with the zeros of $G_{oo}(Z)$. When $G_{oo}(Z)$ is zero we are in a gap, so the possibility is trivial. We are left with the possibility that the only contributions to p_{oo} comes from the bound and localized states, i.e. from the part of the spectrum consisting of discrete poles, or continuous bits which have the 'singular continuity' character.

Here $\underset{\delta\to o^+}{\text{Lim}} \frac{\Delta_o(Z)}{\delta} \to$ a finite quantity $\left.\frac{\partial \Delta_o}{\partial Z}\right|_{Z\to E} (=\Delta_o')$, and since within the continuous spectrum $n_o(Z)$ is non-zero almost everywhere, $p_{oo}(E)$ will be non-zero. Now $G_{oo}(Z)$ may be written as $\sum_i f_i (Z-E_i)^{-1}$, where E_i are the energy eigenvalues corresponding to the eigenfunctions $|\psi_i\rangle$, $f_i = \langle o|\psi_i\rangle\langle\psi_i|o\rangle$ is the probability that an electron in the eigenstate $|\psi_i\rangle$ will be on the site 0. Thus with the help of (1.4) we obtain,

$$P_{oo} = \int_{-\infty}^{\infty} p_{oo}(E)\,dE = \sum_i f_i^2 . \qquad \ldots (1.7)$$

Since $0 < f_i < 1$ with $\sum_i f_i = 1$, we get $0 < P_{oo} < 1$, i.e. $p_{oo}(E)$ varies between 0 and 1.

We examine the consequence of allowing the dimensions of the system to approach infinity. If N be the number of sites in a finite system and $P_N(\Sigma_{o,N};E)$ be the probability distribution of $\Sigma_{o,N}$ for E belonging to the spectrum of infinite ($N=\infty$) system, then following Economou and Cohen[89] and Licciardello and Economou[90] we state that in the localized region $\underset{N\to\infty}{\text{Lim}} P_N(\Sigma_{o,N};E)$ exists whereas it does not exist in the extended region. One can also consider the probability distribution of Im Σ_o i.e. Δ_o. $\underset{\delta\to o^+}{\text{Lim}}\ \underset{N\to\infty}{\text{Lim}}$ $P_N(\Delta_{o,N};E+i\delta)$ exists and is a smooth function of E in the extended regime, whereas in the localized regime $\underset{\delta\to o^+}{\text{Lim}}\ \underset{N\to\infty}{\text{Lim}}$ $P_N(\frac{\Delta_{o,N}}{\delta};E+i\delta)$ exists and is a smooth function of E.

Thus the existence of localized eigenstates depends on the existence of the probability distribution of Σ_o. In order to study the properties of the probability distribution of Σ_o, one has to express it in terms of

~~is resolved by writing a renormalized perturbation expression (RPE)~~ -90-92

known quantities. A perturbative expansion of $\sum_o$ in terms of site energies with hopping integral as perturbation diverges for all energies. The problem is resolved by writing a renormalized perturbation expansion (RPE)[90,91,92] of $\sum_o$:

$$\sum_o(E) = \sum_{n\neq o} V_{on}\left[E-\varepsilon_n-\sum_n^o\right]^{-1}V_{no} + \sum_{\substack{n\neq o\\ n'\neq o,n}} V_{on'}\left[E-\varepsilon_{n'}-\sum_{n'}^{o,n}\right]^{-1} V_{n'n} \times\left[E-\varepsilon_n-\sum_n^o\right]^{-1}V_{no}+\ldots, \qquad \ldots (1.8)$$

or equivalently

$$\sum_o(E) = \sum_{n\neq o} V_{on} \frac{1}{E-\varepsilon_n-\sum_{k\neq n,o} V_{nk}\frac{1}{E-\varepsilon_k-\ldots}V_{kn}+\ldots} V_{no}+\ldots\ldots \qquad \ldots(1.9)$$

The superscripts o,n,...denote that the corresponding quantity has been calculated for $\varepsilon_o,\varepsilon_n,\ldots = \infty$. The summations in (1.8) run over all self-avoiding paths i.e. all paths which begin and end at 0 and do not visit the same site more than once. For a system of finite size both the infinite series and the continued fraction terminate and (1.8) and (1.9) form a closed solution of $\sum_o$. For infinite series we cannot make this statement unless the infinite step iteration procedure implied in (1.9) and the series itself converges in probability. It can be assumed[89,90] that the convergence of the series implies the convergence of the iteration procedure. In one dimensional case, the series terminates at the first step and only the iteration procedure remains. One can show[93] that the latter always converges when the

degree of randomness is non-zero. This was the basis of the statement that in 1-dimensional disordered systems all states are localized. Hence following our previous discussion we infer that the convergence of RPE implies localization and the divergence implies the extension. We may rewrite (1.9) as,

$$\sum_{0,N}(E) = \sum_{M=2}^{N} \sum_{0,N}^{(M)}(E), \qquad \ldots (1.10)$$

where $\sum_{0,N}^{(M)}$ is the sum of all diagrams visiting M sites. If the eigenstates at E are localized then: (a) the probability distribution of $\sum_{0,N}^{(M)}(E)$ converges as $N\to\infty$, and (b) the contributions of all terms $|\sum_{o}^{(M)}(E)|$ where $M > M_o$ are negligible as $M_o\to\infty$. The reason for (a) is as follows. $\sum_{0,N}^{(M)}(E)$ can be expressed in terms of finite number $G_{n,N}^{o,\ldots}$, for each of which the probability distribution converges as $N\to\infty$ (if states at E are localized, probability distribution of $\sum_o$ converges and same is true for all other $\sum_n^o$, $\sum_{n'}^{o,n}$ etc.). Thus if the eigenstates of H corresponding to E are localized, so are the eigenstates of $H^{o,\ldots}$ at E (if any). If (b) is satisfied, (a) is satisfied too[94]. Thus the problem reduces to look at the probability distribution of $\sum_o^{(M)}(E)$ as $M\to\infty$, i.e. of

$$\sum_o^{(M)}(E) \equiv V \sum_{\substack{\text{all diagrams}\\ \text{of order } M(\to\infty)}} \frac{V}{e_1}\cdot\frac{V}{e_2}\cdots\frac{V}{e_M} \qquad \ldots (1.11)$$

Here $e_i \equiv E-\varepsilon_i-\sum_i^{o,n,\ldots i-1}$ and the sum extends over all M-step self-avoiding diagrams starting and ending at 0.

A particular contribution to $\sum_o^{(M)}$ is,

$$T_j^{(M)} \equiv V^M \frac{1}{e_1} \cdot \frac{1}{e_2} \cdots \frac{1}{e_M} \qquad \ldots (1.12)$$

Even if one knows the probability distribution of $T_j^{(M)}$, the problem is not solved since one ought to know the degree of statistical correlation among the various $T_j^{(M)}$. There are roughly $K^M, T_j^{(M)}$ terms contributing to $\sum_o^{(M)}$, where K, the connectivity of the lattice, is related to the number C_M of self-avoiding paths of M steps by the relation, $K = \lim_{M\to\infty} \frac{1}{M} \ell n C_M$. One can proceed with the two limiting cases of 'no correlation' and 'extremely strong correlation'. This has given rise to two schools of thought.

2. NO-CORRELATION CASE

It is easy to see that there is atleast one case where the different contributions due to a certain number of steps are statistically uncorrelated. This is the case of an infinite Cayley tree lattice as shown in the Fig.29. The topology of the Cayley tree indicates that due to the absence of closed polygonal paths on it, the infinite series(1.8) terminates after the first term. Only the second order terms are retained. The sum over n runs only over the nearest neighbours of the site under consideration. If K is the connectivity of the lattice, so that there are (K+1) nearest neighbours, then the first sum in (1.9) runs over (K+1) independent terms and the subsequent sums in the continued fraction have K independent terms. For this case

the problem of localization has been solved exactly by Abou-Chaora et.al.[95] Without going into the details of their method, we briefly mention what they have done. They construct an integral-eigenvalue equation involving the joint probability distribution of the real and imaginary parts of the self-energy and taking advantage of the fact that imaginary part of self-energy tends to zero as δ(imaginary part of energy) tends to zero, they evaluated the mobility edge as the point where the integral equation ceases to have solution. Their theory is thus a theory of the breakdown of localized states. Having known the localized regime from this work we have attempted to determine the nature of the wave functions (i.e. the knowledge of p_{oo} and L_{eff}, the spatial extent) in this regime.

In a disordered system these parameters are configuration dependent and a statistical description demands the knowledge of configuration averages of the type $\langle p_{oo} \rangle$. For a convincing calculation of $\langle p_{oo}(E) \rangle$ we have to resort to more sensitive averaging procedures than the usual effective medium type. To this date no satisfactory calculation of these quantities has been reported, apart from the linear chain case.[95] We have presented a formulation[97] for the calculation of $\langle p_{oo}(E) \rangle$ on a Cayley tree lattice with diagonal disorder and Cauchy probability distribution for site energies. At the outset we have assumed that we have the knowledge of mobility edges calculated by Abou-Chacra et.al.[95]

From eqn.(1.6) and the subsequent discussion, we see that for calculating $\langle p_{oo}(E) \rangle$ in the localized regime we have to have the knowledge of the joint probability distribution of E_o and Δ_o', $\mathcal{F}_+(E_o,\Delta_o')$. We have $\mathcal{F}_+(E_o,\Delta_o') = \mathcal{F}(E_o,\Delta_o')\theta(\Delta_o')$, $\theta(\Delta_o')$ vanishes for negative values of Δ_o' and is unity otherwise. We have to do this because Δ_o and hence Δ_o' is always positive so as to yield positive density of states. In the localized regime we can write (1.6) as

$$p_{oo}(E) = \delta(E-\varepsilon_o-E_o)/(1+\Delta_o'). \qquad \ldots (2.1)$$

$$\begin{aligned} \text{So, } p_{oo}(E) &= \int_{-\infty}^{\infty} d\varepsilon_o \int_{-\infty}^{\infty} dE_o \int_{o}^{\infty} d\Delta_o' p(\varepsilon_o)\mathcal{F}_+(E_o,\Delta_o') \frac{\delta(E-\varepsilon_o-E_o)}{1+\Delta_o'} \\ &= \int_{-\infty}^{\infty} dE_o \int_{o}^{\infty} d\Delta_o' p(E-E_o)\mathcal{F}_+(E_o,\Delta_o') \frac{1}{1+\Delta_o'} \\ &= \int_{-\infty}^{\infty} dE_o \int_{-\infty}^{\infty} d\Delta_o' p(E-E_o)\mathcal{F}(E_o,\Delta_o')\theta(\Delta_o')\frac{1}{1+\Delta_o'} \\ &= \int_{-\infty}^{\infty} dE_o \int_{o}^{\infty} d\Delta_o' p(E-E_o)\,\mathcal{F}(E_o,\Delta_o')\,\frac{1}{1+\Delta_o'}. \qquad \ldots (2.2) \end{aligned}$$

$p(\varepsilon_o)$ is the probability density of ε_o. E denotes the energy measured with respect to E_c, the mobility edge. Evaluation of $\mathcal{F}(E_o,\Delta_o')$ has been elaborated in the following. E_o and Δ_o' on a Cayley tree are given in the localized regime as

$$E_o = \sum_{j=1}^{K+1} \frac{V^2}{E - \varepsilon_o - E_j^o}, \qquad \ldots (2.3a)$$

$$\Delta_o' = \sum_{j=1}^{K+1} \frac{V^2(1+\Delta_j^{o\,\prime})}{(E-\varepsilon_o-E_j^o)^2}. \qquad \ldots (2.3b)$$

The subscript denotes the contribution from the particular site and the superscript denotes the site removed. We have seen that because of the topology of the Cayley tree (K+1) factors in the sum in (2.3) are statistically independent.

For convenience we rewrite (2.3) as

$$\sum_o = \sum_j \frac{V^2}{x} \equiv \sum_j X \,, \qquad \ldots (2.4a)$$

$$\Delta_o' = \sum_j \frac{V^2 y}{x^2} \equiv \sum_j Y \,, \qquad \ldots (2.4b)$$

and
$$E_j^o = E-\varepsilon_o-x \equiv f(x) \,, \qquad \ldots (2.5a)$$

$$\Delta_j^{o\,\prime} = y-1 \equiv g(y). \qquad \ldots (2.5b)$$

$\Delta_j^{o\,\prime}$ never becomes negative, therefore Y and Δ_o' are always positive. Let us denote joint probability distribution of X and Y as $G_+(X,Y)$ for positive Y and $G(X,Y)$ for Y lying anywhere between $-\infty$ and ∞. The similar quantities for E_j^o and $\Delta_j^{o\,\prime}$ are denoted by $F_+(E_j^o,\Delta_j^{o\,\prime})$ and $F(E_j^o,\Delta_j^{o\,\prime})$. We can write the Radon transform[98] F_+ as

$$G_+(X,Y) = \int_{-\infty}^{\infty} d\varepsilon_o \int_{-\infty}^{\infty} dE_j^o \int_0^{\infty} d\Delta_j^{o\,\prime} F_+(E_j^o,\Delta_j^{o\,\prime})\,\delta(E_j^o-f(x))\,\delta(\Delta_j^{o\,\prime}-g(y))\,p(\varepsilon_o) \qquad \ldots (2.6)$$

In further calculations we will require Fourier transforms of these distribution functions. To facilitate this we introduce $\theta(\Delta_j^{o\,\prime})$ to make $\Delta_j^{o\,\prime}$ vary between $-\infty$ and ∞ and thus

get a relation between G and F

$$G(X,Y) = \int_{-\infty}^{\infty} d\varepsilon_o \int_{-\infty}^{\infty} dE_j^o \int_{-\infty}^{\infty} d\Delta^{o'}_j \{F(E_j^o,\Delta_j^{o'})\theta(\Delta_j^{o'})\}\delta(E_j^o - f(x))\delta(\Delta_j^{o'} - g(y))p(\varepsilon_o). \quad \ldots (2.7)$$

We have $G_+(X,Y) = G(X,Y)\theta(Y)$ and $F_+(E_j^o,\Delta_j^{o'}) = F(E_j^o,\Delta_j^{o'})\theta(\Delta_j^{o'})$.

The Fourier transform of (2.7) is

$$G(k_1,k_2) = \frac{1}{(2\pi)^2} \int_{-\infty}^{\infty} dx \int_{-\infty}^{\infty} dy \{F(f(x),g(y))\theta(g(y))\} \int e^{-(k_1X+k_2Y)i} x \int_{-\infty}^{\infty} p(\varepsilon_o)\, d\varepsilon_o. \quad \ldots (2.8)$$

Again in terms of Fourier transform we have

$$F(f(x),g(y))\theta(g(y)) = \int_{-\infty}^{\infty}\int_{-\infty}^{\infty} F(k_1',k_2') e^{i[f(x)k_1' + g(y)k_2']} dk_1' dk_2', \quad \ldots (2.9)$$

so that (2.8) is written as

$$G(k_1,k_2) = \frac{1}{2\pi} \int_{-\infty}^{\infty} dx \int_{-\infty}^{\infty} dk' P(k') F\left(k', \frac{k_2V^2}{x^2}\right) \exp\left[ik'E - ik'x - \frac{ik_1V^2}{x} - \frac{ik_2V^2}{x^2}\right] \quad \ldots (2.10)$$

where $P(k')$ is the Fourier transform of $p(\varepsilon_o)$ and the following definition has been used

$$\delta\left(k_2' - \frac{V^2k_2}{x^2}\right) = \frac{1}{2\pi} \int_{-\infty}^{\infty} \exp\left[i\left(k_2' - \frac{V^2k_2}{x^2}\right)y\right] dy \quad \ldots (2.11)$$

For a Cayley tree we have the following relation between $G(k_1,k_2)$ and $\mathcal{F}(k_1,k_2)$, the Fourier transform of $\mathcal{F}(E_o,\Delta_o')$.

$$\mathcal{F}(k_1,k_2) = \{G(k_1,k_2)\}^{K+1}$$

$$= \left\{\frac{1}{2\pi} \int_{-\infty}^{\infty} dx \int_{-\infty}^{\infty} dk' P(k') F\left(k', \frac{k_2V^2}{x^2}\right) \exp\left[ik'E - ik'x - \frac{ik_1V^2}{x} - \frac{ik_2V^2}{x^2}\right]\right\}^{K+1} \quad \ldots (2.12)$$

Given $P(k') = \exp[-\gamma \mathrm{Sgn}(k')k']$ i.e. Cauchy distribution for site energies, it can be shown by substitution that a solution of (2.12) is given by

$$F(k_1,k_2) = \exp[\{-im_1-n_1\mathrm{Sgn}(k_1)\}k_1+\{-im_2-n_2\mathrm{Sgn}(k_2)\}k_2],$$
$$\mathfrak{F}(k_1,k_2) = \exp[\{-ia-b\ \mathrm{Sgn}(k_1)\}k_1+\{-i\phi-\psi\ \mathrm{Sgn}(k_2)\}k_2], \quad \ldots (2.13)$$

with $m_1-in_1 \equiv \hat{Z}_1$, $m_2-in_2 \equiv \hat{Z}_2$, $a-ib \equiv \hat{\zeta}_1$, $\phi-i\psi \equiv \hat{\zeta}_2$

and
$$\mathrm{Sgn}(k) = +1 \quad , \quad k>0$$
$$= -1 \quad , \quad k<0$$
$$= 0 \quad , \quad k=0$$

With this substitution, the k'-integral becomes,

$$\int_{-\infty}^{\infty} dk'\ e^{-\gamma k'}\exp[i(E-x)-i\hat{Z}_1]k' + \int_{-\infty}^{0} dk' e^{\gamma k'}\exp[i(E-x)-i\hat{Z}_1^*]k'$$
$$= \int_0^{\infty} dk'\ e^{-\gamma k'}[\exp i[E-x-\hat{Z}_1]k' + \exp -i[E-x-\hat{Z}_1^*]k']$$
$$= \int_0^{\infty} dk'\ e^{-(\gamma+n_1)k'}[e^{i(E-x-m_1)k'} + e^{-i(E-x-m_1)k'}]$$
$$= \int_0^{\infty} dk' e^{-(\gamma+n_1)k'}\ 2\cos\{(E-x-m_1)k'\}$$
$$= \frac{2(\gamma+n_1)}{(E-m_1-x)^2+(\gamma+n_1)^2} = \frac{1}{i}\left[\frac{1}{x-T} - \frac{1}{x-T^*}\right]$$

where $T = (E-m_1)+i(\gamma+n_1) = E + i\gamma-\hat{Z}_1$

Thus (2.12) can be written as

$$\exp[\{-ia-b\ \mathrm{Sgn}(k_1)\}k_1+\{-i\phi-\psi\ \mathrm{Sgn}(k_2)\}k_2]$$
$$= \left[\frac{1}{2\pi i}\int_{-\infty}^{\infty} dx\left(\frac{1}{x-T} - \frac{1}{x-T^*}\right)\exp -i\left\{\frac{V^2}{x}k_1 + \frac{V^2}{x^2}k_2\right\}\right.$$
$$\left.\exp.\frac{V^2}{x^2}\{-im_2-n_2\mathrm{Sgn}(k_2)\}k_2\right]^{K+1} \quad \ldots (2.14)$$

If $k_1 > 0$ and $k_2 > 0$, (2.14) reduces to

$$e^{-i\hat{\zeta}_1 k_1 - i\hat{\zeta}_2 k_2} = \left[\exp -i\left\{\frac{V^2}{T} k_1 + \frac{V^2}{T^2} k_2\right\} \exp\left\{\frac{V^2}{T^2} k_2 (-i)\hat{Z}_2\right\}\right]^{K+1},$$

or

$$e^{-\zeta_1 k_1 - \zeta_2 k_2} = \exp\left[-\frac{(K+1)V^2}{Z_1+\xi} k_1 + \frac{(Z_2+i)(K+1)V^2}{(Z_1+\xi)^2} k_2\right], \quad \ldots (2.15)$$

where $Z_1 = i\hat{Z}_1$, $Z_2 = i\hat{Z}_2$, $\zeta_1 = i\hat{\zeta}_1$, $\zeta_2 = i\hat{\zeta}_2$, $\xi = \gamma - iE$, $\zeta_1 = b + ia$, $\zeta_2 = \psi + i\phi$ and $-iT = Z_1 + \xi$.

Comparing the coefficients of k_1 and k_2 we get

$$\zeta_1 = \frac{(K+1)V^2}{Z_1+\xi}, \quad \ldots (2.16a)$$

and

$$\zeta_2 = -\frac{(K+1)(Z_2+i)V^2}{(Z_1+\xi)^2} \quad \ldots (2.16b)$$

These relations are at the origin of the Cayley tree. Z_1 and Z_2 can be obtained by writing analogous expressions for the interior of Cayley tree, and these easily turn out to be

$$Z_1 = KV^2/(Z_1+\xi) \quad \ldots (2.17a)$$

$$Z_2 = -KV^2(Z_2+1)/(Z_1+\xi)^2 \quad \ldots (2.17b)$$

If $k_1 > 0$ and $k_2 < 0$, one easily gets after some algebra the following relations,

$$\zeta_1 = (K+1)V^2/(Z_1+\xi)$$

$$\zeta_2^* = \left\{-(K+1)V^2(Z_2+i)/(Z_1+\xi)^2\right\}^*,$$

which shows that the relations (2.16) and (2.17) which

evaluate a,b, and $\emptyset$, remain unaltered. The other cases, ($k_1<0$, $k_2>0$) and ($k_1<0, k_2<0$) also do not change them.

The two pairs of relations (2.16) and (2.17) yield,

$$\zeta_1 = \frac{(K+1)}{K} Z_1 \equiv b+ia \qquad \ldots (2.18a)$$

and

$$\zeta_2 = \frac{(K+1)}{K} Z_2 \equiv \Psi + i\emptyset \qquad \ldots (2.18b)$$

From (2.17a) we get

$$Z_1 = -\frac{(\gamma - iE)}{2} \pm \frac{1}{2}\left[\gamma^2 - E^2 + 4K - 2i\gamma\epsilon\right]^{1/2}$$

In separating real and imaginary parts of this equation, we encounter two situations.

(a) $(E^2-\gamma^2-4K) > 0$: this gives

$$\text{Re } Z_1 = -\frac{\gamma}{2} + \frac{1}{2} r \sin\theta/2 \qquad \ldots (2.19a)$$

$$\text{Im } Z_1 = \frac{E}{2} - \frac{1}{2} r \cos\theta/2 \qquad \ldots (2.19b)$$

(b) $(E^2-\gamma^2-4K) < 0$: this gives

$$\text{Re } Z_1 = -\frac{\gamma}{2} + \frac{1}{2} r \cos\theta/2 \qquad \ldots (2.20a)$$

$$\text{Im } Z_1 = \frac{E}{2} - \frac{1}{2} r \sin\theta/2 , \qquad \ldots (2.20b)$$

where $\theta = \tan^{-1}\left[2\gamma E / |E^2-\gamma^2-4K|\right]$ and $r = \left[4\gamma^2E^2 + (E^2-\gamma^2-4K^2)\right]^{1/4}$,

and the + or - sign is chosen such that Re Z_1 remains positive. This is to satisfy the natural condition that $\mathcal{F}(E_o, \Delta_o')$ is always positive. This will be clear later when the expression for $\mathcal{F}(E_o, \Delta_o')$ is obtained. With the help of (2.19) or (2.20), and (2.18) we get a and b as

$$b = \text{Re}\,\zeta_1 = \frac{K+1}{K} \text{Re} Z_1 \qquad \ldots (2.21a)$$

$$a = \text{Im}\ \zeta_1 = \frac{K+1}{K}\ \text{Im}\ Z_1 \qquad \ldots (2.21a)$$

From (2.16b) and (2.18b) we get

$$\zeta_2(Z_1) = -\frac{i(K+1)}{(Z_1+\xi)^2+K},$$

which may be converted to the form

$$\zeta_2(\zeta_1) = \frac{-i(K+1)}{(\frac{K}{K+1}\zeta_1+\xi)^2+K}, \qquad \ldots (2.22)$$

Its real and imaginary parts are

$$\psi(\zeta_1) = -(K+1)T/(D^2+T^2), \qquad \ldots (2.23a)$$

$$\phi(\zeta_1) = -(K+1)D/(D^2+T^2), \qquad \ldots (2.23b)$$

where $D = (\gamma+\frac{Kb}{K+1})^2-(\frac{Ka}{K+1}-E)^2+K,$ ... (2.24)

and $T = 2(\gamma+\frac{Kb}{K+1})(\frac{Ka}{K+1}-E).$ ... (2.25)

Now the Fourier inversion of $\mathcal{J}(k_1,k_2)$ as given in (2.13), yields

$$\mathcal{J}(E_o,\Delta_o') = 2\pi\,\frac{b/\pi}{(E_o-a)^2+b^2}\cdot\frac{\psi(\zeta_1)/\pi}{[\Delta_o'-\phi(\zeta_1)]^2+[\psi(\zeta_1)]^2} \qquad \ldots (2.26)$$

Substituting this exact distribution function into (2.2) we get

$$\langle p_{oo}(E)\rangle = 2\pi\int_{-\infty}^{\infty}dE_o\int_{o}^{\infty}d\Delta_o' p(E-E_o)\,\frac{b/\pi}{(E_o-a)^2+b^2}\,\frac{\psi/\pi}{(\Delta_o'-\phi)^2+\psi^2}\,\frac{1}{1+\Delta_o'}$$

$$= 2\pi\int_{-\infty}^{\infty}dE_o\int_{o}^{\infty}d\Delta_o'\,\frac{\gamma/\pi}{(E_o-E)^2+\gamma^2}\cdot\frac{b/\pi}{(E_o-a)^2+b^2}\cdot\frac{\psi/\pi}{(\Delta_o'-\phi)^2+\psi^2}\cdot\frac{1}{1+\Delta_o'}, \qquad \ldots (2.27)$$

where $p(E-E_o) = \dfrac{\gamma/\pi}{(E-E_o)^2+\gamma^2}$, ... (2.28)

is the Cauchy distribution for site energies. Δ_o' and E_o are related through (2.3) in a very complicated manner. This makes the exact solution of (2.27) impossible. To get rid of this trouble, we assume Δ_o' and E_o to be independent of each other like in Anderson's upper limit approximation.[74] This approximation has been discussed in the appendix I, and it has been found that though this approximation is very less rigorous as compared to our line of action still it leads to certain complexities that are crucial. Owing to this assumption of taking Δ_o' and E_o to be independent the simplification enables us to solve the Δ_o' part of (2.27). Calling it to be 'I' we have

$$I = \int_o^\infty \frac{1}{1+\Delta_o'} \frac{\psi(\zeta_1)/\pi}{(\Delta_o'-\phi)^2+\psi^2}\, d\Delta_o'$$

$$= \frac{1/\pi}{(1+\phi)^2+\psi^2}\left[(1+\phi)\left(\frac{\pi}{2}-t\right)+\psi \ln\left|\frac{\cos(\tan^{-1}\frac{1+\phi}{\psi})}{\sin(t+\tan^{-1}\frac{1+\phi}{\psi})}\right|\right], \quad \text{... (2.29)}$$

where $t = -\tan^{-1}\dfrac{\phi}{\psi}$ ... (2.30)

Thus (2.27) reduces to

$$\langle p_{oo}(E)\rangle = \frac{2\gamma b}{\pi}\int_{-\infty}^{\infty} \frac{1}{(E_o-E)^2+\gamma^2}\cdot\frac{1}{(E_o-a)^2+b^2}\cdot I\, dE_o. \quad \text{... (2.31)}$$

This can be conveniently solved numerically using 'Gauss-quadrature' method for integration. Equation (2.31) gives the average probability of localization per unit energy interval. It can be related to the average total extent of

mobility edge. Anderson's original work was extended to determine the mobility edges, by two sets of authors, Economou and Cohen, and Abou-Chacra, Anderson and Thouless. They used renormalized perturbation expansion of self-energy and dealt with the convergence and divergence of the series. The former authors assumed all the terms in the series to be strongly correlated whereas the latter ones took them to be uncorrelated. The convergence of the series implies localization and divergence implies extension.

We have modified the Economou-Cohen criteria by avoiding a mathematical approximation made by them, and have calculated the percolation concentration. This concentration comes out to be 7% and 8% against the corresponding old values of 17% and 24% yielded by two of Economou-Cohen criteria. Percolation studies of localization yield the value 31% . We have made some preliminary studies regarding the influence of short range order on localization, and the meaning of localization of phonons.

The shape of localized wave functions is a subject of great interest in localization studies. Assuming the mobility edge to be known we have studied for a Cayley tree lattice the extent of localized wave function as a function of energy. We have found that the extent of wave-function diverges at the mobility edge — an observation

Imaginary part of (2.35) gives the average density of states. If $(E^2-\gamma^2-4K) > 0$, $\langle n_o \rangle$ is given by,

$$\langle n_o(E) \rangle = \frac{1}{\pi} \frac{(\frac{K-1}{2K}\gamma \mp \frac{K+1}{2K} r \sin \theta/2)}{(\frac{K-1}{2K} E \mp \frac{K+1}{2K} r \cos \theta/2)^2 + (\frac{K-1}{2K}\gamma \mp \frac{K+1}{2K} r \sin \theta/2)^2} \quad \ldots (2.36a)$$

If $(E^2-\gamma^2-4K) < 0$, we have

$$\langle n_o(E) \rangle = \frac{1}{\pi} \frac{(\frac{K-1}{2K}\gamma \mp \frac{K+1}{2K} r \cos \theta/2)}{(\frac{K-1}{2K}E \mp \frac{K+1}{2K} r \sin \theta/2)^2 + (\frac{K-1}{2K} \gamma \mp \frac{K+1}{2K} r \cos \theta/2)^2} \quad \ldots (2.36b)$$

θ and r are given as described earlier after the eqn.(2.20), and out of + and - signs + is taken so as to keep $\langle n_o \rangle$ positive.

2.2 Results and Discussion

We have solved equation (2.31) with the help of the preceding equations for the evaluation of $\langle p_{oo}(E) \rangle$. By integrating $\langle p_{oo}(E) \rangle$ we obtain P_{oo}, introduced in (1.3). These results have been plotted in Fig.30 as a function of disorder parameter γ. The figure shows the results for both K = 3 and K = 1, the linear chain case, taking V = 1. An increase in P_{oo} with increasing γ is always seen. This is the anticipated result but the quantitative behaviour has been reported for the first time for lattice of any K.

After calculating $\langle n_o(E) \rangle$ from (2.36) we calculate the average extent of the wave functions in the localized region with the help of (2.32). The results for K = 1 have

been displayed in Fig.31, and those for K = 3 in Fig.32. The results indicate two very significant features of the wave functions in the localized region. These have been discussed below.

Although Mott[100] has made a number of illuminating conjectures for states near E_c, there has been very little quantitative work on this region of the band. The nature of the states is of great interest because they tell us how localized states near the transition energy change to extended states in a disordered system. Our results are in striking agreement with the contentions of Mott[100]. We have for the first time shown quantitatively that the extent of wave function falls from infinity to a very small magnitude in the vicinity of E_c on the localized portion of density of states. This is related to the Mott's conjecture that the d.c. conductivity at T = 0 falls abruptly to a very small value as soon as the localized region is approached after the transition energy. It should be emphasized that except the efforts by Abram and Edwards[101] no formal proof for this behaviour was so far given, and some authors have thought otherwise [e.g. Cohen[102]]. In the neighbourhood of E_c the extent of wave-function goes very much like that found by Abram and Edwards[101] [$\alpha |E-E_c|^{-3/5}$]. For small γ (~ 1) we find some structures in $\langle L_{eff}^{-1} \rangle^{-1}$, the physical implication of which is unclear. These structures vanish as γ is increased and at a particular energy, $\langle L_{eff}^{-1} \rangle^{-1}$, decreases as γ increases, which is reasonable.

There is another significant feature in the behaviour of $\langle L_{eff}^{-1} \rangle^{-1}$ as the energy approaches the band tail. The

extent of wave function is seen to increase with energy in this region. The behaviour estimated by Abram and Edwards[101] $[\alpha|E-E_c|^{-1/2}$ as $E \to \infty]$ is not correct, as we see that the behaviour obtained by us is congruent with the probabilistic arguments first proposed by Lifshitz[103] and Halperin and Lax.[104]

Let $H = T+V$ be the hamiltonian of the disordered system. T is the kinetic energy operator and is equal to the energy of an electron in host system plus the average potential of the impurities. V is the fluctuation of the impurity potential about the mean value. If $V = 0$ (i.e. no fluctuation), the band edge is decided by the minimum eigenvalues of T. Let the lower and upper band edges be $\underline{E}_o$ and $\bar{E}_o$. If the fluctuations be switched on, the positive fluctuations pull the right band edge to a larger energy and the negative fluctuations pull the left band edge more to the left. For a particular disorder let the new band edges be at $\underline{E}'_o$ and $\bar{E}'_o$. Obviously larger the $(\bar{E}'_o-\bar{E}_o)$, larger will be the potential fluctuation causing this shift. This potential fluctuation has to be large enough to bind states with minimum eigenvalues $\underline{E}'_o$ and $\bar{E}'_o$. The states in the tail should be associated with deep and extensive fluctuations in potential. Because of random nature of impurity distribution, there will always be some region of macroscopic crystal in which we find an unusually high number of attractive impurities

or an unusually small number of repulsive impurities. If the region is sufficiently large and the fluctuation sufficiently deep, then we expect to find a bound state, localized in this region. The probability of finding such a region may be roughly taken to be proportional to c^v, where c is the average concentration of the atoms lying in the deep tail of the distribution and v is the volume of the region. The size of the region containing a fluctuation of sufficient magnitude to produce a bound state increases very rapidly, and hence the probability of finding such strong fluctuations decreases very rapidly as E moves deep into the tail. Therefore the density of states, which goes as c^v, becomes very small. This has been verified. At the same time the increase in the size of the region indicates that the extent of wave function should increase. Our results confirm it directly.

In summary, we have determined the nature of the wave functions in the localized region by calculating the quantities directly related to transport coefficients. The nature of wave functions near E_c and in the extreme tail region has been found to be of special significance. We have been able to make definite statement regarding the nature of wave functions and thus the behaviour of conductivity (at T = 0) near E_c , from the model used here. The conductivity experiences a sudden drop and does not fall gradually to a very small value as E_c is approached

equivalently they have been replaced by infinite potentials. The quantity $\tilde{G}_{n_i}^{o,n_1 n_{i-1}}$ is defined by

$$\ell n\, \tilde{G}_{n_i}^{o,n_1,\ldots n_{i-1}} = \langle \ell n | \tilde{G}^{o,n_1,\ldots n_{i-1}} | \rangle$$
$$= \left\langle \ell n \left| \frac{1}{E-\varepsilon_{n_i}-\sum^{o,n_1,\ldots n_{i-1}}} \right| \right\rangle \quad \ldots (3.3)$$

The L(E) is too complicated for practical calculations. To simplify it Ziman[84] omits the self-energy and obtains

$$L(E) = ZV \exp\left[-\langle \ell n | E-\varepsilon_{n_i} | \rangle\right] \quad \ldots (3.4)$$

where Z is the number of nearest neighbours.

Economou and Cohen[89] have obtained within the framework of an effective medium theory[7] and for symmetrical bands a more sophisticated approximation to L(E) which retains the self-energy. They replaced all the $\tilde{G}$'s in (3.2) by the effective medium Green's function $\tilde{G}_{oo}$ and further simplify as

$$\ell n\, \tilde{G}_{n_i}^{o,n_1,\ldots n_{i-1}} = \langle \ell n | \tilde{G}_{n_i}^{o,n_1,\ldots n_{i-1}} | \rangle$$
$$\simeq \langle \ell n | \tilde{G}_{oo} | \rangle \quad \ldots (3.5a)$$
$$\simeq \ell n \langle | \tilde{G}_{oo} | \rangle \quad \ldots (3.5b)$$
$$= \ell n\, | \langle \tilde{G}_{oo} \rangle | ,$$

where $\langle \tilde{G}_{oo} \rangle = G_{oo}^{eff} = \langle 0 | (E-H_{eff})^{-1} | 0 \rangle = (E-\sum)^{-1}$. G_{oo}^{eff} is the CPA Green's function and $\sum$ is the CPA self-energy, or the effective medium site-energy. Therefore, one gets an

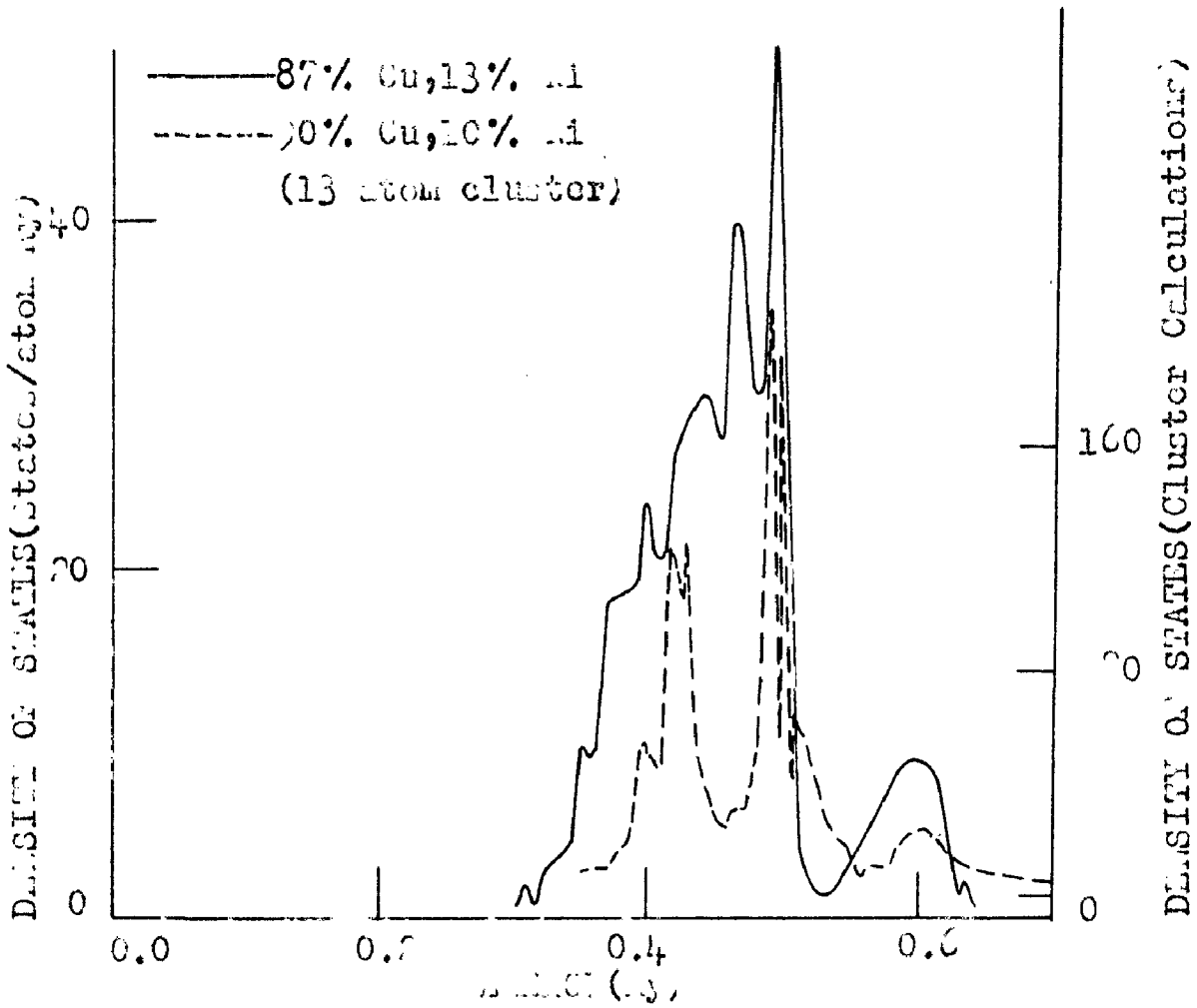

Fig.17. Comparison of densities of states for 90 at.% Cu, 10 at.% Ni alloy (- - - -) obtained from the cluster calculations in ref.50 and for 87 at.% Cu,13 at.% Ni alloy(——) obtained from our calculations.

approximation for L(E) as,

$$L(E) \simeq F(E) = KV \frac{A}{|E-\Sigma|} \qquad \ldots (3.6)$$

A is a constant and is determined by the requirement that in the periodic limit F(E) should be 1 at the band edges i.e. mobility edges move to the band edges. In the (periodic) effective medium $(\Sigma - ZV) < E < (\Sigma + ZV)$, so that

$$\frac{KVA}{ZV} = 1 \qquad \ldots (3.7)$$

or $A = Z/K$ and thus finally

$$F(E) = \frac{ZV}{|E-\Sigma|}, \qquad \ldots (3.8)$$

where Z is the coordination number.

3.1 A New Criterion based on the L(E)-Method.

In this section we report a more sophisticated approximation for L(E) obtained by Licciardello and Economou.[106] For a better calculation of the average in (3.3), an effective Hamiltonian $\mathcal{H}$ is introduced which satisfies the relation,

$$\begin{aligned} \ell n\, \tilde{G}_{n_i}^{o,n_1,\ldots n_{i-1}} &\equiv \left\langle \ell n |\langle n_i| (E-H^{o,n_1 \ldots n_{i-1}})^{-1} |n_i\rangle| \right\rangle \\ &\simeq \ell n |\langle n_i| (E-\mathcal{H}^{o,n_1,\ldots n_{i-1}})^{-1} |n_i\rangle| \\ &= \ell n |\mathcal{G}_{n_i}^{o,n_1,\ldots n_{i-1}}| \qquad \ldots (3.9) \end{aligned}$$

$\mathcal{H}^{o,n_1,\ldots n_{i-1}}$ is a tight binding Hamiltonian with $\varepsilon_n = 0$, $n \neq o$; $n_1,\ldots n_{i-1}$ and $\varepsilon_n = \infty$, $n = o, n_1,\ldots n_{i-1}$. Within this approximation L(E) becomes

$$L(E) \simeq L_e(E) = \lim_{M\to\infty} \left[V^{M+1} \sum{}' \left| \mathcal{G}^{o}_{n_1} \mathcal{G}^{o,n_1}_{n_2} \cdots \mathcal{G}^{o\cdots n_{M-1}}_{n_M} \right| \right]^{1/M} \quad \ldots (3.10)$$

Replacing all the $\mathcal{G}$'s in (3.10) by $\mathcal{G}^{n_{i-1}}_{n_i}$, $L_e(E)$ becomes

$$L_e(E) \simeq KV \left| \mathcal{G}^{n_{i-1}}_{n_i}(E-\Sigma) \right| . \quad \ldots (3.11)$$

Σ is an effective medium self-energy, and[86]

$$\mathcal{G}^{n_{i-1}}_{n_i} = \mathcal{G}_{n_i} - \left[{}_{n_i}n_{i-1} \mathcal{G}_{n_{i-1}n_i} \right] / \mathcal{G}_{n_i} \quad \ldots (3.12)$$

Viewed differently, (3.11) is obtained as

$$\begin{aligned} \ell n\, \tilde{G}^{o,n_1\cdots n_{i-1}}_{n_i} &= \ell n \left| \tilde{G}^{o,n_1,\cdots n_{i-1}}_{n_i} \right| \\ &\simeq \langle \ell n \left| \tilde{G}^{n_i-1}_{n_i} \right| \rangle \quad \ldots (3.13a) \\ &\simeq \ell n \langle \left| \tilde{G}^{n_i-1}_{n_i} \right| \rangle \quad \ldots (3.13b) \\ &= \ell n \left| \langle \tilde{G}^{n_i-1}_{n} \rangle \right| = \ell n \left| \mathcal{G}^{n_{i-1}}_{n_i} \right| . \end{aligned}$$

Thus from (3.2) we again get (3.11).

The following section (3.2) contains an error and it is regretted that this was included without adequate analysis of the matter. You may please ignore this section and its conclusions.

improving upon the approximation involved in eqns.(3.5b) and (3.13b). Let $\tilde{H}$ be the Hamiltonian involved in $\tilde{G}$, so that $\tilde{G}_{oo} = \langle 0 | (E-\tilde{H})^{-1} | 0 \rangle$, and $\tilde{H} = H_{eff} + V$ giving $G^{eff} = (E-H_{eff})^{-1}$, the Green's function of a reference system. Then we have

$$\begin{aligned} \ell n\, \tilde{G}^{o,n_1,\cdots n_{i-1}}_{n_i} &\simeq \langle \ell n \left| \tilde{G}_{oo} \right| \rangle \\ &= \langle \ell n \left| \langle 0 | (E-\tilde{H})^{-1} | 0 \rangle \right| \rangle \end{aligned}$$

$$= \left\langle \ell n \left| \langle 0 | (E-\underline{H}_{eff}-\underline{V})^{-1} | 0 \rangle \right| \right\rangle$$

$$= \left\langle \ell n \left| \langle 0 | (E-\underline{H}_{eff})^{-1} | 0 \rangle \langle 0 | \{\underline{I}-(E-\underline{H}_{eff})^{-1}\underline{V}\}^{-1} | 0 \rangle \right| \right\rangle$$

$$= \left\langle \ell n \left| G_{oo}^{eff} \langle 0 | \{I-\underline{G}^{eff}\underline{V}\}^{-1} | 0 \rangle \right| \right\rangle$$

$$= \left\langle \ell n | G_{oo}^{eff} | \right\rangle + \left\langle \ell n \left| \langle 0 | \{I-\underline{G}^{eff}\underline{V}\}^{-1} | 0 \rangle \right| \right\rangle \quad \ldots (3.14)$$

Thus the approximation involved in (3.5b) is equivalent to neglecting the second term in (3.14). G_{oo}^{eff} is the CPA or generalized CPA Green's function. To study whether the approximation of neglecting the second term of (3.14) is crucial we have devised a method of calculating this term exactly.

Since we have configurational averages involved, we have the advantage of using the property

$$\frac{1}{N}\langle \mathrm{Tr}\underline{X} \rangle = \frac{1}{N}\mathrm{Tr}\,\langle \underline{X} \rangle = \langle 0' \langle \underline{X} | 0 \rangle = \langle\langle 0 | \underline{X} | 0 \rangle\rangle \quad \ldots (3.15)$$

Therefore (3.14) can be written as

$$\left\langle \ell n | \langle 0 | (1-\underline{G}^{eff}\underline{V})^{-1} | 0 \rangle | \right\rangle = \left\langle | \langle 0 | \ell n (1-\underline{G}^{eff}\underline{V})^{-1} | 0 \rangle | \right\rangle$$

$$= \frac{1}{N}\left\langle \mathrm{Tr} | \ell n (1-\underline{G}^{eff}\underline{V})^{-1} | \right\rangle$$

$$= \frac{1}{N}\left\langle \ell n \det (1-\underline{G}^{eff}\underline{V})^{-1} \right\rangle$$

$$= -\frac{1}{N}\left\langle \mathrm{Tr} | \ell n (1-\underline{G}^{eff}\underline{V}) | \right\rangle \ldots (3.16)$$

The problem thus reduces to the evaluation of $\ell n(1-\underline{G}^{eff}\underline{V})$, which is done as follows. Let $\underline{B}$ and $\underline{B}(\lambda)$ be two matrices defined as

$$\underline{B} = \left[\underline{\tilde{G}}\,\underline{V} + \frac{1}{2}\underline{\tilde{G}}\,\underline{V}\,\underline{\tilde{G}}\,\underline{V} + \ldots . \right] \quad \ldots (3.17)$$

and $$\underline{B}(\lambda) = \left[\lambda\tilde{\underline{G}}\,\underline{V} + \frac{\lambda^2}{2}\tilde{\underline{G}}\,\underline{V}\,\tilde{\underline{G}}\,\underline{V} + \ldots\right] \qquad \ldots (3.18)$$

Thus $$\tilde{\underline{G}}^{-1}\underline{B}(\lambda) = \underline{T}(\lambda), \qquad \ldots (3.19)$$

where $\underline{T}$ is the total t-matrix of the system defined earlier. From (3.18) we have

$$\int_0^1 \frac{\underline{B}(\lambda)}{\lambda}\,d\lambda = \tilde{\underline{G}}\,\underline{V} + \frac{1}{2}\tilde{\underline{G}}\,\underline{V}\,\tilde{\underline{G}}\,\underline{V} + \frac{1}{3}\tilde{\underline{G}}\,\underline{V}\,\tilde{\underline{G}}\,\underline{V}\,\tilde{\underline{G}}\,\underline{V} + \ldots$$
$$= -\ell n(1-\tilde{\underline{G}}\,\underline{V}) \qquad \ldots (3.20)$$

or $$-\int_0^1 \frac{\underline{T}(\lambda)}{\lambda}\,\tilde{\underline{G}}\,d\lambda = \ell n(1+\tilde{\underline{G}}\,\underline{V}) \qquad \ldots (3.21)$$

Thus we have for (3.16)

$$-\frac{1}{N}\left\langle \mathrm{Tr}\left|\ell n(1-\underline{G}^{\mathrm{eff}}\underline{V})\right|\right\rangle = \frac{1}{N}\left\langle \mathrm{Tr}\left|\int_0^1 \frac{\underline{T}(\lambda)}{\lambda}\,\underline{G}^{\mathrm{eff}}\,d\lambda\right|\right\rangle$$
$$= \left\langle \left|\int_0^1 \frac{\langle 0|\,\underline{T}(\lambda)\,\underline{G}^{\mathrm{eff}}\,|0\rangle}{\lambda}\,d\lambda\right|\right\rangle \ldots (3.22)$$

We have seen in Chapter 2 that $\underline{T}$ can be expanded in terms of atomic t-matrices and within single-site approximation we have $\langle 0|\underline{T}(\lambda)|0\rangle \simeq t_o(\lambda)$. Also $\underline{G}^{\mathrm{eff}}$ is site diagonal in single-site approximation, so that (3.22) can be written as

$$-\frac{1}{N}\left\langle \mathrm{Tr}\left|\ell n(1-\underline{G}^{\mathrm{eff}}\underline{V})\right|\right\rangle = \left\langle \left|\int_0^1 \frac{t_o(\lambda)G_{oo}^{\mathrm{eff}}}{\lambda}\,d\lambda\right|\right\rangle$$
$$= \left\langle \left|\int_0^1 \frac{v_o G_{oo}^{\mathrm{eff}}}{1-\lambda v_o G_{oo}^{\mathrm{eff}}}\,d\lambda\right|\right\rangle \qquad \ldots (3.23)$$
$$\equiv Y$$

Thus having known G_{oo}^{eff} from CPA, (3.23) is exactly calculable. Equation (3.14) can now be written in the form

$$\ell n\,\tilde{G}_{n_i}^{o,n_1,\ldots n_{i-1}} \simeq \ell n\left|G_{oo}^{\mathrm{eff}}\right| + Y \qquad \ldots (3.24)$$

Therefore the modified form of criterion (3.8) is

$$L_m^I(E) = KV \exp\left[\ell n|G_{oo}^{eff}|+Y\right] \qquad \ldots (3.25)$$

The modified form of the criterion (3.11) is

$$L_m^{II}(E) = KV \exp\left[\ell n|G_{11}^{o\ eff}|+Y'\right] \qquad \ldots (3.26)$$

where $$Y' = \left\langle\left|\int_o^1 \frac{v_o G_{11}^{o\ eff}}{1-\lambda v_o G_{11}^{o\ eff}}\, d\lambda\right|\right\rangle \qquad \ldots (3.27)$$

and $$G_{11}^{o\ eff} = G_{11}^{eff} - \left[G_{01}^{eff}\ G_{10}^{eff}\right] / G_{11}^{eff}\ , \qquad \ldots (3.28)$$

where $$G_{10}^{eff} = G_{01}^{eff} = (E - \Sigma)\left[G_{11}^{eff}\ (E - \Sigma)\right] - 1 \qquad \ldots (3.29)$$

The last relation is the same as Eq.(2.12) of Chapter 4. There it was derived for a nearest neighbour pair along with a 2x2 matrix for self-energy. Here in the single site frame work we have put $\Sigma_2 = 0$.

It is necessary to normalize all the localization functionsso as to fulfil the requirement mentioned before (3.7). The mobility edge should coincide with the band edge in the periodic limit. The arguments leading to (3.7) yield the normalization constant for $L_e(E)$ in (3.11) to be Z/K. The normalization constant for both L_m^I and L_m^{II} is obtained in the following way. Calling it to be A, we have,

$$L_m^{I(II)} = A.KV \exp\left[Y\right]_{E=ZV} = 1,$$

because G_{oo}^{eff} and $G_{11}^{o\ eff}$ both tend to 1/ZV as disorder tends to zero and E tends to the periodic system's band

edge. In the periodic limit if we take x = 0(concentration of say A atoms) then y = 1-x=1 and therefore $v_o = \varepsilon_B$ (as $\sum = 0$), so Y reduces to the following

$$Y = \left| \int_o^1 \frac{\varepsilon_B}{1 - \lambda\varepsilon_B} \, d\lambda \right| = \ell n(1-\varepsilon_B).$$

Therefore $A = 1 / [KV(1-\varepsilon_B)]$,

and $$L_m^I = \exp[\ell n|G_{oo}^{eff}| + Y] / (1-\varepsilon_B) \quad \ldots (3.30)$$

$$L_m^{II} = \exp[\ell n|G_{11}^{o\ eff}| + Y] / (1-\varepsilon_B) \quad \ldots (3.31)$$

Numerical results for $F(E)$, $L_e(E)$, $L_m^I(E)$ and $L_m^{II}(E)$ are displayed in Fig.33 for $\delta = 1$ and 2 and $x = 0.1$ and 0.05. It is indicated that $F(E)$ and $L_e(E)$ greatly overestimate the localization as compared to their modified versions obtained by us. For $x = 0.1$, no localization is seen through L_m^I and L_m^{II} for both $\delta = 1$ and 2, although for δ 2 all states are localized if seen through $F(E)$ and $L_e(E)$. It is more instructive and a reliable test of conformity to compare the percolation limit of concentration, x_c, obtained from the four criteria. Percolation concentration, x_c, is the maximum concentration of impurity at which Anderson transition does not occur even as $\delta \to \infty$. Some direct numerical estimates (see e.g. ref.106) indicate it to be 0.31 and, $F(E)$ and $L_e(E)$ yield respectively 0.17 and 0.25 for simple cubic.[106] If simple cubic lattice be assumed to have parabolic shape of density of states, then L_m^I and L_m^{II} respectively indicate 0.07 and 0.08 values for x_c. Thus there is hardly any agreement, with the value 0.31.

This shows that the approximation, $\langle \ell n|\ldots|\rangle \simeq \ell n\langle|\ldots|\rangle$ leads to a fortuitous agreement. A more critical study is under process.

3.3 Localization and Short Range Order

Our study was motivated by the fact that complete disorder is possible only in principle and that in practice it is doubtful whether the 'annealing' temperature is high enough or the 'quenching' fast enough (in the preparation of sample) to guarantee total randomness, so there will always be some local order present. Moreover, it is now possible to measure the degree of localorder (see e.g. Mozer et al. Phys.Rev.175, 868(1968)), hence, instead of trying to remove local order it would seem worthwhile to make it an adjustable parameter and study its effects. The knowledge of short range order gives information about clustering or anticlustering of like atoms. It will be shown further that clustering or anticlustering show effects near the band edges of the density of states. Also, there are the regions where localization is seen. Therefore, short range order should show significant changes in localization.

Local order cannot be introduced in any of the single-site theories (say CPA) because they completely ignore the correlations among the lattice sites. One should therefore use atleast two-site cluster theory. We have used the pair calculation discussed in Chapter 4, and introduce

the short range order in the following manner. Suppose σ is short range order parameter such that the probabilities for A-A, A-B(B-A) and B-B configurations of a nearest neighbour pair are respectively, $P_{AA} = c^2\sigma$, $P_{AB} = c-c^2\sigma = P_{BA}$ and $P_{BB} = 1-2c+c^2\sigma$, where c is the concentration of A atoms. Thus $\sigma = 1$ implies complete randomness and $\sigma = 1/c$ implies complete A-A order.

The computational results are shown in Figs.34 and 35 for simple cubic density of states with $c_A = 0.1$ and 0.2, and $\delta = 1$. For $c_A = 0.1$, σ takes the values 1,4 and 6, and for $c_A = 0.2$, it takes the values 1,1.5 and 2.5. Starting from the completely random case, as σ increases, P_{AA} and P_{BB} increase by equal amount and P_{AB}(or P_{BA}) decreases by the same amount. As a result of this, affinity for the formation of A-A and B-B pairs increases. This will cause the segregation of A-A and B-B pairs, until at $\sigma = 10$ for $c_A = 0.1$ and $\sigma = 5$ for $c_A = 0.2$ when complete segregation should take place (i.e. absence of A-B order). We can describe this situation as: for $c_A = 0.1$, P_{AA} will be 0.1, i.e. if one of the sites is known to be A then the other will be A with probability 1. Thus, in the cases under consideration with increasing σ we have an increasing tendency for the formation of small A-atom clusters in the sea of large B-atom clusters. This will give rise to larger fluctuations in potential as compared to the case when there is complete disorder. Switching over to the discussions like in Sec.2.2 of this chapter, we see that the eigenvalues

of the Hamiltonian of the disordered system (H=T+V, T= Kinetic energy operator, V = fluctuation in potential) should shift to the energies more on the right and left of the density of states. The effects of changing σ^- should dominate at the top of the alloy density of states where the impurity (A) band is situated. The reason is the following. The ends of the alloy density of states contain the maximum effects due to fluctuations. The concentration of A atoms being small only the positive fluctuations are significant. The negative fluctuations can be ignored because there is very little chance of small clusters of B atoms being embedded in larger A-atom clusters.

The above considerations allow to make the following conjectures. With increasing σ^-, density of states should be stretched to form long tail at the top-side of the band and a little stretch on the bottom side. The localization should increase as σ^- increases. Our results for the aforesaid parameters are in conformity with these theoretical qualitative contentions.

The $c_A = 0.1$ case: For complete disorder ($\sigma^- = 1$) a band of extended states sandwitched between bands of localized states is seen in the impurity band region. Very little localization is seen at the bottom edge. For $\sigma^- = 4$, the structure in the impurity band is eroded and a gradual fall of density of states is seen. The band of

extended states also vanishes and all impurity states become localized. The localization at the bottom increases slightly. As σ further increases to 6 , the impurity band looks like a long tail of the main band. Localization at the top and bottom of the band increases.

The c_A = 0.2 case: The variations in the shape of density of states with varying σ are like those explained for c_A= 0.1 case. For σ = 1 the band of the extended states in the impurity subband is bigger as compared to c_A = 0.1 case. As σ increases this band of extended states shrinks. The localization at the bottom of the band also increases gradually.

4. LOCALIZATION OF PHONONS:

There is only a little knowledge available about localization of phonons in disordered systems. Some insight into the problem has been given by Economou[107] and Bell[108]. We have just started studies in this direction from the very beginning, starting from the meaning of localization of phonons. So far we have only assimilated some qualitative knowledge and some quantitative knowledge obtained by adaptation of the results for electronic systems into phononic systems. Both the systems respond to localization phenomenon broadly in the similar fashion, but there are some subtle differences.

Following general behaviour is found for phonons in disordered alloys:

(a) An impurity atom which is sufficiently light and strongly bound will vibrate in a mode which has a higher frequency than any of the modes of the pure host crystal. The amplitudes of the atoms vibrating in this 'local mode' are, to a greater or lesser extent, localized around the impurity site. The degree of localization depends on the interatomic forces and on the mass of the impurity atom relative to a host atom. The smaller the mass of the impurity, the more localized at the impurity site is the local mode.

(b) An impurity atom which is sufficiently heavy and weakly bound will produce a 'resonant mode' at a frequency within the band of lattice-vibrational (phonon) frequencies of the pure host crystal. The greater the mass of the impurity atom relative to the mass of a host atom, the lower will be the 'resonant frequency' and the more readily apparent will be the effects of the resonant mode.

Various experimental techniques have been applied (or are in principle applicable) to such studies. Among these are the Mossbauer effect, infrared absorption, Raman and Brillouin scattering, diffuse x-ray scattering, coherent and incoherent inelastic neutron scattering etc.(for references see Maradudin[109](1966)). Of these, coherent inelastic neutron scattering is considered to be the most powerful.[110] From the neutron scattering profiles one can deduce the intensities, energies and energy widths (inverse lifetimes)

of the individual modes of vibration. Without giving details we state that these quantities are also easily obtainable through theoretical techniques and respectively correspond to the spectral density, real part (which gives the shift in energy with respect to the host band) and imaginary part of self-energy. Thus one can easily obtain the frequencies (energies) and the degree of localization (spatial extent) of local and resonance modes. A qualitative discussion of this follows.

For illustration the density of states, self-energy and spectral densities for various parameters have been displayed in Figs.37 and 38. They have been obtained through CPA discussed in Chapter 2. The constituents possess the Debye form of phonon density of states. The spectral density $\mathcal{A}(\vec{q},\omega)$ can give a vague information about the localization or delocalization of a phonon (or electron) state. Localization in $\vec{q}$-space indicates delocalization in coordinate space (uncertainty principle), and vice-versa. $\mathcal{A}(\vec{q},\omega)$ gives distribution of ω's for a particular $\vec{q}$, hence the informations about localization are obtained by looking at $\mathcal{A}(\vec{q},\omega)$'s at a particular ω for a series of $\vec{q}$'s ranging over the whole allowed range. For alloys $\mathcal{A}(\vec{q},\omega)$ shows two peaks (for large mass-ratio and small concentration of light impurity), one sharply distributed about a central energy (lorenzian in shape) and another very flat in shape. The first shows

the quasi-particle nature of the excitations and is related to the plane wave like eigenstates of host crystal. The other flat peak is extended over a large $\vec{q}$ - space, indicating localization in $\vec{r}$-space. This is consistent as seen from the density of states and $\mathcal{A}(q,\omega)$ for $\epsilon = -2$ (i.e. mass ratio = 3/1) and $c = 0.75$ (conc. of heavy atoms). If ϵ is reduced and c is increased, $\mathcal{A}(\vec{q},\omega)$ is seen to be affected for large $\vec{q}$'s only. This means comparatively more localization in $\vec{q}$-space, thus delocalization in $\vec{r}$-space (cf. Fig.35). This is what one expects. In the region of main band the Lorenzian character of $\mathcal{A}(\vec{q},\omega)$ is consistent with the small magnitude of $\mathrm{Im}\Sigma$ (imaginary part of self-energy) in this region (see Fig.37(b) for $c = 0.5$ and 0.75). Small $\mathrm{Im}\Sigma$ means small damping of states because of impurities , i.e. the states in this region have large life time ($\alpha\, 1/\mathrm{Im}\Sigma$). Life time tells that if an eigenstate be assigned an energy it will stay at that energy for the time proportional to $(\mathrm{Im}\Sigma)^{-1}$ before it diffuses to the neighbouring energies. The strongly damped, non-Lorenzian character of $\mathcal{A}(\vec{q},\omega)$ in the region of impurity band is consistent with large $\mathrm{Im}\Sigma$ i.e. small life time.

For resonance mode (in-band mode) the state of affairs is slightly different. A crude physical explanation of the resonance mode can be given as follows. We consider the case of a very heavy impurity coupled very weakly to the surrounding host crystal. At very low frequencies

because of infinitesimal translation it vibrates in phase with the neighbours in the host crystal. However, as the normal mode frequency increases, because of its heavy mass and (or) weak binding to neighbours, it begins to lag more and more behind the neighbours, until a frequency is reached at which it vibrates 180° out of phase with the surrounding lattice in a kind of local optical vibration mode. The frequency at which this occurs is called the frequency of resonance mode. The mean square vibration amplitude of the impurity atom as a function of its frequency is sharply distributed about the resonance mode frequency. Resonance mode is not spatially localized in the way a local mode is localized. Since it lies in the allowed frequency range of the host lattice,the vibration of the heavy impurity is transferred to the neighbouring light atoms. Resonance mode appears like a hump or shoulder on the low frequency side of the density of states (c.f. density of states for c= 0.05 and 0.25). This description facilitates the understanding of the Fig.36(a). The line shape of a mode with a frequency slightly lower or higher than that of the resonance (this can be roughly known from the density of states plots) tends to have a shoulder or pronounced tail over the resonance region. When the line shape peaks right at the resonance, it is symmetric but broad.

The resolution broadened line shapes[110] obtained from neutron inelastic scattering profiles taken for a series

of $\vec{q}$-vectors are comparable with the spectral density discussed here. The two look alike for both, the local mode and resonance mode. The width at half maximum of a line shape belonging to a particular energy $[\sum_{\vec{q}} \mathcal{A}(\vec{q},\omega)]$ gives the inverse life time of that energy state(90);this is thus comparable to the Im Σ obtained theoretically.

It is always more illustrative to do calculations for realistic systems rather than the models as discussed just now. In Fig.1 we have displayed density of phonon states for Cu-Au alloys for 3% and 9.3% Au. These systems have been widely scanned (see ref.90 and the references therein). The resonance mode due to heavy impurity (Au) is clearly shown. The real and imaginary parts of Σ (Fig.38) are in very good agreement with the experimental data (for comparison se ref.110).

We now proceed further to study the localization problem more rigorously rather than the qualitative arguments given above. We take the analogy with the problem of electrons and define phonon localization in Anderson-sense.

Suppose $U_\alpha(o,o) = U_o$ is the amplitude of displacement of an atom at 0^{th} site and at $t = 0$. Then the localization criterion would require, $U_\alpha(o,\infty) \neq 0$ at $t = \infty$. To be more explicit suppose $U_X(o,o) = U$, then the criterion would be, $|\vec{U}(o,\infty)|^2 = U_X^2(o,\infty) + U_Y^2(o,\infty) + U_Z^2(o,\infty) \neq 0$,i.e. the quantity of interest is $\lim_{t\to\infty} |\vec{U}(o,t)|^2$.Alternatively,given arbitrarily

small η, we can always find a finite number $M(\eta)$ of lattice sites which contain all but η of the total amplitude. To quantify the concept we introduce a participation ratio which gives the proportion of atoms in a system contributing effectively to the energy of a given mode.

In the case of electrons the localization is found symmetrically on the both ends of a band. Unlike this the situation in the case of phonons appears to be entirely unsymmetrical mainly because all the frequency distributions start from the zero of frequency. Further it appears that the states lying in the low frequency region of the density of states, attributed mainly to the vibration of heavy atoms can not be localized in the Anderson sense. A small displacement given to a heavy atom surrounded by light atoms, will always be transferred to the neighbouring atoms. This also suggests that the eigen-frequencies less than ω_m, the maximum eigen-frequency in the spectrum of the heavy atom, should not be localized. To guess the localization of higher frequencies ($>\omega_m$) we understand in the following manner. Consider the situation where mass ratio is sufficiently large and the concentration of light atoms is sufficiently small so that the impurity band is separated. The main band is mainly constituted due to heavy atoms and very little of light atoms. The top of this band is due to clusters of light atoms surrounded by heavy atoms. The movement of the light atoms

is damped by the surrounding heavy atoms, thus reducing the eigenvalue. If the cluster of light atoms is sufficiently large to have an eigenfrequency greater than ω_m, it will trap the eigenstate ofthe corresponding eigenfrequency. These clusters will of course be not very large in size because the eigenvalues that they can accommodate are still quite smaller than those in the impurity band. As the edge of this band is approached the size of the cluster required increases. The impurity band is constituted of so high eigenvalues that they are scarcely taken by heavy atoms, so it is mainly due to very large clusters of light atoms. However, the presence of few heavy atoms cannot be ignored in principle. These heavy atoms tend to reduce the eigenvalue, so the lower portion of the impurity band has the effects due to the clusters of heavy atoms embedded among light atoms. The situation in this band can be conceived in terms of the configurations shown in Fig.39. Large clusters of light atoms containing small clusters of heavy atoms as shown in (I) correspond to the lower portion of the impurity band. As the size of the small cluster of heavy atoms reduces the eigenvalue increases. Since the large clusters of light atoms are further enveloped by the heavy atoms, the eigenstates are localized in this region. There is also possibility of finding clusters of light atoms open at atleast two boundaries of the crystal, like in (II). They

give rise to the extended states. The probability of occurrence of such clusters is proportional to the concentration of light atoms. As one approaches the higher eigenvalues, the effect of heavy atoms reduces rapidly. So that the topmost eigenfrequencies are thought to be due to very large clusters of light atoms as shown in (III). If their concentration is quite small, there will be very few such clusters but they will be enclosed by heavy atoms, thus creating localized states of very high eigenfrequency.

It is interesting that in the results reported in the following all such features are revealed. It is important to state that as $M \to \infty$ (the weight of heavy atoms), $\omega_m \to 0$, thus making all the states localized provided concentration of heavy atoms is larger than a critical value. This may correspond to the Anderson transition for electron states.

Without working out the localization problem for phonons from the very beginning as has been done for electrons, we transform the two localization criteria for electrons reported in eqns.(3.6) and (3.11) to the case of phonons. This is done with the comparison of the equations of motion for electrons and phonons in a disordered system,

$$(\epsilon_i - E)\, a_i = V \sum_{\delta} a_{i+\delta} \qquad \text{(electrons)} \qquad \ldots (4.30)$$

$$(m_i \omega^2 - ZK)\, u_i = -K \sum_{\delta} u_{i+\delta} \qquad \text{(phonons)} \qquad \ldots (4.31)$$

The electron wave function is given by $\psi = \sum_i a_i |i\rangle$,
u_i is the displacement of i^{th} particle of mass m_i,
K is the coupling constant for oscillations, ω is the eigenfrequency of the oscillation, E is the eigenvalue and V is the hopping integral between nearest neighbours. Comparison of the two equations yields the following correspondences,

$$\left.\begin{aligned} \varepsilon_i &\rightarrow m_i\omega^2 \\ E &\rightarrow ZK \\ V &\rightarrow K \end{aligned}\right\} \qquad \ldots (4.32)$$

Now we will derive the correspondence between the forms of self-energy, in which it is commonly used in the calculations of electronic and phononic properties. For that we compare the single-particle Green's function in the two cases,

$$G_{11}^{\text{electron}}(E-\Sigma) = \frac{1}{N}\sum_k \frac{1}{E-\Sigma - ws(k)} \qquad \ldots (4.33)$$

$$G_{11}^{\text{phonon}} = \frac{1}{mN}\sum_k \frac{1}{\omega_k^2 - \omega^2(1-\tilde{\varepsilon})} \qquad \ldots (4.34)$$

where $s(k) = \frac{1}{Z}\sum_\delta e^{ik\delta}$

and w = half width of energy distribution function. $\tilde{\varepsilon}$ is the self energy for phonons as defined in Chapter 2. It is very simple to see that

$$\omega_k^2 = \frac{ZK}{m}(1-s(k)) \qquad \ldots (4.35)$$

So (3.34) can be written as

$$G_{11}^{\text{phonon}} = \frac{1}{N}\sum_{k} \frac{1}{ZK(1-s(k)) - m\omega^2(1-\tilde{\varepsilon})} \qquad \ldots (4.36)$$

Replacing E by ZK in (4.33) we get for phonons,

$$G_{11}^{\text{phonon}} = \frac{1}{N}\sum_{k} \frac{1}{ZK - ws(k) - \Sigma} \qquad \ldots (4.37)$$

Comparison of (4.36) and (4.37) yields the correspondence,

$$\left.\begin{array}{l} \Sigma \rightarrow m\omega^2(1-\tilde{\varepsilon}) \\ w \rightarrow ZK \end{array}\right\} \qquad \ldots (4.38)$$

The correspondences (electron→phonon) (4.32) and (4.38) transform the localization criterion (3.6) as

$$\begin{aligned} F(\omega) &= \frac{ZK}{|ZK - m\omega^2(1-\tilde{\varepsilon})|} \\ &= \frac{m\omega_m^2/2}{|m\omega_m^2/2 - m\omega^2(1-\tilde{\varepsilon})|} \\ &= \frac{1}{|1-2X^2[1-\tilde{\varepsilon}(X)]|}, \end{aligned} \qquad \ldots (4.39)$$

Using the relation $ZK = m\omega_m^2/2$, where ω_m is the maximum frequency in the frequency spectrum of the host. $X = \omega/\omega_m$ in dimensionless units. For the transformation of the criterion (3.11) we have to transform the Green's function occurring in (3.12),

$$\mathcal{G}\, n_i(E-\Sigma) = \frac{1}{N}\sum_k \frac{1}{E-\Sigma(E) - ws(k)}$$

$$\equiv \frac{1}{N}\sum_k \frac{1}{ZK-m\omega^2(1-\tilde{\epsilon})-ZKs(k)}$$

$$= \frac{1}{N}\sum_k \frac{1}{m\omega_k^2 - m\omega^2(1-\tilde{\epsilon})}$$

$$= \frac{1}{m}\int_0^{\omega_m} \frac{\rho_o(\omega')\,d\omega'}{\omega'^2-\omega^2(1-\tilde{\epsilon})}$$

$$= \frac{1}{m\omega_m C}\int_0^1 \frac{\rho_o(X'\omega_m)\,dX'}{X'^2-X^2[1-\tilde{\epsilon}(X)]} \qquad \ldots (4.40)$$

Here $X' = \omega'/\omega_m$, ρ_o is the unperturbed density of states of the host lattice, and C is the normalization constant, i.e.

$$\int_0^{\omega_m} \rho_o(\omega')\,d\omega' = C \qquad \ldots (4.41)$$

The only thing to be resolved in (4.40) is to write $\rho_o(X'\omega_m)$ in ter s of $\rho_o(X')$ which involves dimensionless variable for frequency. Equation (4.41) is equivalent to

$$\frac{1}{C}\int_0^{\omega_m} \rho_o(\omega')\,d\omega' = 1 = \int_0^1 \rho_o(X')\,dX'$$

or

$$\frac{1}{C}\int_0^1 \rho_o(X'\omega_m)\,\omega_m\,dX' = 1 = \int_0^1 \rho_o(X')\,dX'$$

so that we get

$$\rho_o(X') = \frac{\omega_m}{C}\,\rho_o(\omega_m X') \qquad \ldots (4.42)$$

Thus we have,

$$\mathcal{G}_{n_i}^{\text{phonon}} = \frac{1}{m\omega_m^2} \int_0^1 \frac{\rho_o(X')dX'}{X'^2 - X^2[1-\tilde{\varepsilon}(X)]} \qquad \ldots (4.43)$$

Substitution of this into (3.11) through (3.12) is straightforward and finally yields the criterion,

$$L_e(X) = \frac{3}{8}\left| D - \frac{4[\{\frac{1}{2} - X^2[1-\tilde{\varepsilon}(X)]\}D-1]^2}{D} \right| \qquad \ldots (4.44)$$

where $D \equiv \int_0^1 \frac{\rho_o(X')dX'}{X'^2 - X^2[1-\tilde{\varepsilon}(X)]}$ ... (4.45)

We have calculated $\tilde{\varepsilon}(X)$ and D within CPA as discussed in Chapter 2. The results for Cu-Au alloys (the density of state, F(X) and $L_e(X)$) have been shown in Fig.40(a,b,c,d). The criterion L_e pushes the mobility edges more inside the band as compared to F. For Cu_{25} Au_{75}, all states in the impurity band have been shown to be localized by L_e whereas F shows quite a large amount of extended states in the middle of the impurity band. Other features of the localized states are as conjectured above except the one which states that localization should be observed among the states with eigenfrequencies ω_m(defined there). If this was to hold, we should not have obtained localization before X = 0.6, but we do obtain it for $Cu_{50}Au_{50}$ alloy. The error may be assigned to CPA. The self energy and D obtained in CPA may yield an overestimation of localization and the same quantities obtained through a very sophisticated technique may correct it. Besides this for calculating

the d nsity of states for alloys (with arbitrary concentration of Au), the integral form of Green's function involves the unperturbed density of states of Cu and no force constant changes have been taken into account, which should be quite different for Cu and Au. Our experience from the calculations for Si-Ge alloys tells that if instead of ρ_o^{Cu}, ρ_o^{Au} is used in the calculation of Green's function, the essential features remaining unchanged, the alloy density of states in the two cases should have a marked shift.

Keeping in view these discrepancies, we can say that the Economou-Cohen criteria originally obtained for electron localization, are able to describe some features of the phonon localization. However, it should not be taken seriously to be a very good theory (for phonons also) as we have seen in the previous section. A more consistent theory is yet to come out specially for phonons. It is important to indicate that all the theories to deal with localization are for the models that are far from reality. In realistic systems very little localization is expected because of long range hopping which is completely omitted in the theory. There are other important factors also, such as off-diagonal disorder, which should be incorporated into a theory to make it apt for realistic systems.

5. THEORY OF MATTIS AND YONEZAWA — A REFUTAL:

Recently Mattis and Yonezawa[111] (MY) have proposed a new criterion for locating mobility edges in a three dimensional disordered medium. It is completely alienated from the concepts introduced in the preceding sections and incorporates an altogether different concept of localization. The criterion relates the mobility gap to regions of anomalous dispersion of quasi-particles. They construct a wave packet, which in this region becomes an incoming spherical wave packet and grows unphysically as it approaches the origin and then ceases to exist at large t. The conclusion that there is a sink at r= 0, is related to localized eigenstates. We have pointed out [112] some unphysical outcomes of the criterion. It starts with $\langle G \rangle$, which can never yield localization.

The MY criterion is essentially based on the following considerations. One considers the single particle dispersion relation obtained after averaging the retarded single-particle Green's function:

$$\langle G(\omega) \rangle = G_k^o(\omega) + G_k^o(\omega) \Sigma_k(\omega) \langle G_k(\omega) \rangle \qquad \ldots (5.1)$$

Here $$\Sigma_k(\omega) = R_k(\omega) - i\Gamma_k(\omega), \qquad \ldots (5.2)$$

is the self-energy. The single particle dispersion relation is given by

$$\omega = \varepsilon_k + R_k(\omega). \qquad \ldots (5.3)$$

MY construct a spherical wave packet about a central energy given by (5.3). This is written after some simplifications as,

$$F(\vec{r},t) = -\exp(-i\omega_o t \mp i\vec{k}_o.\vec{r}) \left[\pi\rho_o(\varepsilon_{k_o})/k_o r\right] \times \exp\left[-r\Gamma_o/|V_o|\right] \int_{-\infty}^{\infty} d\Omega f(\Omega) \exp\left[-i\Omega(t-\mu^* r/|V_o|)\right], \quad \ldots (5.4)$$

where $V_o = (d\varepsilon_k/dk)_{k=k_o}$, $\Omega = \omega-\omega_o$, $f(\Omega)$ is the envelope function and $\mu^* = \left[1-dR_k(\omega)/d\omega\right]_{\omega=\omega_o}$ is the dispersion parameter. $\Gamma_k(\omega)$ is assumed to be small $\left[\Gamma_o \simeq \Gamma_k(\omega_o)\right]$ as well as slowly varying. MY argue that in the region of anomalous dispersion given by

$$\mu^* = \left[1- \frac{dR_k(\omega)}{d\omega}\right]_{\omega=\omega_o} \leqslant 0 \quad \ldots (5.5)$$

the states are localized with the equality sign locating the mobility edge. The spherical wave-pocket $F(\vec{r},t)$ built out of the energy states for which (5.5) is satisfied does not correspond to outgoing spherical waves, but rather to incoming spherical waves indicating a sink at r = 0. Equivalently the region where (5.5) holds has been assigned to the localized states.

We have shown in the following that (5.5) leads to negative density of states in the localized region, which is unphysical. Subsequently we see that the line of action adopted by MY yields only extended states. $\langle G_k(\omega)\rangle$ can be written in terms of ε_k and $\Sigma(k,\omega)$ as,

$$\langle G_k(\omega)\rangle = \frac{1}{\omega-\varepsilon_k-\Sigma(k,\omega)} . \quad \ldots (5.6)$$

This has a pole at $\omega_k - i\Gamma_k$ (for small Γ_k), where ω_k is given by the solution of (5.3). Expanding the denominator about $\omega_k - i\Gamma_k$, we get,

$$\left\langle G_k(\omega) \right\rangle = \frac{1}{(\omega - \omega_k + i\Gamma_k(\omega))\left(1 - \frac{\partial \Sigma_k}{\partial \omega}\right)_{\omega=\omega_k} + \ldots} \qquad \ldots (5.7)$$

At $\omega=\omega_k$, Im $\left\langle G_k \right\rangle$ is written as

$$\mathrm{Im}\left\langle G_k(\omega) \right\rangle = \frac{-\Gamma_k\left[1 - \frac{\partial R_k}{\partial \omega}\right]_{\omega=\omega_k}}{\left[\frac{\partial \Gamma_k}{\partial \omega}\right]^2_{\omega=\omega_k} + \left[1 - \frac{\partial R_k}{\partial \omega}\right]^2_{\omega=\omega_k}} \qquad \ldots (5.8)$$

Therefore to keep the density of states positive one always has

$$\left[1 - \frac{\partial R_k}{\partial \omega}\right] > 0. \qquad \ldots (5.9)$$

Thus $\mu^* < 0$, which is the MY criterion, is never satisfied. $\mu^* = 0$ is trivially satisfied in the region of no density of states.

The reasons for our assertion that the MY states are extended are easily understood in the light of the work by Anderson[86] and Economou and Cohen.[89] We present below essentially their arguments in the present context.

(a). In constructing the wave packet, MY use the Green's function that has the translational symmetry of the regular lattice. If the system contains the localized

states, they are necessarily localized in some finite part of space within the system, where a strong enough fluctuation in the potential has occurred, thereby making the Green's function translationally non-invariant. The effect of averaging this Green's function is placing such a localized state at all the equivalent sites of the lattice, and thus destroying the local character. The argument has been stated in references(65) and (68) in terms of the analytical properties of the Green's function. For a N-site lattice, we can write the Green's function in the site representation as

$$G_{oo} = \langle 0|G|0\rangle = \sum_{\alpha=1}^{N} \frac{\langle 0|\alpha\rangle\langle\alpha|0\rangle}{E-E_\alpha} = \sum_{\alpha=1}^{N} \frac{f_{\alpha N}}{E-E_\alpha}, \quad \ldots (4.10)$$

where $|\alpha\rangle$'s denote the eigenstates of the system. Now we can divide the sum into two parts-one over the extended states and the other over the localized states,

$$G_{oo} = \sum_i \frac{f_{iN}}{E - E_i} + \sum_j \frac{f_{jN}}{E - E_j}, \quad \ldots (4.11)$$

but $f_{iN} \alpha\ 1/N$ for extended states,
and $f_{jN} \alpha\ e^{-\beta\vec{R}_j}$ for localized states,

where $\vec{R}_j$ is the distance of 0 site from the site where jth state is localized. As we take the limit $N \to \infty$, the first sum becomes an integral leading to the familiar branch cut in the Green's function, while the second term has most peculiar analytical structure. Though the number

and packing of localized states increases as $N \to \infty$; the second term remains a dense distribution of discrete poles, some of which have very small residues and the others have residues of order unity. From the above argument it is clear that this must be a basic property of Green's function describing localized states. The Green's function that MY use has only a branch cut which should correspond to extended states only.

(b) Another demonstration of this argument may be seen by considering the quantity P_{oo}, defined earlier. It is given as follows

$$P_{oo} = \lim_{s \to o} \frac{s}{\pi} \int G_{oo}(E-is) G_{oo}(E+is) dE. \qquad \ldots (4.12)$$

Plugging the Green's function that is employed by MY we get,

$$P_{oo} = \lim_{s \to o} \frac{s}{\pi} \int \sum_k \sum_{k'} \frac{1}{E-\epsilon_k+\sum_k(E+is)} \cdot \frac{1}{E-\epsilon_{k'}-\sum_{k'}(E-is)} dE \qquad \ldots (4.13)$$

But $\sum_k(E \pm is) = R_k(E) \mp i \Gamma_k(E)$, $\qquad \ldots (4.14)$

so that $P_{oo} \to 0$ for such a form of self-energy.

(c) For a disordered system the calculation of the wave-function $F(\vec{r},t)$ involves off-diagonal part of the Green's function as well. It is not clear that if we ignore the off-diagonal part of Green function, we will be correctly describing the situation, particularly in the presence of localized states. MY's formulation takes into account only the diagonal part of Green's function.

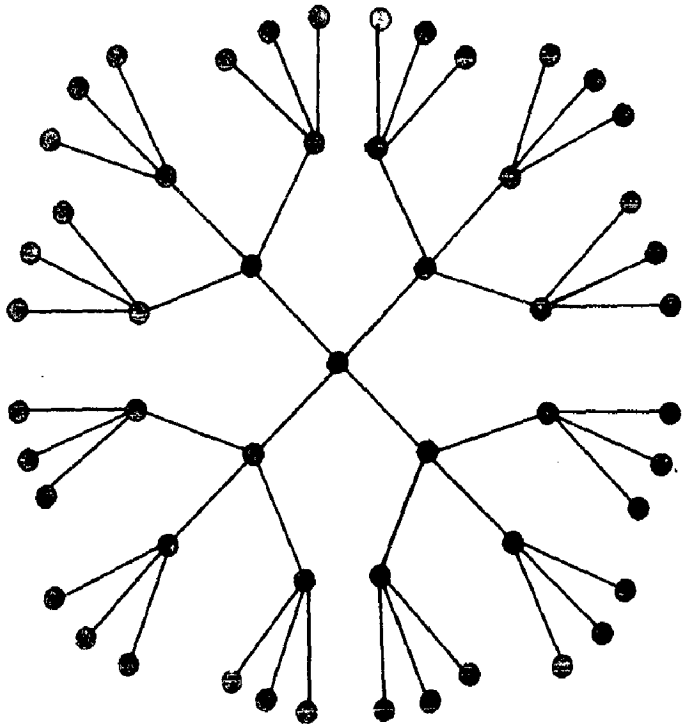

Fig. 9. A section of a Cayley tree lattice with $z = 3$.

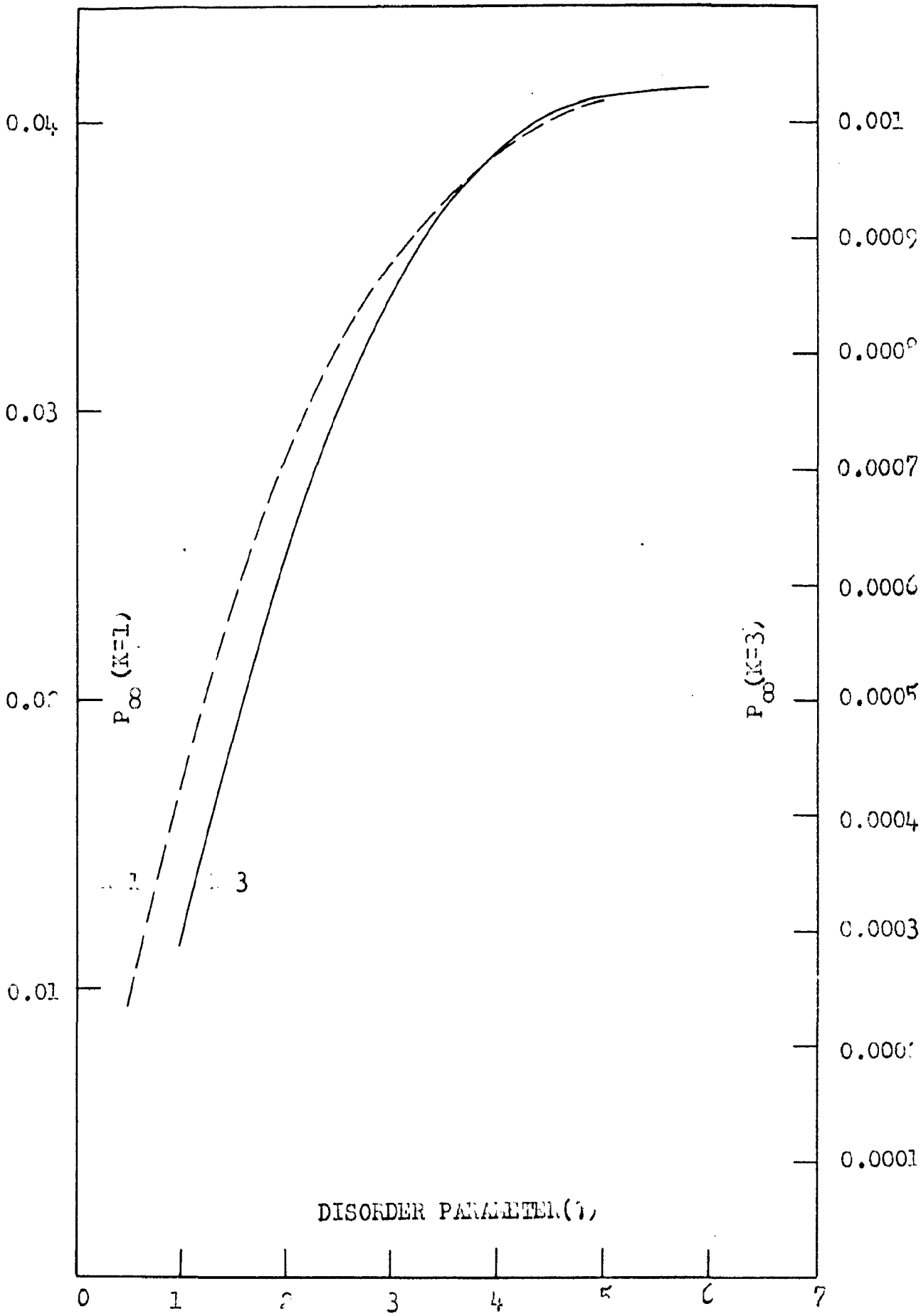

Fig.30. Probability P_{oo}, that an electron remains on 0th site after infinite time has elapsed, versus disorder parameter γ.

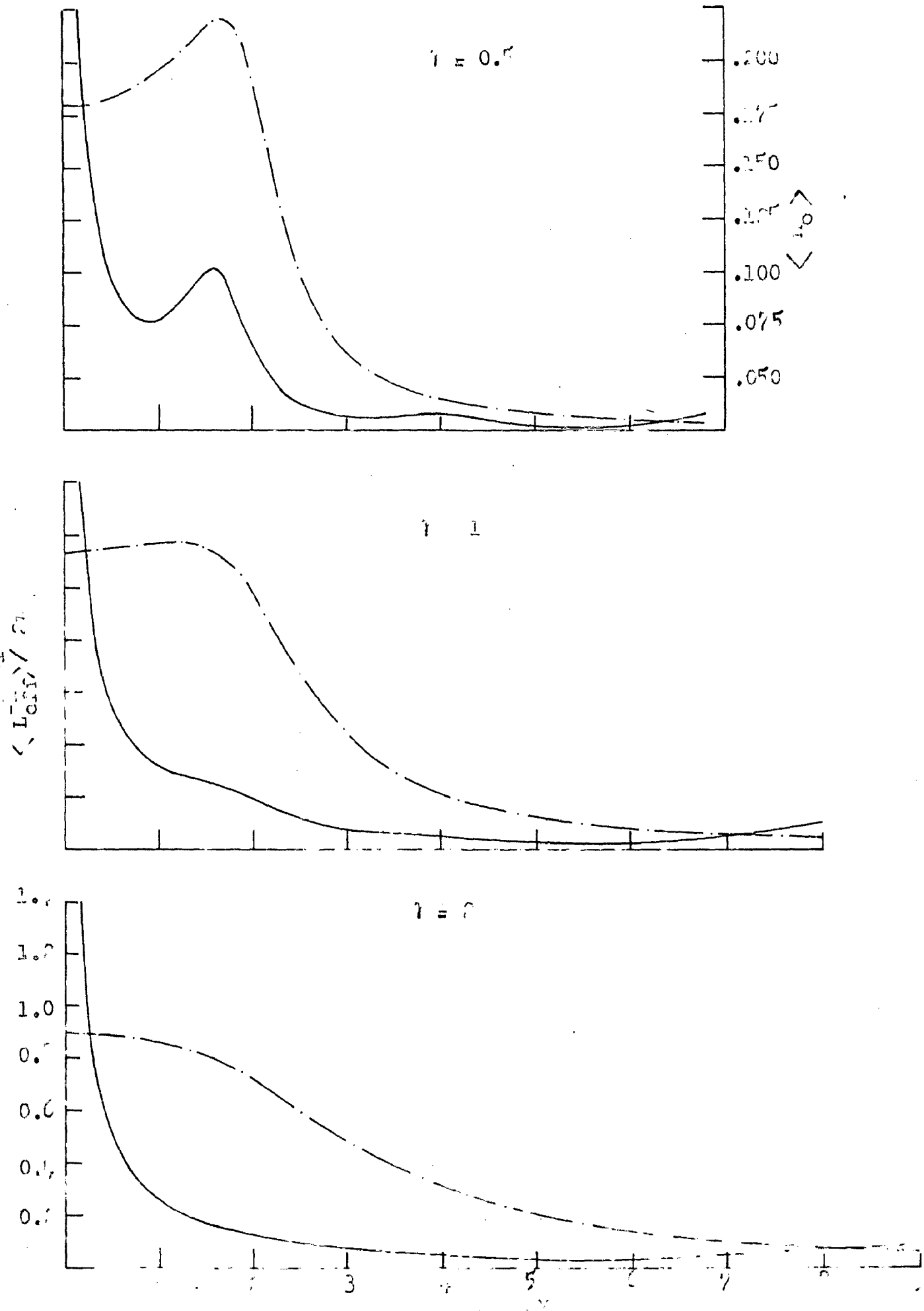
.200
.150
.100
.075
.050
1.0
0.8
0.6
0.4
3
5
7

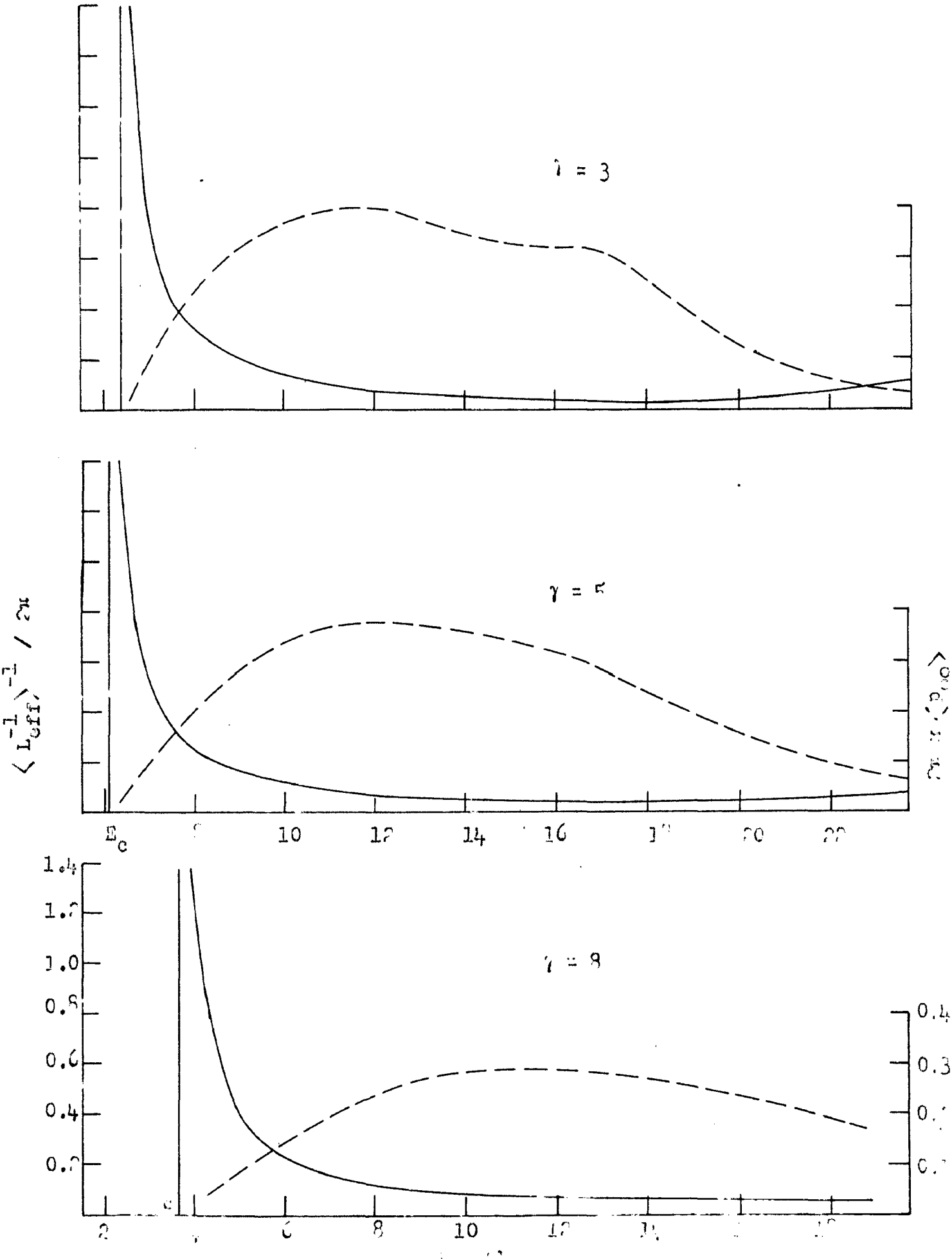

...3. Plots of $\langle L_{eff}^{-1}(L) \rangle^{-1}$ (———) and $\langle \rho_{eff}(L) \rangle$ (- - -) for Cayley trees with K = 3.

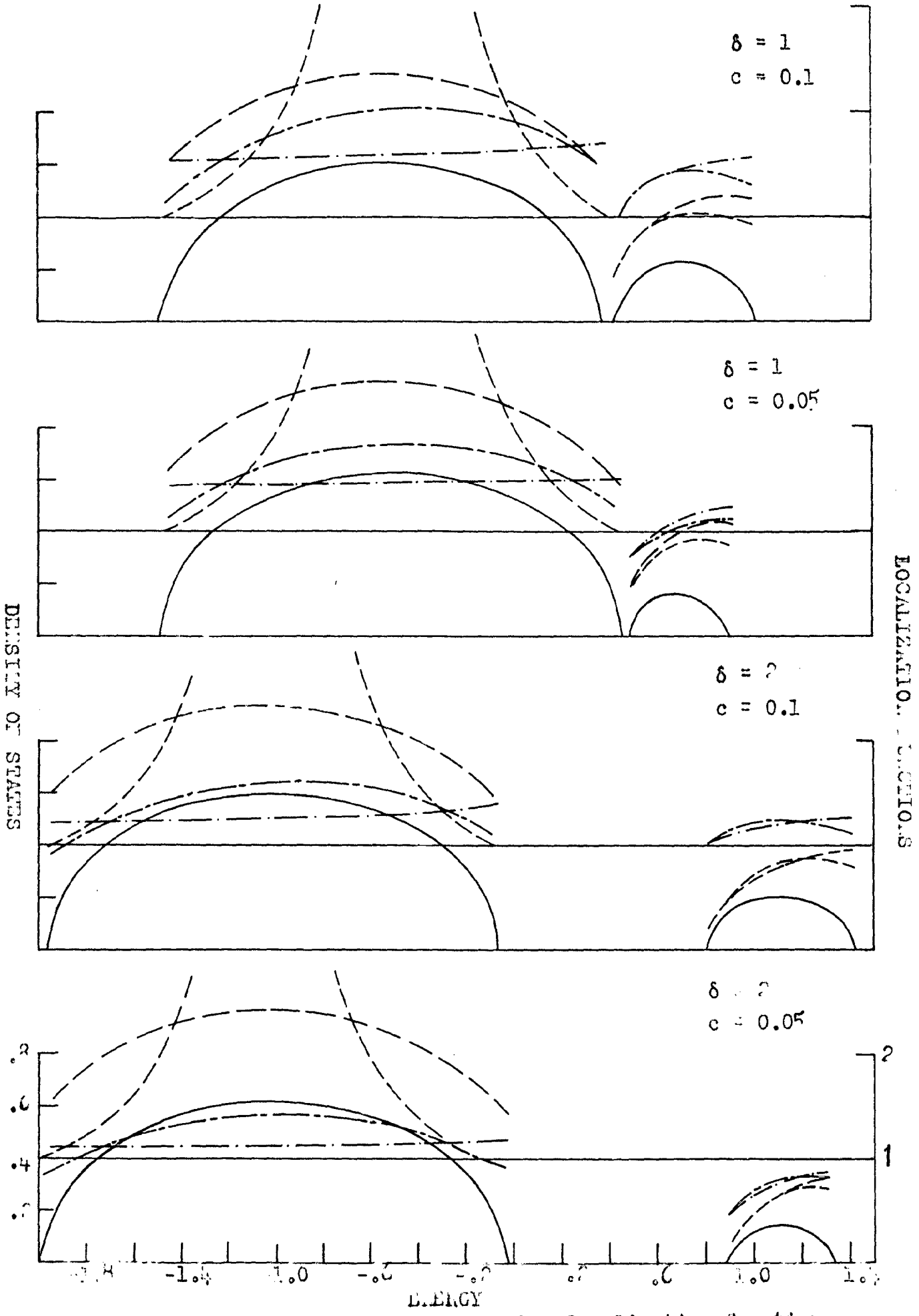

Fig.33. Plots of the two Economou-Cohen localization functions, $L_c(E)$ (——) and $L_c(E)$ (— — —), and the corresponding modified functions, $L_m^I(E)$ (—·—·—) and $L_m^{II}(E)$ (—··—··—); (——) shows Anderson density of states.

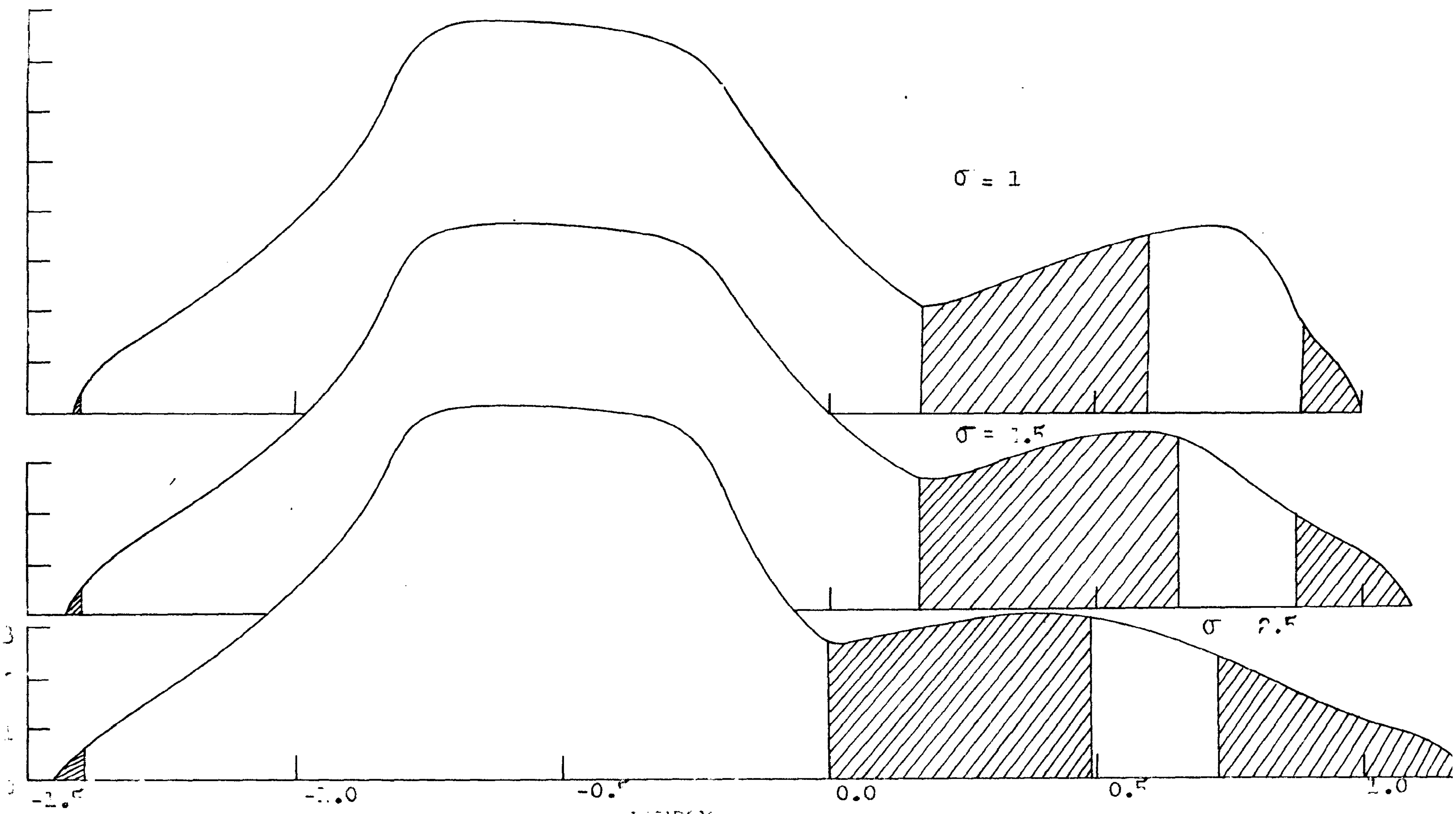

Fig. 37, Longitudinal eigenstates for c_x = 0.?; δ = ?. σ takes the values 1, 1.5 and 2.5.

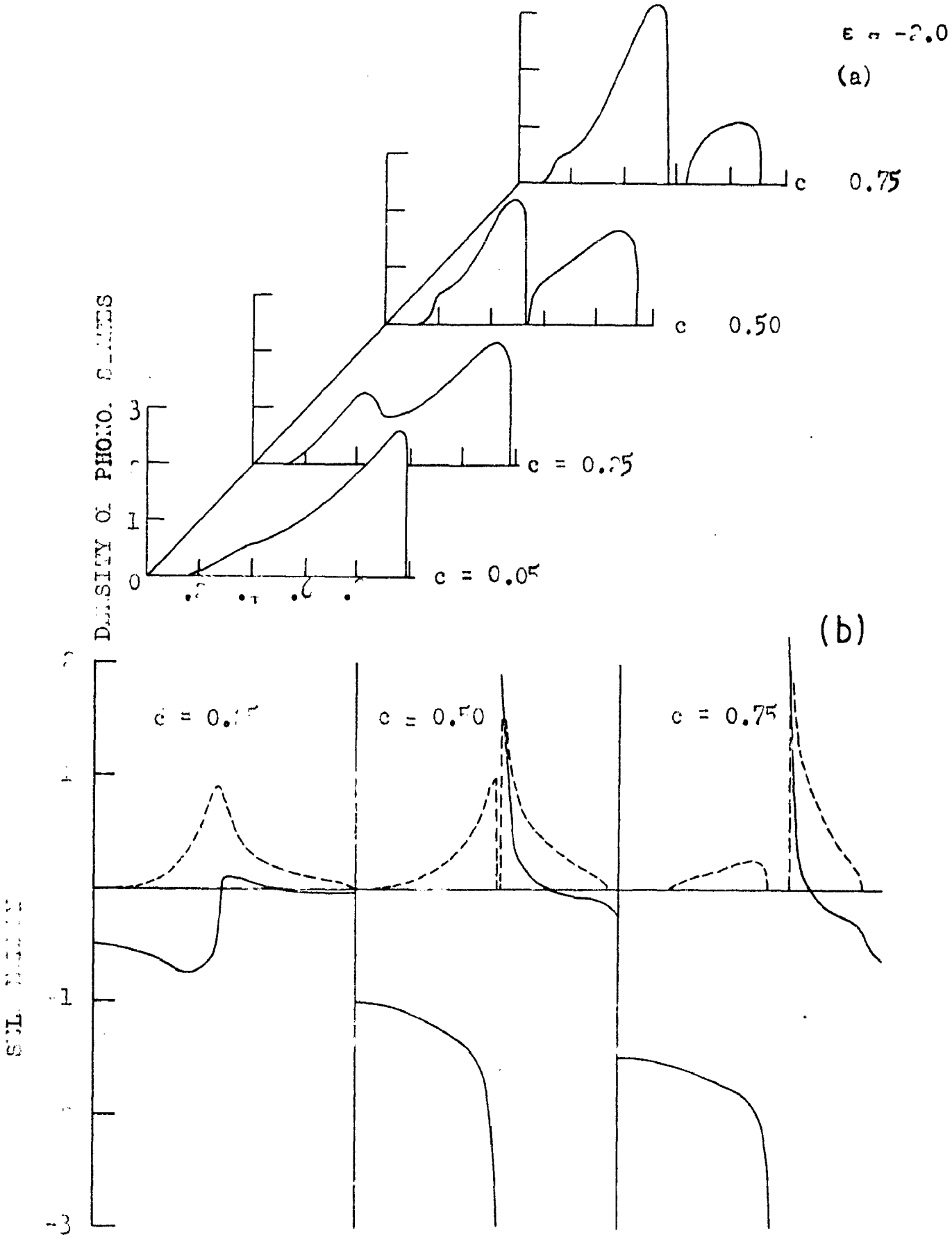

1.37. [illegible] for (a) density of photo[illegible] and (b) self-energy. ε = -2 and c_A = 0.05, 0.25, 0.50 and 0.75. [illegible] have Debye density [illegible] (——) and (----) respectively show the real and [illegible]

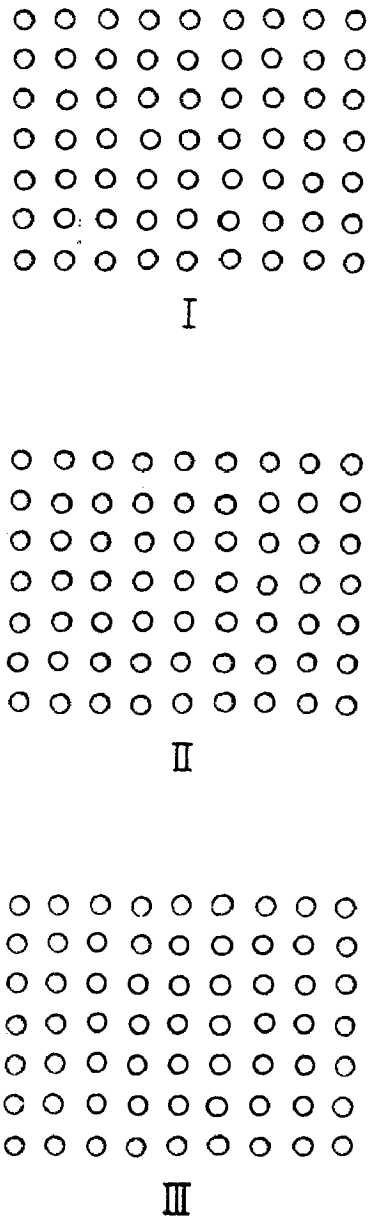

Fig.39. Hypothetical configurations depicting localization and extension of vibrational modes in disordered lattices.

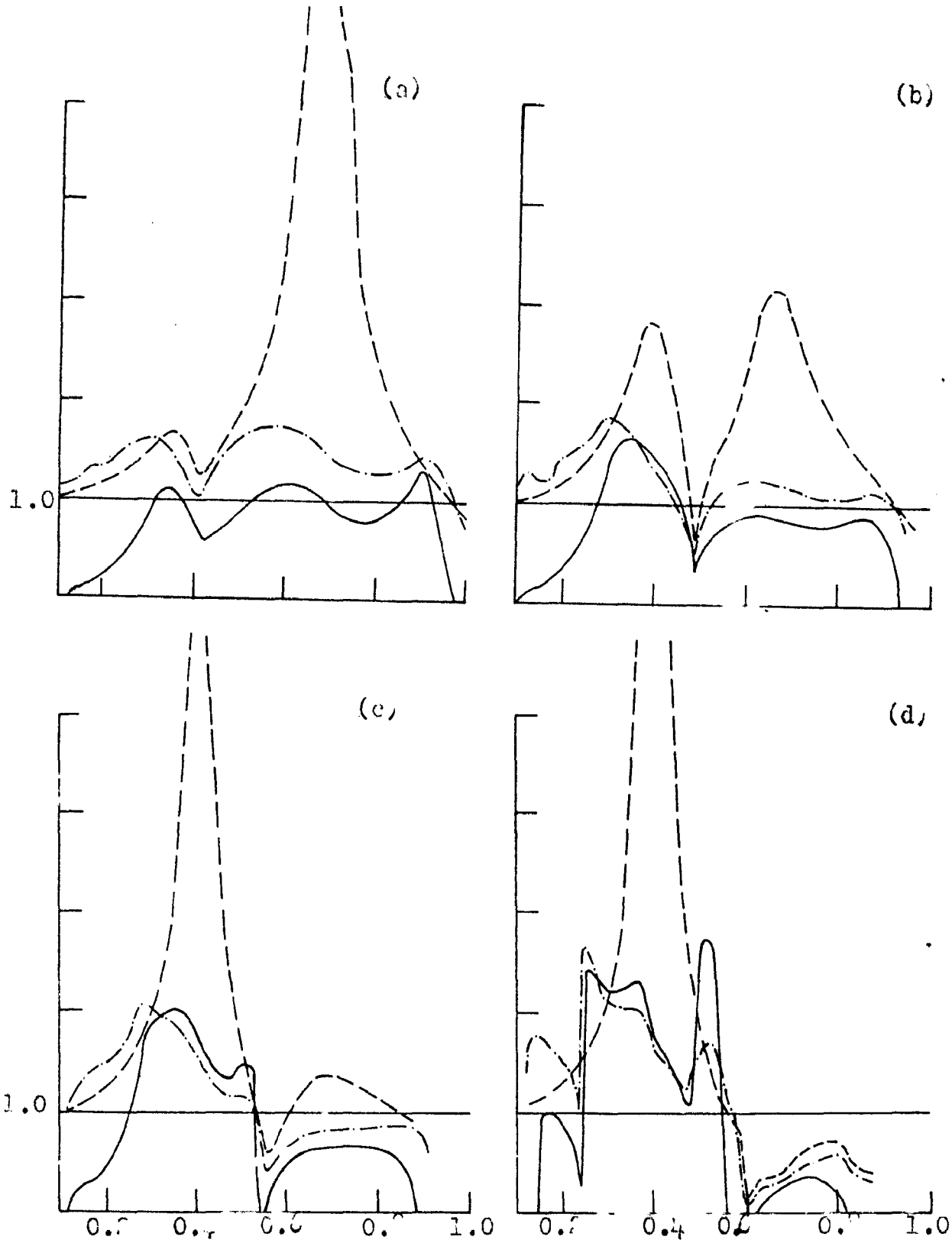

Fig.+0. Plots of Economou-Cohen localization functions adapted for phonons for Cu-Au alloys containing (a) 25% Au, (b) 50% Au, (c) 75% Au and (d) 90% Au. (----) and (-·-·-) show the plots of eqns.(7.39) and (7.41) respectively, (——) show the densities of states.

APPENDIX I.

ANDERSON'S UPPER LIMIT APPROXIMATION.

Anderson has argued that an upper limit to the width of the site energy distribution necessary to produce localized states could be obtained by ignoring the real part of the self-energy. A similar argument can be made here. The argument is that a very small value of $E-\varepsilon_j-E_j$ produces a very large value of Δ_i', but also produces a very large value of E_i. If eqn.(2.3) of Chapter 5 is iterated again, Δ_i', which now occurs on the right hand side of the equation, is large, but $(E-\varepsilon_i-E_i)^2$ is also large, so there is no particularly large effect from this term. Thus under the approximation that the effect of E_o over Δ_o' is negligible, we write Δ_o' as

$$\Delta_o' = \sum_{j=1}^{K+1} \frac{V^2(1+\Delta_j^{o\,\prime})}{(E-\varepsilon_o)^2} \equiv \sum_{j=1}^{K+1} \frac{V^2(1+\Delta_j^{o\,\prime})}{x^2} \quad \ldots (I1)$$

The joint probability distribution $\mathcal{J}(E_o,\Delta_o')$ then splits as

$$\mathcal{J}(E_o,\Delta_o') = f_1(E_o)f_2(\Delta_o'), \quad \ldots (I2)$$

and the expression for $\langle p_{oo}(E)\rangle$ is simplified as

$$p_{oo}(E) = \int_{-\infty}^{\infty} p(E-E_o)f_1(E_o)dE_o \int_o^{\infty} f_2(\Delta_o')\frac{d\Delta_o'}{1+\Delta_o'} \quad \ldots (I3)$$

It follows from the equations (2.1) and (2.32) of Chapter 5 that $\langle 1+\Delta_o' \rangle$ is related with the participation ratio (roughly proportional to the number of sites over which the wave function is spread). So for the calculation

of $\langle L_{eff} \rangle$ ($\sim \langle L_{eff}^{-1} \rangle^{-1}$) we can solve separately the second integral in (I3). At this stage it is necessary to make it clear that one has to resort to the calculation of $\langle 1/(1+\Delta_o') \rangle$ as $\langle \Delta_o' \rangle$ does not exist. To check this one should study the form of $f_2(\Delta_o')$ for very large Δ_o' or equivalently by studying the form of f(s) [Laplace transform of $f_2(\Delta_o')$] for very small s. Following Abou-Chacra et al.[74] one can show that

$$f(s) \approx 1 - A s^{\beta} \quad , \qquad 0 < \beta < 1/2 \qquad \ldots (I4)$$

for small s. This means $\partial f/\partial s\big|_{s\to o} \to \infty$, i.e. $\partial f_2/\partial \Delta_o'\big|_{\Delta_o' \to \infty} \to \infty$ or $f_2(\Delta_o')$ falls off too slowly as $\Delta_o' \to \infty$. Therefore Δ_o' does not exist. But $\langle 1/(1+\Delta_o') \rangle$ does exist. Following the same line of action as in section 2 of Chapter 5 we get

$$F(k) = \left\{ \frac{1}{2\pi} \int_{-\infty}^{\infty} p(\varepsilon_o) d\varepsilon_o f_2\left(\frac{kV^2}{x^2}\right) \exp\left(-\frac{ikV^2}{x^2}\right) \right\}^{K+1} \qquad \ldots (I5)$$

For Cauchy distribution of site energies, $p(\varepsilon_o) = \gamma/\pi\,/(\varepsilon_o^2+\gamma^2)$, eqn.(I5) is solved,

$$F(k) = \left\{ f_2\left(\frac{kV^2}{\zeta_o^2}\right) \exp\left(-\frac{ikV^2}{\zeta_o^2}\right) \right\}^{K+1} , \qquad \ldots (I6)$$

where $\zeta_o = E + i\gamma$. Taking solutions of this equation as $F(k) = e^{-\alpha|k|}$ and $f_2(k) = e^{-\beta|k|}$, we get

$$\exp.(-\alpha|k|) = \exp\left(-\beta \frac{(K+1)V^2}{\zeta_o^2}|k|\right) \exp\left(-i \frac{|k|V^2(K+1)}{\zeta_o^2}\right),$$

so that

$$\alpha = \frac{(K+1)V^2}{\zeta_o^2}(\beta+i) \qquad \ldots (I7)$$

Solving this for the interior of Cayley tree, we get

$$\beta = \frac{KV^2}{\zeta_o^2}(\beta+i) \equiv \Psi + i\emptyset \ ,$$

with
$$\Psi = \frac{2\gamma EKV^2}{(E^2-\gamma^2-KV^2)^2+4\gamma^2E^2}, \qquad \ldots (I8)$$

and
$$\emptyset = \frac{KV^2(E^2-\gamma^2-KV^2)}{(E^2-\gamma^2-KV^2)^2+4\gamma^2E^2} \ . \qquad \ldots (I9)$$

With the help of this we get for the origin of Cayley tree,

$$\alpha = \frac{(K+1)V^2}{\zeta_o^2}(\Psi + i\emptyset+i) \equiv \Gamma + ia$$

with
$$\Gamma = \frac{(K+1)V^2[\Psi(E^2-\gamma^2)+2\gamma E(1+\emptyset)]}{(E^2-\gamma^2)^2+4\gamma^2E^2}, \qquad \ldots (I10)$$

and
$$a = \frac{(K+1)V^2[(1+\emptyset)(E^2-\gamma^2)-2\gamma E\Psi]}{(E^2-\gamma^2)^2+4\gamma^2E^2} \qquad \ldots (I11)$$

From (I3) we get

$$\left\langle L_{eff}^{-1}\right\rangle \equiv \frac{\Gamma}{\pi}\int_o^\infty \frac{d\Delta_o'}{(\Delta_o'-a)^2+\Gamma^2}\cdot\frac{1}{1+\Delta_o'} \ , \qquad \ldots (I12)$$

because the Fourier inversion of F(k) yields,

$$f_2(\Delta_o') = \frac{\Gamma/\pi}{(\Delta_o'-a)^2+\Gamma^2} \qquad \ldots (I13)$$

Equation (I12) can be solved to give

$$\left\langle L_{eff}^{-1}\right\rangle = \frac{1/\pi}{(1+a)^2+\Gamma^2}\left[(1+a)\left(\frac{\pi}{2}-t\right)+\Gamma\ell n\left|\frac{\cos(\tan^{-1}\frac{1+a}{\Gamma})}{\sin(t+\tan^{-1}\frac{1+a}{\Gamma})}\right|\right].$$

$$\ldots (I14)$$

where $t = -\tan^{-1}\left(\frac{a}{\Gamma}\right)$ ... (I.15)

The results for $\left\langle L_{eff}^{-1}\right\rangle^{-1}$ look very much like those shown in figures 31 and 32 except that the feature, that $\left\langle L_{eff}^{-1}\right\rangle^{-1}$ increases as E moves deep into the deep tail, is lost.

BIBLIOGRAPHY

1. J.A. Krumhansl, Proceedings of the International Symposium on Amorphous Magnetism, Detroit, 1972 (Plenum Press). p.15.

2. P.Soven, Phys.Rev.156, 809(1967).

3. D.W.Taylor, Phys.Rev.156, 1017(1967).

4. M.Lax, Rev.Mod.Phys.23, 287(1951).

5. S.F.Edwards, Phil.Mag.6, 617(1961).

6. J.L. Beeby and S.F.Edwards, Proc.Roy.Soc.(London) A274, 395(1963).

7. B.Velický, S.Kirkpatrick and H.Ehrenreich, Phys.Rev.175, 747(1968).

8. F.Yonezawa and K.Morigaki, Prog.Theor. Phys.Suppl.No.53 (1973).

9. Vipin Srivastava and S.K.Joshi, Phys.Rev.B8, 4671(1973).

10. D.N.Zubarev, Usp. Fiz.Nauk.71, 71(1960) [Sov.Phys.-Usp.3, 320(1960)].

11. For reference see G.Lucovsky, M.H.Brodsky and E.Burstein, Phys.Rev.B2, 3295(1970).

12. M.Balkanski, R.Besserman and J.M. Besson, Solid State Commun.4, 201(1961).

13. D.W.Feldman, M.Ashkin and James H.Parker Jr., Phys.Rev. Lett.17, 1209(1966).

14. M.A.Renucci, J.B.Renucci and M.Cardona, in Proceedings of the Second International Conference on Light Scattering in Solids, edited by M.Balkanski (Flammarion, Paris, 1971), p.326.; Solid State Commun.9, 1651(1971).

15. W.J.Brya, Solid State Commun, 12, 253(1973).

16. J.P. Dismukes, L. Ekstrom and R.J.Paff, J.Phys. Chem.68, 3021(1964).

17. A.Ghose, H.Palevsky, D.J.Hughes, I.Pelah. and C.M. Eisenhauer, Phys.Rev.113, 49(1959).

18. G.Dolling, Inelastic Scattering of Neutrons in Solids and Liquids (International Atomic Energy Agency, Vienna, 1963) Vol.II, p.37.

19. G.Dolling and R.A. Cowley, Proc.Phys.Soc.London, 88, 463(1966).

20. R.K.Chang, Brad Lacina and P.S.Pershan, Phys.Rev. Letters, 17, 755(1966).

21. N.X.Xinh, Westinghouse Research Laboratories Scientific Paper no.65-9F5-442-P8,1965(unpublished).

22. A.A.Maradudin, Astrophysics and the Many Body Problem (Benjamin, New York,1963).

23. A.E.Cosand and W.G.Spitzer, J.Appl.Phys.42, 5241(1971)

24. A.E.Cosand, J.Appl.Phys.42, 5230(1971).

25. N.Wakabayashi, R.M.Nicklow and H.G.Smith,Phys.Rev.B4, 2558(1971).

26. N.Wakabayashi, Phys.Rev.B8, 6015(1973).

27. J.S.Lannin, Solid State Commun.12,947(1973).

28. C.Benoit à la Guillaume and M.Voos, Phys.Rev.B10, 4995(1974).

29. P.Soven, Phys.Rev.B2, 4715(1970).

30. B.L.Gyorffy, Phys.Rev.B5, 2382(1972).

31. A.Bansil, H.Ehrenreich, L.Schwartz and R.E.Watson, Phys.Rev.B9, 445(1974).

32. J.A.Clark and P.G.Dawber, J.Phys.F,2, 930(1972).

33. Vipin Srivastava and S.K.Joshi, Proceedings of the International Conference on Vacuum Ultraviolet Radiation Physics (Hamburg, 1974).

34. Vipin Srivastava and S.K.Joshi, Phys.Rev.B12, 2871(1975).

35. E.A. Owens and L.Pickup, Z.Krist.88,116(1934).

36. B.Mozer, D.T.Keating and S.C.Moss, Phys.Rev.175, 868(1968)

37. E.I.Zornberg, Phys.Rev.B1,244(1970).

38. B.Segall, Phys.Rev.125, 109(1962).

39. G.A.Burdick, Phys.Rev.129, 138(1963).

40. H.Friedman and W.W.Beeman, Phys.Rev.58, 400(1940).

41. J.Clift, C.Curry and B.J.Thompson, Phil.Mag.8,593 (1963).

42. J.C.Love, F.E.Obenshain and G.Czjzek, Phys.Rev.B3, 2827(1971).

43. L.V.Azaroff, and B.N.Das, Phys.Rev.134, A 747(1964).

44. D.H.Seib and W.E.Spicer, Phys.Rev.B2,1676(1970).

45. D.H.Seib and W.E.Spicer, Phys.Rev.B2,1694(1970).

46. S.Kirkpatrick, B.Velický and H.Ehrenreich, Phys.Rev. B1, 3250(1970).

47. G.M.Stocks, R.W.Williams and J.S.Faulkner, Phys.Rev.B4, 4390(1971).

48. P.Soven, Phys.Rev.151, 539(1966).

49. G.F.Koster and J.C.Slater, Phys.Rev.96,1208(1954).

50. D.House, B.L.Gyorffy and G.M.Stocks, J.de Phys.35, C4-81(1974).

51. Vipin Srivastava and S.K.Joshi, Phys.Rev.B(1976)(to appear in 15th June-issue).

52. R.J.Elliott,J.A.Krumhansl, P.L.Leath, Rev.Mod.Phys.46, 465(1974), and the references therein.

53. F.Cyrot-Lackmann and F.Ducastelle, Phys.Rev.Letters.27, 429(1971).

54. L.Schwartz and H.Ehrenreich, Phys.Rev.B6,2923(1972).

55. F.Cyrot-Lackmann and M.Cyrot, J.Phys.C5,L209(1972).

56. Vipin Srivastava and S.K.Joshi, J.Phys.F3,L 179(1973).

57. E-Ni Foo,H.Amar and M.Ausloos, Phys.Rev.B4,3350(1971).

58. E-Ni Foo,S.M.Bose and M.Ausloos, Phys.Rev.B7,3454(1973).

59. T.Horiguchi, C.C.Cohen and T.Morita, Solid State Commun. 13, 957(1973).

60. V.Čapek, Phys.Status Sol.(b) 52, 399(1972).

61. F.Ducastelle, J.Phys.F2,468(1972).

62. F.Ducastelle, J.de Phys., Paris 33 C3, 269(1972).

63. R.N.Aiyer, R.J.Elliott, J.A.Krumhansl and P.L.Leath, Phys.Rev.181,1006(1969).

64. B.G.Nickel and J.A.Krumhansl, Phys.Rev.B4, 4354(1971).

65. W.H.Butler and W.Kohn, J.Res.Natl.Bur.Stand.(USA) A74, 443(1970).

66. W.H.Butler, Phys.Letters. 39 A, 203(1972).

67. H.J.Fischbeck, Phys.Stat.Sol.(b) 62, 425(1974).

68. K.F.Freed and M.H.Cohen, Phys.Rev.B3, 3400(1971).

69. N.F.Berk and R.A. Tahir-Kheli, Physica 67, 501(1973).

70. K.Nuzeki, Solid. State Commun.12,267(1973).

71. P.R.Best and P.Lloyd, J.Phys.C8, 2219(1975).

72. F.Brouers, F.Cyrot-Lackmann and M.Cyrot, Phys.Rev. B7,4370(1973).

73. F.Brouers, F.Ducastelle, F.Gautier and Van der Rest, J.Phys.F3,2120(1973).

74. W.H.Butler, Phys.Rev.B8, 4499(1973).

75. P.L.Leath, J.Phys.C6,1559(1973).

76. W.H.Butler, Phys.Rev.B8,4499(1973).

77. M.Tsukada, J.Phys.Soc.Jap.32, 1475(1972).

78. K.Moorjani, T.Tanaka, M.M.Sokoloski and S.M.Bose, J.Phys.C,7,1098(1974); J.de.Phys.35,C4-153(1974).

79. F.Brouers and J.Van der Rest, J.Phys.F2,1070(1972).

80. J.A.Blackman, N.F.Berk and D.M. Esterling, Phys.Lett. 35A, 205(1971).

81. J.A.Blackman, D.M.Esterling and N.F.Berk, Phys.Rev.B4, 2412(1971)

82. F.Ducastelle, J.Phys.C7,1795(1974).

83. F.Cyrot-Lackmann, J.de Phys.,35,C4-109(1974), and the references therein.

84. L.Schwartz and E.Siggia, Phys.Rev.B5, 383(1972).

85. Vipin Srivastava and S.K.Joshi, under preparation.

86. P.W.Anderson, Phys.Rev.109,1492(1958).

87. D.J.Thouless and Last, private communication.

88. M.H.Cohen, H.Fritsche and S.R.Ovshinsky, Phys.Rev. Letters, 22,1065(1969).

89. E.N.Economou and M.H.Cohen, Phys.Rev.Letters.25, 1445(1970); Phys.Rev.B5,2931(1972).

90. D.C.Licciardello and E.N.Economou, B11,(3697(1975).

91. E.Feenberg, Phys Rev.74,206(1948).

92. K.M.Watson, Phys Rev.105,1388(1957).

93. E.N.Economou and M.H. Cohen, Phys.Rev.B4,396(1971).

94. E.N.Economou, Proceedings of the New Delhi Winter School(1972).

95. R.Abou-Chacra, P.W.Anderson and D.J.Thouless, J.Phys. C6,1734(1973); R.Abou-Chacra and D.J.Thouless, J.Phys.C7,65(1974).

96. E.N.Economou and C.Papatriantafillou, Phys.Rev. Lett.32, 1130(1974).

97. Vipin Srivastava,Abhijit Mookerjee and, S.K.Joshi,under preparation.

98. I.M.Guelfand, M.I.Graev and N.Ja.Vilenkin, Les Distributions, tome 5,Dunod, Paris (1970).

99. P.Lloyd, J.Phys.C2, 1717(1969).

100. N.F.Mott, Phil.Mag.22,7(1970);N.F.Mott and E.A.Davis, Electronic Processes in Non-Crystalline Materials, Clarendon Press, Oxford (1971).

101. R.A.Abram and S.F.Edwards, J.Phys.C5,1183(1972).

102. M.H.Cohen, J.Non-Cryst.Solids 2,432(1970), and J.Non-Cryst.Solids 4,391(1970).

103. I.M.Lifshitz, Usp.Fiz.Nauk 83, 617(1964) [Sov.Phys.Usp.7, 549(1965)].

104. B.I.Halperin and M.Lax, Phys.Rev.148,722(1966), and Phys.Rev.153,802(1967).

105. J.M.Ziman, J.Phys.C2,1230(1969).

106. D.C.Licciardello and E.N.Economou, Sol.St.Comm.15,969(1974)

107. E.N.Economou, Solid St.Comm.9,1317(1971).

108. R.J.Bell, Rep.Prog.Phys.35,1315(1972).

109. A.A.Maradudin, Solid State Physics, edited by F.Seitz and D.Turnbull (Academic Press Inc.New York),18,273-420; 19,1-134.

110. E.C.Svensson and W.A.Kamitakahara, Can.J.Phys.49,2291(1971).

111. D.C.Mattis, and F.Yonezawa, Phys.Rev.Lett.31,828(1973).

112. Deepak Kumar, Vipin Srivastava and S.K.Joshi,unpublished.

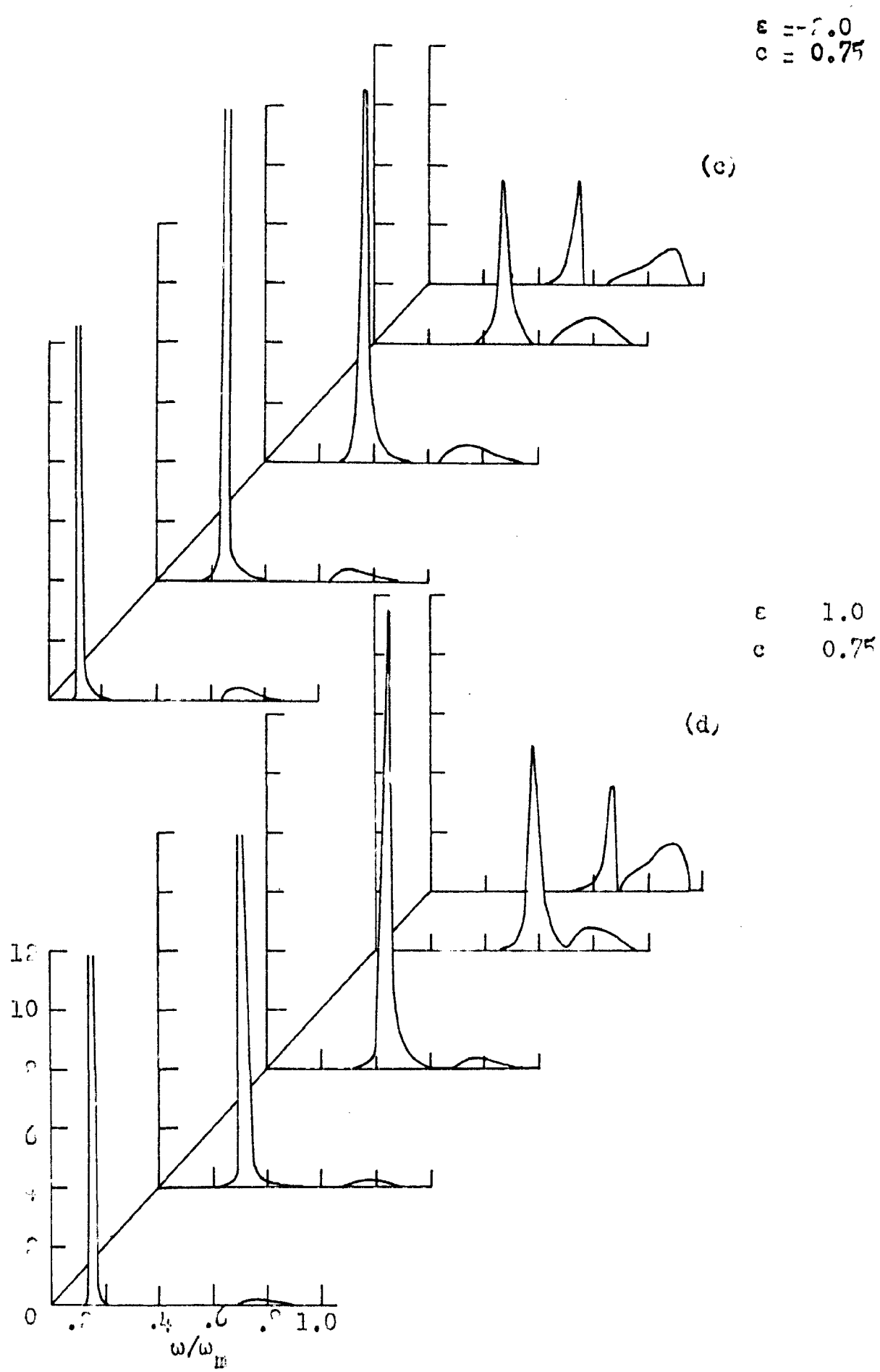

Fig. 3.6(c,d). CPA spectral functions for phonons:
(c) $c = 0.75$, $\varepsilon = -2.0$; (d) $c = 0.75$, $\varepsilon = 1.0$.

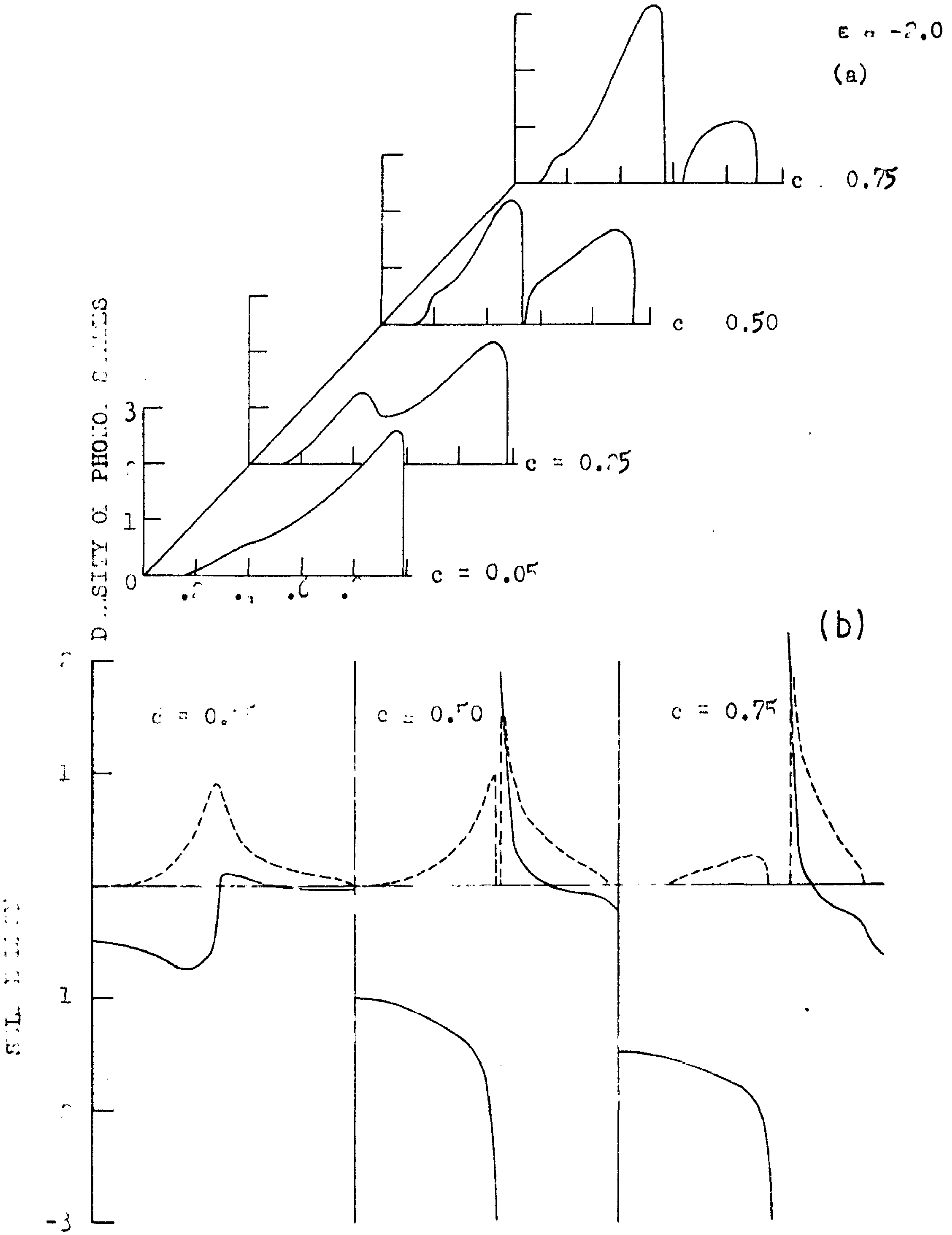

[illegible]57. CPA results for (a) den[illegible] of phono[illegible] and (b) self energ[illegible]. ε [illegible] and c [illegible] 0.0[illegible], 0.[illegible]0 and 0.7[illegible] [illegible] B have Debye density of states. (---) and (—) [illegible] the real and imaginary part of self energy.

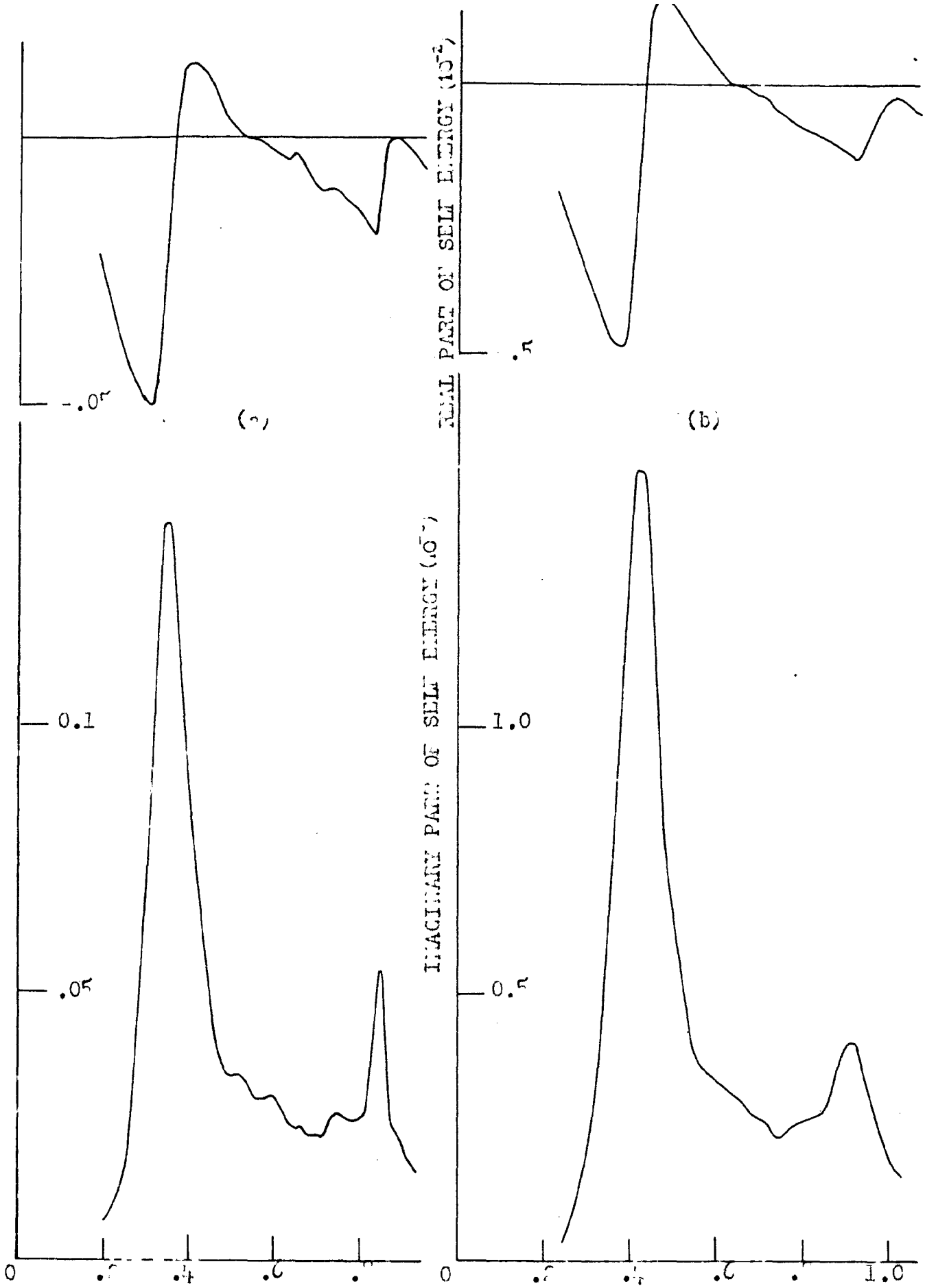

Fig.3. Real part (upper curves) and imaginary part (lower curves) of phonon self energy (CPA) for Cu Au alloys with (a) 3% and (b) 9.3% Au.

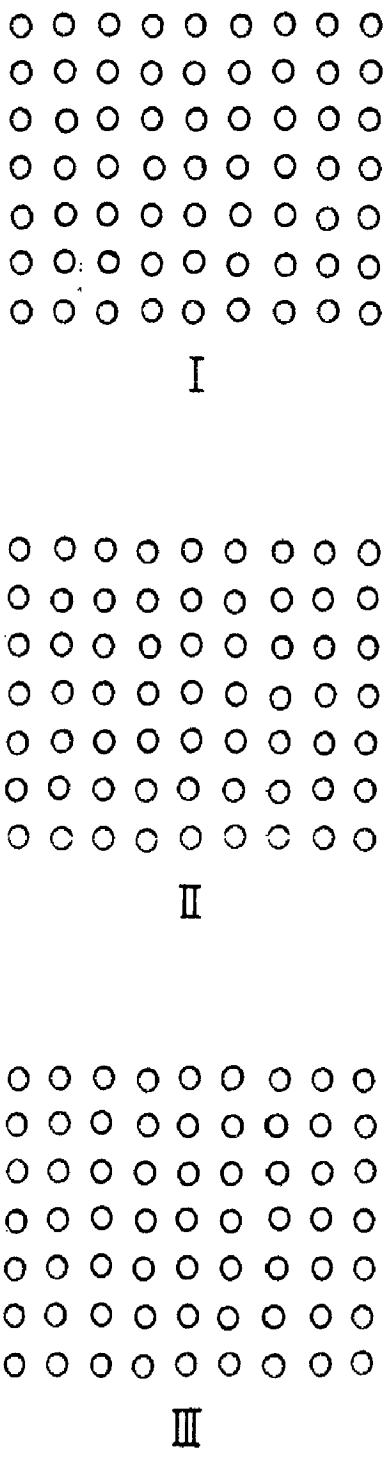

Fig.39. Hypothetical configurations depicting localization and extension of vibrational modes in disordered lattices.

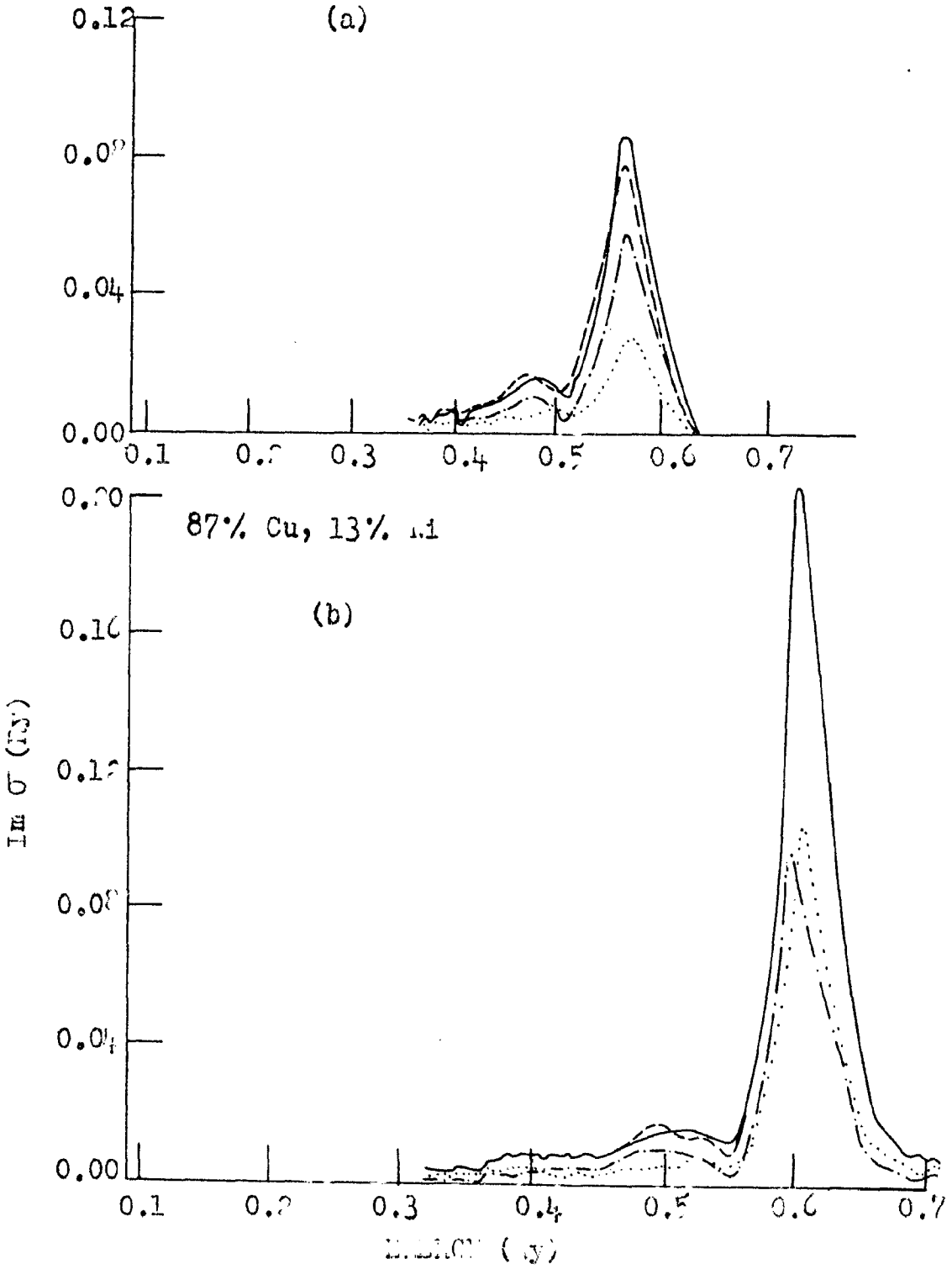

Fig.14. The Im $\sigma(E)$ versus energy plots calculated with methods employing eqn.(1.21) (——) and eqn.(1.25) (----). (a) shows the same for coherent pseudopotential method and (b) shows them for CPA. (.....) and (—·—·—) respectively belong to the e_g and t_{2g} contributions to the total Im σ obtained through eqn.(1.21).

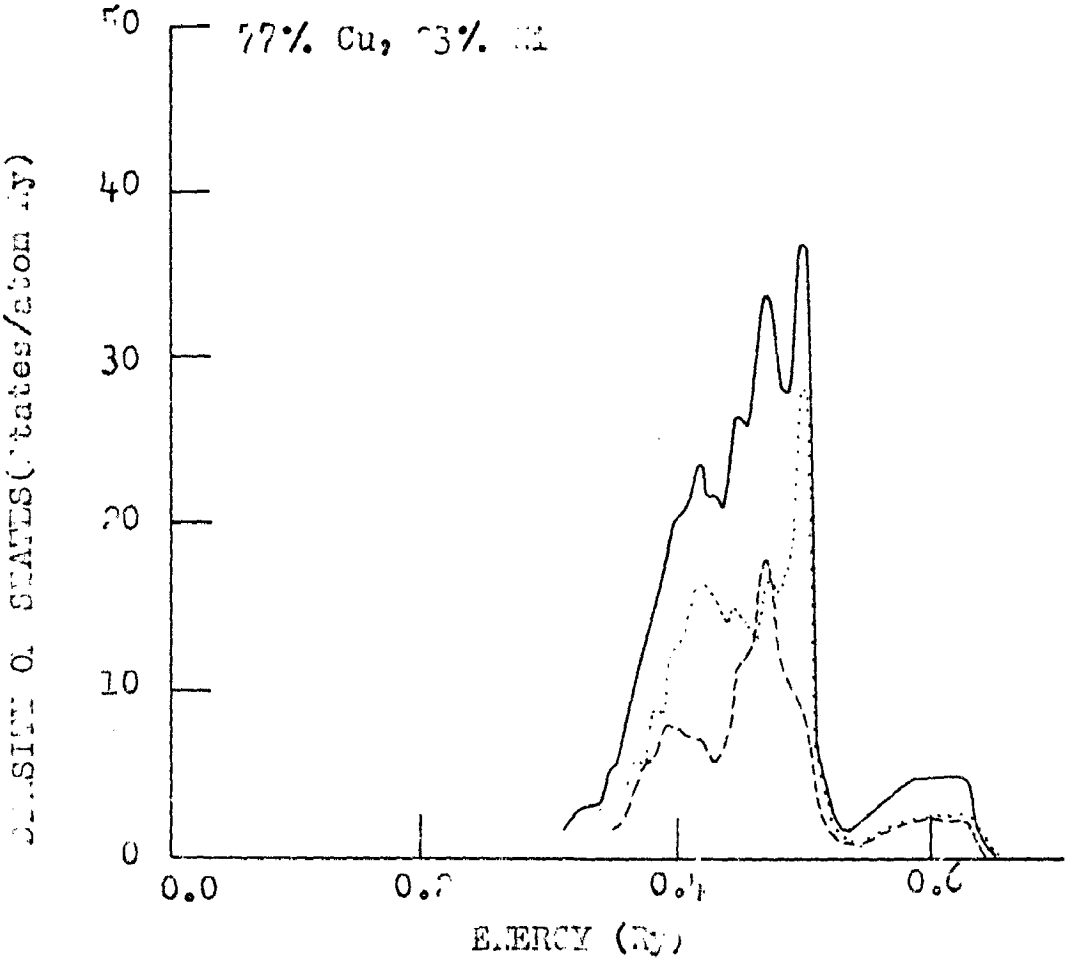

Fig.1. Densities of states using equations (1.48) and (1.49). (———) denotes total densities of states, (-----) the e_g component, and (••••) the t_{2g} component of total densities of states.

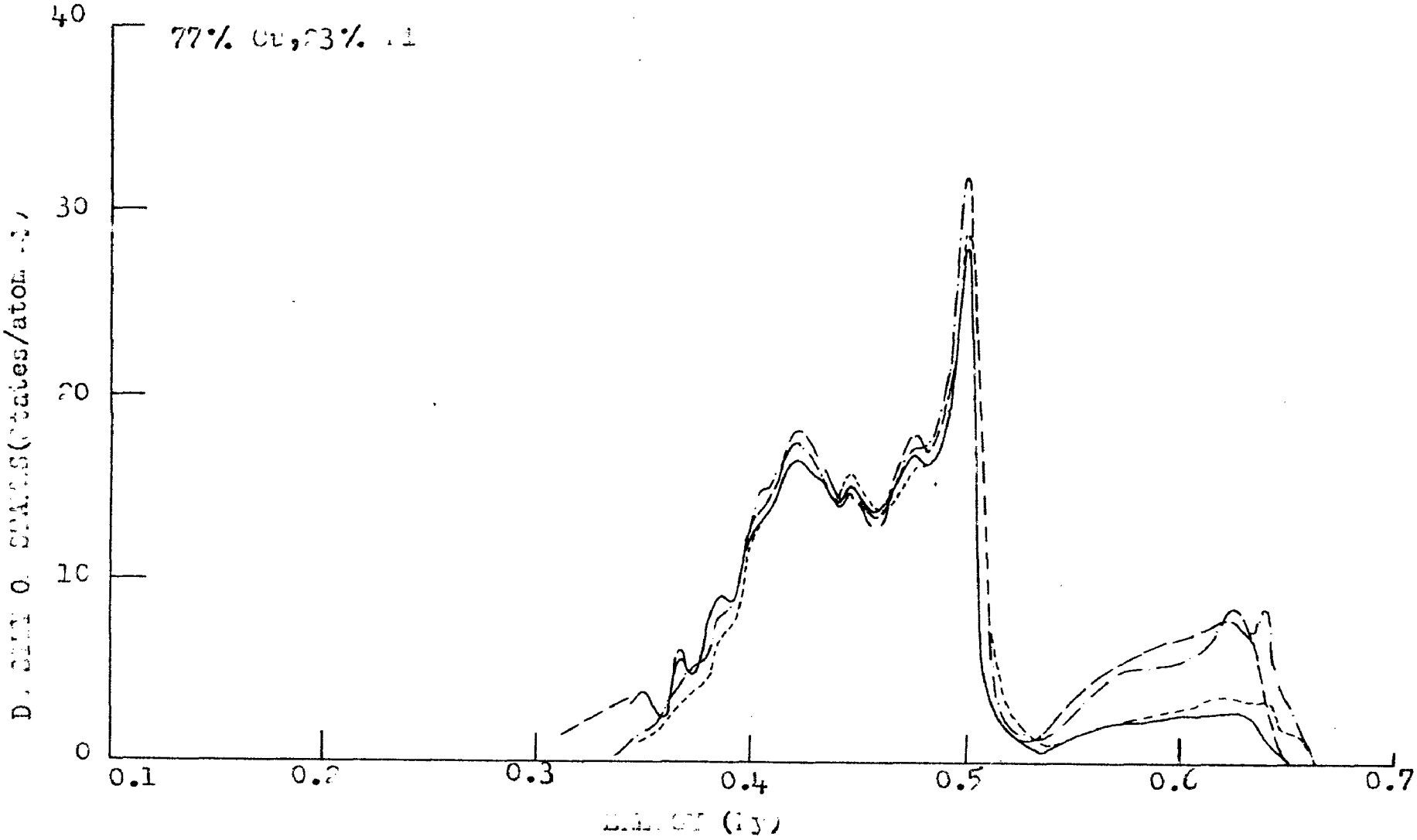

Fig.1: The t_{2g} component of the densities of states calculated through the approaches (i) and (ii), given respectively by eqn.(1.47) and by (1.45), (1.46) and (1.48) within the two self-consistent methods given by eqn.(1.41) and (1.55). (——) and (– – –) show $\rho_{t_{2g}}$ obtained from (i), and (----) and (·–·–) are obtained from (ii).